LASER-INDUCED SURFACE MODIFICATIONS FOR OPTICAL APPLICATIONS

Tahseen Jwad

Department of Mechanical Engineering

School of Engineering

University of Birmingham

This dissertation is submitted for the degree of Doctor of Philosophy

June 2018

ABSTRACT

Surface treatments by laser processing have gained significant attention due to the achievable surface properties along with the selectivity that cannot be realized with other methods. The focus of this research is on investigating and developing laser-based treatment methods, i.e. laser-induced surface oxidation, laser-induced oxygen reduction, and laser-induced periodic surface structures (LIPSS), to address the requirements of specific applications in optics, aesthetics, and anti-counterfeiting, e.g. colour marking and the fabrication of optical devices and diffraction holograms. A single spot oxidation method is proposed to control the size of the oxidation area and its thickness on titanium substrates. A pixel resolution down to the beam spot size with high spatial control is achieved. To produce diffraction optical devices on glass substrates by direct writing, another method is proposed. Especially, the method is implemented and validated for fabricating two-level phase-type Fresnel Zone Plates (FZPs) with a nanosecond laser by converting a titanium film on a glass substrate into titanium dioxide patterns with a thickness controlled at the nano-scale. The flexibility and applicability of laser-induced oxidation is extended with a method for erasing colour marks selectively by employing a laser-induced oxygen reduction. Finally, a method for producing LIPSS patterns with varying orientations is developed and then validated for fabricating diffraction gratings on metallic surface.

DEDICATION AND ACKNOWLEDGEMENTS

I dedicate this thesis to my family, I would not have made it this far without your constant encouragement and support.

I would like to show my deepest gratitude to my main supervisor, Prof. Stephan Dimov, and to Dr. Haider Butt for their guiding and supporting me during the years of research.

I would like to thank the Iraqi Ministry of Higher Education and Scientific Research (MOHESR) for the financial support of during my PhD research.

My thanks and appreciation go to all my friends and my colleagues, for the love, care, support, and trust that you have provided.

TABLE OF CONTENTS

TABLE OF FIGURES

LIST OF TABLES

LIST OF PUBLICATIONS

Journal Publications

1. **Jwad, T.**, Deng, S., Butt, H., & Dimov, S. (2016) Laser induced single spot oxidation of titanium, Applied Surface Science, 387, 617-624.

2. **Jwad, T.**, Deng, S., Butt, H., & Dimov, S. (2018) Fabrication of TiO2 Thin Film-Based Fresnel Zone Plates by Nanosecond Laser Direct Writing. Journal of Micro and Nano-Manufacturing, 6(1), 011001 (9 pages).

3. **Jwad, T**., Walker, M. and Dimov, S., 2018. Erasing and rewriting of titanium oxide colour marks using laser-induced reduction/oxidation. Applied Surface Science, 458, pp.849-854.

4. **Jwad, T.**, Penchev, P., Nasrollahi, V., & Dimov, S. (2018) Laser induced ripples' gratings with angular periodicity for fabrication of diffraction holograms, Applied Surface Science, 453, 449-456.

Other publications

5. Deng, S., **Jwad, T**., Li, C., Benton, D., Yetisen, A.K., Jiang, K., Dai, Q. and Butt, H., 2017. Carbon Nanotube Array Based Binary Gabor Zone Plate Lenses. Scientific Reports, 7(1), p.15256.

6. Nasrollahi, V., Penchev, P., **Jwad, T**., Dimov, S., Kim, K. and Im, C., 2018. Drilling of micron-scale high aspect ratio holes with ultra-short pulsed lasers: Critical effects of focusing lenses and fluence on the resulting holes' morphology. Optics and Lasers in Engineering, 110, pp.315-322.

CHAPTER 1 : INTRODUCTION

1.1   Motivation

Laser-based surface treatments have attracted a myriad of research interests due to the selectivity that laser can provide, along with the unique surface properties that cannot be achieved by other methods. Laser-based surface modifications are the result of either surface structuring, chemical composition modification or physical proprieties altering. Generally, such laser treatment methods involve one or a number of the following processing mechanisms: shock-waves, melting, ablation, laser surface-wave interaction, quenching, shock penning [1, 2].

A number of optical, aesthetic, mechanical, thermal, electrical, chemical, and tribological applications can benefit by employing these surface modification methods [1, 3]. The focus of this research is on investigating and developing further three of these methods, i.e. laser-induced surface oxidation, laser-induced oxygen reduction, and laser-induced periodic surface structures (LIPSS), to address the requirements of specific applications in optics, aesthetics, and anti-counterfeiting, e.g. colour marking and the fabrication of optical devices and diffraction holograms.

Laser-induced surface oxidation for colour marking applications on different metal surfaces such as titanium and stainless steel is a well-known method and it has been studied comprehensively by a number of researchers [4-6]. However, although laser-induced oxidation offers significant advantages compared with other oxidation methods, such as anodizing, due to its selectivity, it is still underutilised and needs further research to benefit fully from the achieved high processing resolution. In particular, such further development of

this technology can address requirements to contain the oxidation within the smallest possible processing area and thus to increase the processing resolution. Additionally, the use of laser-induced oxidation can be broadened beyond its main colour marking application area by developing capabilities for direct writing of optical devices and thus to take advantage of its relatively low processing cost, selectivity and control of the oxide thickness at nanometre scale.

Another constraint in using laser-induced oxidation for colour marking is that its application is limited to few metals such as titanium, tantalum and niobium. This is due to the unique combination of refractive indices of these metals and their oxides that cannot be obtained on other metals together with their high reactivity to oxygen at elevated temperatures. Therefore, a solution is required to broaden the use of this technology to other materials, e.g. glass. An additional limitation that the literature review revealed is that there are no available erasing methods other than ablating the coloured surfaces. Thus, a selective way of erasing and rewriting oxides-based colours is important to increase the process' flexibility.

Colour marks by light diffraction rather than by thin film interference is also achievable by applying ultrafast pulsed lasers (femtosecond) by generating ripples with a periodicity similar to the laser source wavelength [7]. Such self-organised ripples are called laser-induced periodic surface structures (LIPSS) and they can be utilised in different application areas as diffraction gratings [8, 9]. The fact that the ripples' orientation is dependent on the laser source polarization vector can be explored to develop new capabilities for a range of optical applications. In particular, capabilities for controlling the LIPSS orientation in real time during the laser beam scanning of surfaces can be developed together with their potential applications.

1.2   Research aims and objectives

The overall aim of this research is to investigate the capabilities and limitations of laser-induced surface modification technologies, i.e. laser-induced oxidation, laser-induced oxygen reduction and LIPSS, and then to develop them further to address the requirements of existing and potential new optical applications. In particular, the research is focused on overcoming some of the limitations of these technologies in terms of processing flexibility, necessary devices, software, and control strategies for broadening their use, especially to create the necessary implementation pre-requisite for fabricating surfaces with optical functionalities.

In order to meet this aim, the main objectives of this research are as follows:

1. *To create means for controlling the selectivity of laser-induced oxidation process down to a beam spot size level and thus to have a local control of the oxides' spatial resolution at microns scale together with a thickness control at nanometre scale.* This will be achieved by developing, implementing and validating a novel laser processing technology for imprinting colour images on titanium surfaces.

2. *To extend the capabilities of laser-induced oxidation to any material and thus to create the necessary prerequisites for applying this colour marking technology for direct writing of optical devices.* The feasibility of producing oxides' film as light phase shifter will be investigated with the objective to imprint diffraction optical elements on glass substrates, e.g. to produce cost effectively Fresnel zone plate (FZP). As part of this research, a model for determining the oxide thickness and the FZP geometry will be developed that take into account the FZP functional wavelength, focusing length and the refractive index of the oxide film.

3. *To investigate the feasibility of using laser-induced reduction and thus to convert titanium dioxides into either lower oxides or into titanium and thus to erase the oxide-based colours selectively.* The laser processing domain for achieving this together with the possibility of rewriting different colours over the erased titanium dioxides will be investigated to determine any interdependences between the erased and the new generated colours.

4. *Finally, to develop capabilities for controlling the orientation of LIPSS within the laser spot size or even a smaller area selectively and thus to create pre-defined patterns of LIPPS orientations.* A laser processing setup with a motorized polarizer together with its controller for following a specific speed function will be designed and implemented to allow the synchronization of the $\lambda/2$ wave plate rotation with the laser scanning speed along the beam path. The objective is to create capabilities for fabricating diffraction-based holograms by producing LIPSS with a varying orientation.

1.3   Thesis organization

This thesis consist of seven chapters, the research objectives are introduced in this chapter while the literature review is presented in Chapter 2. The research carried out to achieve these four objectives is reported in Chapters 3 to 6, respectively. The summary of the contribution to knowledge, the general conclusions and future research directions are presented in Chapter 7. The contents of these chapters are outlined below.

Chapter 2 presents a literature review of methods used for laser-induced surface modifications by oxidation, reduction and LIPSS formation with a specific focus on their

capabilities, limitations and potential applications while pointing out on open issues and key research directions for their further development.

Chapter 3 presents a method for controlling the selectivity of laser-induced oxidation process for colour marking applications. The novelty aspect of the proposed method is achieving a spatial resolution down to the beam spot size and an oxide thickness control in the nanometre scale.

Chapter 4 reports the development of capabilities for applying laser-induced oxidation on any material and demonstrates the use of this colour marking technology for imprinting cost-effectively FZP on glass substrates. In this chapter, an original method is proposed to colourise a glass substrate using laser-induced oxidation. Another aspect is the use of the generated films to produce diffraction optical devices such as FZP's

Chapter 5 presents a method for erasing colour marks produced with laser-induced oxidation by employing laser-induced oxygen reduction selectively and thus to convert titanium dioxides into either lower oxide or into titanium. To the best of our knowledge, the proposed erasing method was validated for the first time.

Chapter 6 describes the development of a method for creating pre-defined patterns of LIPPS orientations by real time control of laser processing polarization vector along the beam scanning path.

Chapter 7 summarises the contributions to knowledge and the general conclusions of this research and also outlines future research directions.

CHAPTER 2: Literature review

2.1 Introduction

Light amplification by stimulated emission of radiation (LASER) has attracted many researchers since the first laser built by Maiman in 1960 [10, 11]. Laser has been involved as a main or secondary processing media in almost all applications. Numerous applications have been industrialised in many areas including, but not limited to, medicine, measurements and inspections, optics and communications, and manufacturing. Laser unique properties, such as high spatial coherence and monochromaticity, are behind the huge interest of using laser in industrial applications, as well as in scientific investigations [12].

Laser can be classified, based on its active medium, into gas, liquid, and solid-state. Alternatively, based on its wavelengths, it can be classified into near-ultraviolet, visible, and near-infrared. Another classification is based on the duration of the laser emission (pulsed laser or continuous wave). Pulsed laser is also sub classified, based on the pulse duration, into ultrashort (picosecond and femtosecond laser), short (nanosecond), and long (millisecond).

In manufacturing, laser has played a fundamental role in the development of number of applications. This is due to the fact that laser can interact with most materials (e.g., metals, ceramics, and polymers) and composite materials, in both transparent and opaque states. Nevertheless, laser is considered as a cheap, fast, clean, non-contact, and accurate tool of manufacturing. As a result, it has become a pioneer in machining (i.e., cutting, shaping, and drilling), welding, and surface chemical and physical modification (e.g., surface hardening, annealing, recrystallization, gladding, patterning, deposition, and chemical transformation).

Laser-induced surface modification can be classified into two main classes, physical modification and chemical modification. Surface physical modification using laser is usually based on surface ablation to create a micro or sub-micro structures on the surface thus obtaining a specific functionality. In the case of chemical modifications, the composition of the surface is modified either by melting and inserting some alloying elements or by using specific gases to alter the composition of the melted surface and gain the required surface properties.

2.2 Laser-matter interaction

Laser-matter interaction depends mainly on the laser parameters along with the material optical and thermal properties. The most effective laser parameters that should be taken into consideration in laser-matter interactions are laser fluence, wavelength, polarization, and pulse duration.

Laser fluence can be defined as the ratio of energy to unit area; it usually represents the energy flux of pulsed laser. While in the case of a continuous wave (CW) laser, the quantity measurement of the laser power is represented by the intensity.

Laser wavelength is another important parameter in laser-matter interactions. Since a laser beam is a source of light, it suffers reflection, absorption, transmission, and scattering as Figure 2 illustrates. These light related phenomena are totally dependent on the laser wavelength, since a material could be transparent to a specific wavelength but opaque to another. Similarly, the absorption and reflection of laser by matter are functions of laser wavelength. Another essential parameter that affects the interaction is the laser pulse duration, which plays an important role in the ablation rate, and the precision and quality of the processed part [13].
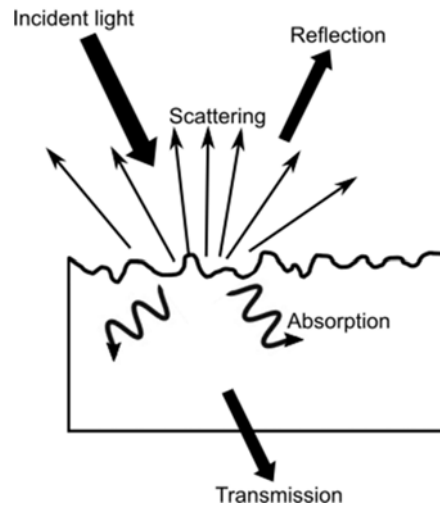
Figure 2 Light-matter interaction and its optical phenomena
(Reflection, Scattering, absorption, and transmission)
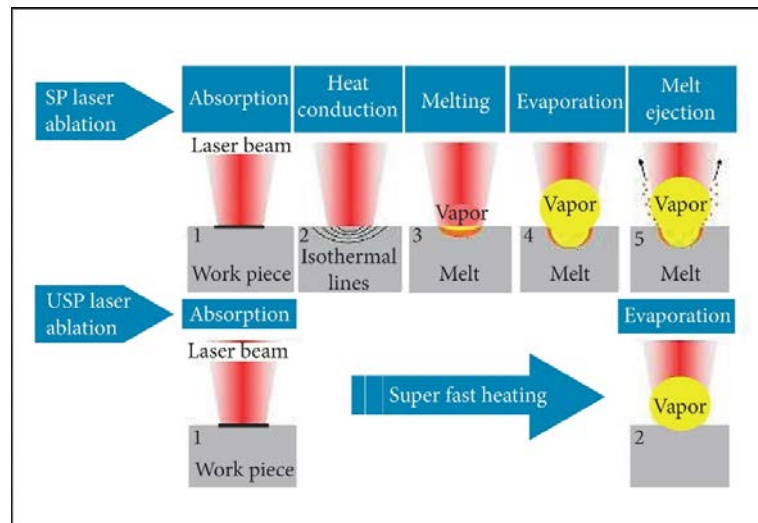
Figure 1 Laser surface heating, melting and vaporization depending on two pulse duration
time scales, short pulse (SP) and ultrashort pulse (USP) [14].

The pulse duration also affects the provided pulse peak power, which is a function of the

pulse duration and the pulse energy. Figure 1 shows laser-material interaction for short pulse

laser (SP) and for ultrashort pulse (USP); examples of these are a nanosecond and

femtosecond laser, respectively. When the laser energy is absorbed locally in the electron

system, electrons collide with each other leading to their thermalization. This will heat up the

lattice eventually, depending on the material's electron-phonon relaxation time [13].

Therefore, the time scale of the pulse determines the type of laser-material interaction, which can be thermal for long and short pulses (longer than the electron-phonon relaxation time) or athermal for ultrashort pulses (shorter than the electron-phonon relaxation time). This in turn will affect the size of the heat-affected zone, which affects the quality and mechanical properties of the processed target. Figure 3 illustrates the heat-affected zone for continuous waves, and nanosecond and femtosecond pulsed laser.
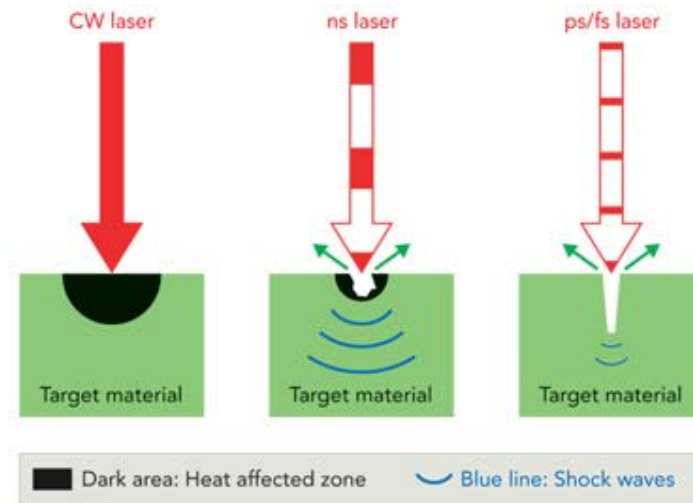
Figure 3 Laser material interaction basic for different types of lasers (CW, ns, and fs) [13].

2.3 Oxidation of metals

The oxidation of metal surfaces in rich-oxygen environments is a well-known phenomenon and it happens spontaneously for most metals and semiconductors [12]. For some metals (like iron), the oxidation is a continuous process and it stops once all the metal has been converted into metal oxide; for other metals (such as Al, Nb, Si, Ti, Ta), the native oxide layers prevent further oxidation when their thickness is enough (usually 1-10 nm) to terminate the oxygen diffusion.

Although the oxidation of metal as a consequence of laser processing (i.e. cutting, machining, polishing) is not preferred [15], increasing and controlling the oxide thickness are desirable for many applications such as mechanical, chemical, electronic, optical, and aesthetic. Therefore, many oxidation methods have been developed through the years in order to control the surface oxide thickness on various metals [12]. These oxidation techniques include, but are not limited to, thermal oxidation, thermochemical oxidation, plasma oxidation, chemical oxidation, electrolytic oxidation (anodizing), chemical vapour deposition, physical vapour deposition, plasma deposition, laser deposition, and laser-induced oxidation [16]

2.3.1 Laser-induced oxidation

Laser-induced oxidation has advantages over other oxidation methods, as most of these methods are expensive, time consuming, and hazardous (as they required dealing with chemical and electrical power) [17]. The thickness of the oxide films that formed by these methods is usually non-homogeneous and, for some methods, non-controllable. Nevertheless, these treatment methods are non-selective, which is one of the most important limitations [17].

Laser-induced surface oxidation is a thermochemical process resulting from laser-metal interaction [18] and it is a type of high temperature gas corrosion[16]. Localized heating using laser is the most commonly applied method for the aim of oxidation [15], as laser is preferred for applications requiring high precision and localization [17]. The advantages of laser-induced oxidation over other methods include, but are not limited to, the following [12, 17]:

- Relatively lower bulk temperatures.
- Different types of oxide formation.
- Lateral oxidation resolution down to laser wavelength.

- Spatial and temporal precise control.

- Localization.

- Short processing time for small areas.

- High repeatability.

Regardless of the simplicity, straightforwardness, and the above mentioned advantages of laser-induced oxidation, there are some disadvantages associated with the use of laser for oxide film formation, such as the low throughput, the formation of cracks, and the roughness of the generated film [12]. However, some of these disadvantages could be overcome by optimizing the laser processing parameters.

Laser-induced oxidation is not a new technique. A number of groups of Soviet researchers pioneered the use of laser in oxidation throughout the 1970s and published the first studies of the laser-induced oxidation mechanism on different metals [15]. However, the blossom of laser-induced oxidation started at the end of that decade [15]. The ability and importance of the selectivity in the oxidation process using laser have been mentioned in a published work by Veiko et al. [19] at the beginning of 1970s in which they state "thus we may speak of localization of chemical reactions by use of the laser" [15].

Initiation of the metal oxide using laser can be achieved either by using continuous-wave (CW) or pulsed laser [15]. The use of the former is more controllable in terms of the provided energy, while the latter can lead to a relatively fast melting of the surface. In a work published in 1969, Asmus and Baker [20] attributed the increase of CW CO_2 laser absorption by the metallic targets to the formation of surface oxide film [15, 21]. The same results were obtained by Arzuov et al. [21] for tungsten, molybdenum, aluminium, and copper. They found that the oxidation of targets irradiated by laser is not due only to melting and it could happen

11

below the metal melting point, as in the case of tungsten and molybdenum. However, the absorptivity is increased by several-fold when the temperature is increased to the melting temperature due to the oxidation of the metal [21]. Then Arzuov et al. [22] proposed a method to calculate the optical and diffusion constants as well as the thickness of the generated oxide film.

The importance of the optical constants and the thickness of the generated thin film of oxide do not only affect the absorptivity of the incident laser. They also affect the provided intensity of the laser due to the thin film interference phenomenon. This fact has driven Arzuov's group to study the effect of interference on the losses of the provided laser power, which in turn affect the heating of metals, and they developed a theoretical model to considered these losses [23]. They later extended the work to include, at different stages, the effect of laser wavelength [24], the effect of the incident angle and laser polarization on the absorptivity [25]. Pulsed laser has also been used for surface oxidation (as reported by a number of Soviet scientific groups, such as Veiko et al.) in the 1970s [26].

Laser-induced oxidation occurs when the metal surface is heated in an O_2-rich environment; this heat is generated as a result of laser-metal interaction. In particular, the absorbed laser energy is converted into collective atomic vibrations (and thus into heat) with the presence of O_2, consequently the reaction occurs [15]. Similar to the formation of the native oxide, the formation of the oxide layer using laser passes through the following consecutive steps [12, 18] as illustrated in Figure 4:

1. Transportation of oxygen to the metal surface.
2. Adsorption of oxygen.
3. Transfer of the free electrons from the surface to the adsorped oxygen.

4. Diffusion of the metal ions through the layer.

5. Formation of new oxide film.

The main difference between the native oxide layer and the one generated using laser is the oxide thickness: a few nanometres for the native oxide, while it can exceed 100 nm with the laser assistance. This is due to the high temperature resulted by the laser-matter interaction, which will increase the rate of reaction as they are directly proportional [18]. The high temperature allows more free electrons and ions to be generated and transported through the oxide film. Furthermore, the high temperature will generate some defects such as vacancies [12] thus resulting in further oxide growth.
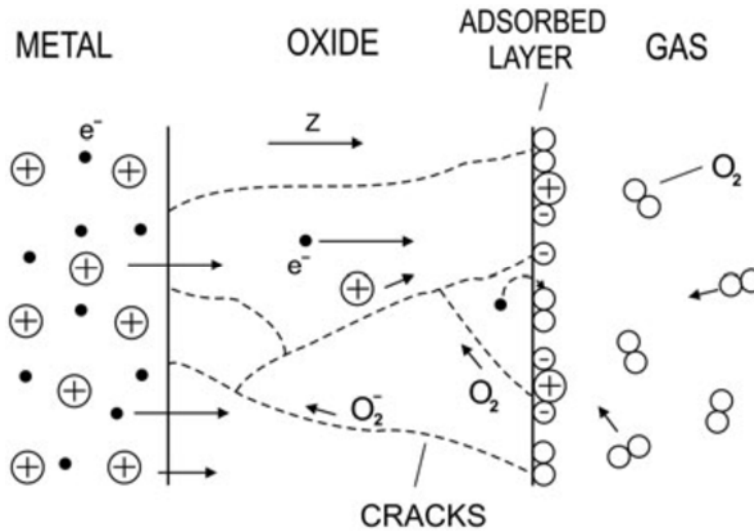
Figure 4 Model for surface oxidation of metals. The metal ions diffuse to the surface to react with oxygen. [12]

The oxidation rate and the oxide thickness are influenced by laser parameters and they differ from one material to another (they might even differ for the same material depending on environmental conditions) [18]. The most effective laser parameters in the oxidation process are the pulse time scale, the laser wavelength, and the fluence [18].

Generally, it has been experimentally shown that the oxide thickness formed by laser-induced oxidation is time scale dependant. For a continuous wave laser, the generated film thickness is 1-10 nm, while it is 10-100 nm and 10 nm for 1 ms and 100 ns pulsed laser, respectively [18].

2.3.1.1 Laser-induced oxidation of titanium

Titanium (Ti) is considered as one of the most important materials in the industry. It was discovered by William Gregor and named by Klaproth after the titans Greek mythology [27, 28]. Although it is the fourth most abundant metal in the crust of the Earth [27], titanium is relatively an expensive material. It has attracted a significant interest due to its chemical and mechanical superior properties. Its unique strength to density ratio, formability, along with its good corrosion, erosion, oxidation, and fatigue resistance make it distinguished among other metals [27].

Titanium can form solid solutions with the majority of the substitutional elements [28]; this increases its ability to be alloyed with other materials achieving extra properties in its alloy form, as a combination of different properties [27]. As a result of these superior properties, there is a wide range of applications for titanium in industry. It has found applications in chemical, general and automobile engineering, as well as in architecture, and even the fashion and jewellery industries; however, the lions share in the use of titanium and its alloys has been in the aerospace and biomedical areas.

The high reactivity of titanium with oxygen at elevated temperatures could be problematic, especially in the production process of titanium, which is one of the reasons behind the high price of titanium, as a special atmosphere (inert gas or vacuum) is required during the production process [29]. However, one of the main advantages of this high reactivity of titanium with oxygen is the superior corrosion resistance that the native oxide layer provides [29]. Increasing the thickness of this native oxide is preferable for some applications.

Similar to the oxidations of metals in general, the oxidation of titanium can be achieved through different methods (e.g., as Sol-Gel, thermal, hydrothermal, solvothermal, anodizing, chemical and physical vapour deposition, laser-induced oxidation) [28, 30-32].

Since its commercial production one century ago, titanium dioxide (TiO_2) has been of considerable interest to both researcher and industrialists due to its unique properties [30]. Titanium dioxide is a semi-conductive material that exists in some crystalline forms, such as rutile, anastasi, and brookite [33]. However, anastasi and rutile are the most famous forms of TiO_2. Its high corrosion resistance, nontoxicity, high chemical stability, biocompatibility, low cost, stable phase, comparable thermal coefficient, and highly oxidation power [33-36] have widened its areas of use. Titanium dioxide is used as a pigment in paints and the food industry [30], as well as in photovoltaic, photocatalytic, photo-electrochromic, optical, sensing and biomedical applications [30, 33].

As mentioned earlier, the oxidation of metals during laser processing is not preferred, especially when super surface finish is required [15]. However, the deliberate generation of a thin oxide film on metallic surfaces using laser is required for many applications. Forming a thin film of titanium oxides on titanium substrate reported in early 1980s, Akimov et al. [37] reported the formation of TiO_2 on Ti substrate using millisecond pulsed laser for the first time

in 1980 [15, 38]. Strakovskii [39] studied the ignition of Ti using CW laser and he studied the effect of the generated titanium oxide on the absorption of the laser and on the ignition of Ti foil. Research investigations of processing titanium with laser for the sake of oxidation have continued until the new era of using the process for colour marking applications.

2.3.2 Laser colour marking

Generally, laser can be used as a marking tool through the generation of marks on different types of materials. The marks could be achieved by removing layers, changing the topography of the surface, modifying the chemical composition, or by a colour centre activation [1].

Laser colour marking is one of the main applications of the laser-induced oxidation of metals. It mainly shown on titanium, tantalum and stainless steel. The generated thin film of the metal oxide on the metal surface appears in different colours depending on the oxide thickness and the optical properties of both the metal and its oxide, based on thin film interference phenomena. Laser colour marking is vital in many aerospace, automotive, medical, optical, and anti-counterfeit applications [3]. Logos, decorative design, product and functional information are mostly imprinted using laser colour marking with high speed and good quality [40] on cables, medical and electronic devices, implants, and surgical instruments [1, 12, 41]. ASTM F983 and F86 standards [42, 43] for the permanent marking of implant components advised that the marking should not affect the mechanical property, corrosion resistance, and implant performance [42, 43], and of course the marking material should be nontoxic. TiO_2, which is the predominant structure of oxide generated on the oxidized Ti substrate [15], fulfils all these requirements as it is nontoxic, biocompatible, and exhibits negligible solubility in most of the solvents [44].

Generating colours using laser for decoration was first reported in 1998 by Carey et al. [45], followed by the first comprehensive study of the use of laser-induced oxidation to colourise the surface by Langlade et al. in 1998 [46]. However, the use of this method for the colour marking application on metallic substrate is reported by Zheng [47-49] in 2000. He produced different colours on stainless steel and titanium just by controlling the laser parameters in a controlled oxygen environment; the colours shown to be durable in various alcoholic, acidic, and alkaline solutions [48]. Zheng et al. [50] showed that the colours depend on the thickness of the generated oxide layer which, in turn, depends on the concentration of the oxygen, laser fluence, and the overlapping of the scanned beam. Rusconi et al. [51] applied the method for decoration and drawing on metallic objects.

Many other researchers have imprinted coloured drawings on metallic surfaces using laser colour marking [52-55]; Figure 5 shows different colour marking on titanium substrate. As it is clear in the figure, the imprinted drawings were limited to high scale drawings such as logos.

Two main strategies are used to mark the items using laser marking, direct scanning or mask [56]. In the first method, the laser beam is moved over the surface of the workpiece. In this case, the path of the beam will be along the required marks. In the second method, a mask containing the features to be marked is placed over the workpiece and one single shot of the unfocused beam interacts with the surface through the mask.

Other marking techniques such as chemical etching, engraving, mechanical stamping, and inkjet are outdone by laser marking. This is due to the advantages of laser over other techniques; these advantages relate to its cleanness, high processing speed, minimal defects,

17

unrequired fixtures, ability to mark complicated surfaces, and suitable for inline use [40, 56].

Table 1 compares laser marking and other marking processes.

Figure 5 Examples of colour laser marking on titanium (plate size: 100*100 mm^2). [54]

Table 1 Advantages of laser marking vs. other marking technologies [57]

Marking process	Speed	Durability	Image flexibility	Contrast
Laser marking	Good	Good	Good	Good
Chemical etch	Good	Good	Poor	Poor
Photo etch	Good	Good	Poor	-
Ink jet	Good	Poor	Good	Moderate
Mechanical stamping	Good	Good	Poor	Poor
Nameplates	N/N	Moderate	Poor	Good
Casting/molding	Good	Good	Poor	Poor
Pneumatic pin	Moderate	Good	Moderate	Poor
Vibratory pencil	Poor	Good	Good	Poor
CO_2 mask marker	Good	Moderate	Poor	Moderate

2.3.3 Thin film interference

Generating colours via laser oxidation has been reported on different materials, such as titanium, stainless steel, tantalum and aluminium; however, the generated colours are different from one material to another. Similar to colours generated by metal anodizing, the colours generated via laser oxidation were attributed to thin film interference phenomena. Although thin film interference of the generated oxide layer using laser was studied by Arzuov et al. [23], they did not study the effect of the phenomena on the appearance of the metal but on the absorption of the incident laser. Zheng et al. [48, 50] attributed the generated colours to the interference effect and they showed that the generated colours depend on the oxide thickness which, in turn, depends on the laser processing parameters.

Interference can be defined as a linear superposition of coherent waves with different phases [58, 59]. In thin films, the light is reflected from and transmitted through the interfaces of the film, as a result they interfere with each other. Since the waves originate from the same source of light, all of these waves are usually coherent [59].

As the generated oxide layer is semi-transparent to the visible light, thin film interference occurs when the film is subjected to white light. Part of the incident waves is reflected from the upper surface of the oxide, while the other part is propagated through the oxide and reflected back from the substrate. These parts of waves may interfere with each other or even with the incident waves. The type of interference (constructive or destructive) is determined by the phases and amplitudes of these waves [59].

The phase of the reflected part is subjected to a phase delay of π as it reflects from a dielectric. While the propagated part is subjected to phase change due to its propagation through the oxide (see Figure 6).

The phase and amplitude of each of the waves reflected from and transmitted through the interfaces of the film are a function of the refractive indices, the thickness of the layers, the number of layers and their order, as well as the light incident angle and its wavelength.

Since the film thickness is less than the coherence length of the wave packet, which is around 1.6λ for white light [60], interference occurs when the amplitudes and the phases of the waves dependent on the thickness of the film. As a result, different thicknesses lead to different colour appearances. The phases and amplitudes of the reflected and transmitted waves at any interface can be calculated using Fresnel coefficient of reflection as below [58, 61].

$$r_{ab} = \frac{n_a \, \cos\theta_a - n_b \, \cos\theta_b}{n_a \, \cos\theta_a + n_b \, \cos\theta_b} \qquad \text{For s-polarization}$$

$$r_{ab} = -\frac{n_a \, \cos\theta_b - n_b \, \cos\theta_a}{n_a \, \cos\theta_b + n_b \, \cos\theta_a} \qquad \text{For p-polarization}$$

Where (a) and (b) are the number of any consecutive layers, n_a and n_b are the refractive indices of these layers, θ_a and θ_b are the angles of incidence and refraction respectively as illustrated in Figure 6.

For a three layers system the total reflection, which is the summation of the partial reflectances from two interfaces, is calculated using the following equation [59, 61].

$$r = \frac{r_{12} + r_{23}e^{i2\delta}}{1 + r_{12}\, r_{23}e^{i2\delta}}$$

where: r_{12}, and r_{23} - the reflection coefficients in any two mediums, i.e. air-TiO_2 and TiO_2-Ti respectively in this research as illustrated in Figure 6 and can be calculated using Fresnel's equations of reflection above. δ - the phase gain per single penetration in TiO_2 film and is

20

equal to $(2\pi \, d/\lambda) \sqrt{n_2{}^2 + \sin^2\theta_2}$ where: d is the TiO₂ film thickness; λ is the wavelength of the incident wave.
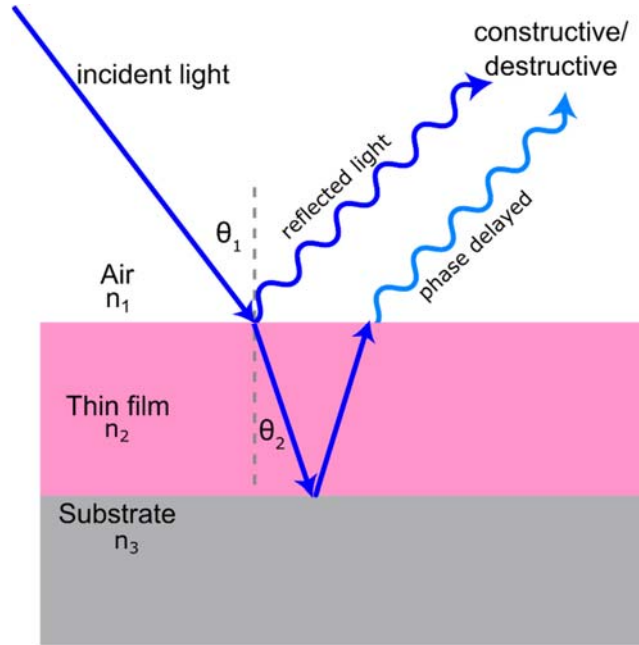
Figure 6 thin film interference phenomenon

Although most researchers agree that the generated colours are a result of light interference, some others argue that some oxides have their own colours by nature, which contributes to the appearance of oxides. The natural colours of the oxides are resulted as the oxides absorb some wavelengths and reflect others. The electrons of the oxides absorb the photons, get excited and promoted to a higher level, then they emit photons with specific wavelengths depending on their energy gap.

Langlade et al. [46] indicated that the resulted violet and blue colours maybe due to Ti₂O₃ and Ti₃O₅, respectively. Lavisse et al. [62] also denied that the observed colours were related to thin film interference as the measured oxide thickness was more than five microns. Perez del Pino et al. [63] supported this opinion as different compositions of oxide were found in

21

different film colours. However, Adams et al. [64] refuted that by arguing that a similar

sequence of colours was generated with vapour deposition of TiO_2 when its thickness

increased within the same range of the one generated with laser. Later Perez del Pino et al.

[36] supported this opinion when they found that the refractive indices and thickness of the

oxide layers were almost the same for the identical colours obtained by laser and anodizing;

they concluded that the colours are a result of a light interference phenomenon in both cases.

Hamadi et al. [65, 66] found that similar colours have different XRD spectrum, thus they

concluded that colours do not correlate to the composition.

The two main factors determining the resulting colours are the thickness and the optical

constants of the oxide film.

2.3.3.1 Thin film thickness

As mentioned above, the thickness of the metal oxide is one of the predominant factors that

contribute to the appearance of the processed area. Therefore, almost all the researchers who

have studied the laser colourising of metal have measured the thickness of the oxide layer of

different colours. Langlade et al. [46] were the first to measure the generated films for

different colours. However, their measurements were in micron scale, as 12, 20, and 100 μm

for yellow, purple, and grey respectively. These measured thicknesses were higher by three

orders from the one obtained later, as Zheng et al. [48, 50] measured the thickness to be tenths

of nanometres. In their first study, Perez del Pino et al. [63] reported the thickness of the film

to be in hundreds of nanometres [63] with high uncertainty, but later they corrected the results

by measuring a maximum thickness of 166 nm for the greenish pink [36]. Later on, most of

the reported oxide thickness was in nanometres scale (up to 120-160 nm for the light blue).

Perez del Pino et al. [36] found that, as the oxide thickness is linear depending on the voltage

in the case of anodization, it is also linearly dependant on the accumulative fluence in the case

22

of laser processing. Skowronski et al. [6, 16] derived an empirical equation between the laser accumulative fluence and the thickness of the film; they agreed that the oxide thickness depends linearly on the fluence.

This huge difference in the measurements of the oxide thickness by different researchers is likely to be due to the fact that the measurements were conducted using different techniques. Firstly, each measurement method has its own error, which is different to another. Secondly, using an optical microscope to measure the cross-section of the processed substrate is not accurate as it is difficult sometimes to differentiate the borders between the oxide layer and the metal. Furthermore, the measured oxide thickness includes all of the different compounds of the metal oxide regardless its optical properties, which is not the case when non-direct optical methods of measurements (such as ellipsometry) are used. A thin film of metal oxide could have different compounds along the depth of the oxide, some transparent and other opaque. Processing titanium substrate, for example, will generate a titanium oxide layer containing both TiO_2 (near the surface) and TiO with Ti_2O (underneath); TiO_2 is a ceramic and it is transparent to the visible light, while both TiO and Ti_2O are opaque as they have a metallic character [64, 67]. Ellipsometry and other non-direct optical methods depend on the reflectivity of the processed substrate for different wavelengths of light. Therefore, the measured thickness represents the transparent layer only.

2.3.3.2 Film composition and its optical properties

After the oxide thickness, the second main property playing a key role in thin film interference is the optical properties of the oxide. In particular, the refractive index affecting the phase delay when the light propagates through the oxide resulted in a wavelength dependant interference (constructive or destructive) that leads to different colour appearance.

In order to determine the optical properties of the generated oxide, the phase and composition of the oxide must be identified.

In general, a number of stable Ti-O phases (such as such as Ti_2O, TiO, Ti_2O_3, Ti_3O_5, and TiO_2) can be generated using laser, as number of researchers reported. However, TiO_2 (rutile) is the most stable and is the main structure of oxide generated on the surface of the oxidized Ti substrate [15]. The composition of the formatted oxide varies with the depth starting from TiO_2 at the top surface towards a lower oxide underneath [38].

Merlin et al. [68] reported that the generated film is mostly TiO_2 along with some Ti_2O_3 and TiO underneath. Similar oxide compositions of the colour film generated by anodizing the titanium substrate were reported [69]. Conversely, Perez del Pino et al. [36] found that the anodizing film is only TiO_2 along the depth, unlike the film generated by laser which is a mixture of several titanium oxides. Perez del Pino et al. [35, 63, 67] state that all the oxide layers, generated by any laser parameters, consist of a thick compact layer of TiO and Ti_2O covered by a thin granulated film of Ti_2O_3 and TiO_2 initiated at higher accumulated fluence. Akman et al. [70] also found that the oxygen concentration decreases by depth and the layer consists of TiO_2, TiO, Ti_2O. Similarly, in the composition obtained by Lavisse et al. [71] using EDS, XPS, SIMS, and Raman spectroscopy, small amounts of carbon and nitrogen were also detected as an indication of the existing of titanium oxy-carbo-nitride. Adams et al. [64] agrees that the generated oxide layer consists of three sublayers of different composition of titanium oxide and they are (from top to bottom) TiO_2, TiO, and TiO_xN. They stress that the middle and the third layer do not affect the appearance as TiO prevent the light to propagate through it, thus these layers should not be counted in the calculation of the interference. The existence of nitrogen in the oxide layers was confirmed by Skowronski et al. [6] as they reported similar oxide phases and compositions. The same group found that the top

layer is not pure TiO_2 as there was some nitrogen as well [16]. However, the nitrogen exists in very low concentration and the layer is transparent as well. Hamadi et al. [65, 66] found that not only rutile is formed on the surface but also other TiO_2 structures (such as anastasi) when higher accumulated fluence is applied.

Lawrence et al. [72] found that the film consists of TiO at the top and Ti_6O underneath, though they do not mention the laser processing parameters of the measured sample nor its colour. This composition could be correct for samples processed with low laser fluence, which corresponded to golden colour. Ageev et al. [73] justifies the differences in the measured compositions of oxides between researchers due to the difficulty in the interpretation of the measured data. They used a theoretical chemical-thermodynamic model to predict the quantitative, qualitative and phase composition of the formed oxide. A layer consisting of TiO_2 at the top, then Ti_2O_3 and TiO underneath was predicted and the result was in agreement with the measured one. A similar model to predict a time dependant temperature diffusion profile with respect to the laser parameters was conducted by Lavisse et al. [62]

Apart of some differences in the compositions of the layers of oxide, almost all the researchers agreed that the top layer is a transparent TiO_2 and the lower layers are low titanium oxides (TiO and Ti_2O). Due to the metallic character of TiO and Ti_2O [64, 67], they have complex refractive indices at the visible wavelengths, which means they are not transparent to the light. This is representative by the imaginary part (k) of their complex refractive indices, which is called the extinction coefficient, as it represents the attenuation of light due to absorption. As a result, these phases exhibit a light absorption [36] opposite to TiO_2, which can be described as transparent material. Therefore, only TiO_2 should be included in the interference calculations since the complex refractive index of TiO [74] at the

visible wavelengths is almost the same as the one of pure titanium [75, 76] in both its real (n) and imaginary (k) parts.

Generally, the refractive index of titanium dioxide is found to be in the range of 2.4-2.8 for the visible range of spectrum [77, 78]. For laser-generated titanium dioxide, Perez del Pino et al. [36] measured the refractive index of the film to be around 2.4; they found that this value is the same for all the generated films of colours unlike the anodized surfaces where the refractive indices vary from 2.1 to 2.3. However, Skowronski et al. and Antonczak et al.[6, 16] use spectroscopic ellipsometry to measure the refractive index of the generated film of oxide and they found that the refractive index is not fixed and it increases as a function of the applied laser fluence. The same group reported the refractive index of the generated film of TiO_2 is in the range of 2.4-2.7 for the visible wavelengths [79, 80]. It is worth mentioning that the refractive index of titanium dioxide in both of its forms (amorphous or crystalline) is almost equal [68].

2.3.3.3 Thin film appearance

A range of colours can be obtained on titanium substrate using laser-induced oxidation. However, the appearance of the oxide film can be slightly affected by factors other than the film thickness and the refractive index, since the colours result from thin film interference phenomena; the appearance of the oxide film can also be affected by the white light intensity as a function of wavelength and the viewing angle.

Few different colours (such as metallic gray, golden yellow, yellow, orange, brown, purple, blue, and light blue) can be differentiated on titanium substrates. Changing the laser parameters will not lead to the production of other colours (such as green) but will produce

different shades of the previously mentioned colours. This has been proven theoretically and

experimentally as shown in Figure 7 and Figure 8, respectively.
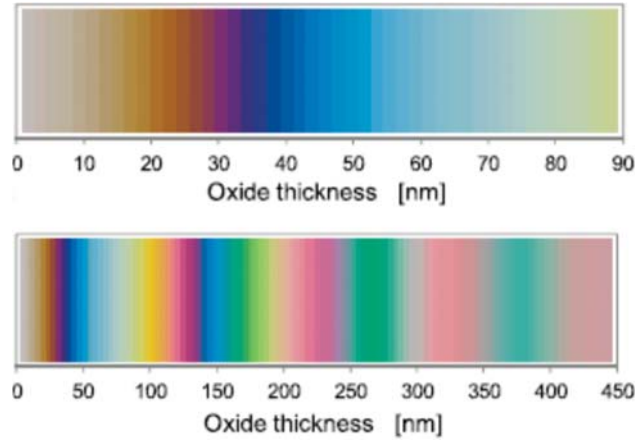
Figure 7 the sequences of colours obtained on titanium substrate as a function of oxide layer
thickness [54]

Different interference models and experimental studies have been conducted by researchers.

Antonczak et al. [54] studied the influence of different laser parameters, such as initial

temperature, focal position, x-y position, power and speed, on the generated colours. They

compared the resulting colours to the one generated by the film interference model and

showed that red and purple are the most sensitive to change in any of the laser parameters,

while gold and blue are less sensitive. Skowronski et al. [79, 80] studied the optical properties

of TiO_2/Ti/glass system, they showed that the obtained sequence of colours, which is relating

to TiO_2 thickness, is similar to the one obtained by laser. In addition, they built interference

models, where they included the roughness of the surface, the native oxide, intermix layers

between the titanium and the titanium dioxide. Veiko et al. [55] introduced an empirical

model to connect the resulting colours to laser parameters using chromaticity coefficients by

the reflectance of the generated film. The fluence caused a specific oxide thickness (and thus

a specific colour) has been proven by Antonczak et al. [16] to be able to be delivered through

two or more stages by reprocessing the surface with lower laser fluence. Veiko et al. [81, 82]

proved that the same range of colours could be generated on the different materials through

depositing a layer of pure titanium and then processing it by laser. They proposed the

technique for jewellery colourisation of silver and gold plates. Lecka et al. [83] applied a

protective layer on the laser generated colours and studied the influence of this layer on the

appearance of the surface using the interference model. It is worth mentioning that the

reproducibility of colours proved to be high, even on small surfaces [84].
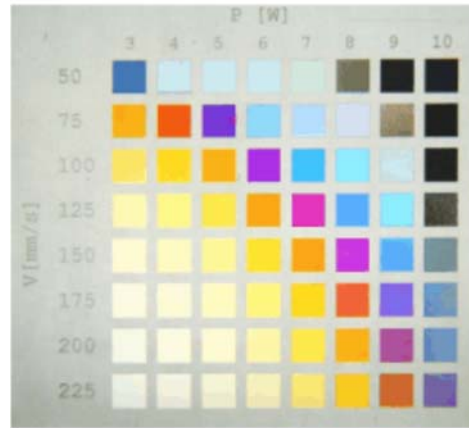
Figure 8 colours resulted from different oxide thicknesses generated using different laser parameters [54]

2.3.4 Layer texture, topography, and cracks

Titanium substrate covered by titanium oxide is an example of a hard film–soft substrate

system [72]. Laser-induced oxidation of metallic substrate is achieved by shallow melting the

substrate using laser fluence below the ablation threshold and close to the melting threshold.

Although the process does not involve any material removal, the topography of the surface is

not smooth sometimes and it suffers from some variation in the surface height (waviness).

This variation, which usually results from the non-uniform distribution of the energy of the

beam or the employed scanning strategy, is generally low but it could reach few microns. In addition to that, the generated film seems to be accompanied by micro cracks as Figure 9 illustrates. These cracks are noticed to exist with different density in almost all films regardless of their colour and thickness. It is believed to be generated due to fast heating/cooling processes with any used laser parameters. The crack formation, their density, and the effect of laser processing parameters has been investigated by number of researchers. Perez del Pino et al.[67] investigated the influence of the scanning speed and the overlapping distance on the morphology of the treated surfaces. They stated that since the TiO_2 is more fragile than titanium and its other oxides, the cracks generate as a result of accumulative tensile stress developed after solidification. Gyorgy et al. [85] studied the topography of the formed film; they noticed that the initial generated micro cracks are converted into droplets, then turn into dome shapes by increasing the number of pulses. The influence of the laser fluence on the morphology was also studied by Lavisse et al. [71, 86] and they found that the roughness and the crack density increase with the fluence. However, they noticed that the very smooth films, which are generated using low laser fluence, still suffer from cracks. Lawrence et al. [72] conducted a study on the influence of laser processing parameters on different surface properties such as the crack formation, hardness, elastic modulus, and the conductivity of the generated film. They found that both the hardness and the elastic modulus of the formed film (which equal to 15 GPa and 200 GPa, respectively) are insensitive to the laser processing parameters. They attributed the formation of the cracks to the residual stresses resulting from the differences in the coefficients of thermal expansion between the film and the substrate. Although they found the cracks existing in all the films (extending through the thickness of the films), they noticed that higher accumulative fluence leads to an increase of the fracture toughness. However, the crack formation and the roughness were

found by Antonczak et al. [16] to be reduced by increasing the accumulative fluence. In terms of the grain size of the cracks, Akman et al. [70] found it directly proportional to the fluence, which is an indication to the low crack formation. They investigated a scratch damage test of the oxide film and they found that the minimum scratch hardness of the treated surface (which increases by increasing the fluence) is double than the one of the substrates. Although there was some delamination of some oxides during the micro-scratch test, they concluded that the titanium oxide film has a good adhesion on the substrate.

Pan et al. [88] investigated the crack growth theoretically and experimentally, and they also found that the high fluence treated surfaces have low cracks which are attributed to the melting happening at high fluence. Similar results were obtained by Espejo et al. [87] as they connected a low crack density film to high laser processing fluence; they also found that the cracks are penetrated few microns in the substrate.

To conclude, the cracks and the waviness can be minimized or terminated by optimizing the laser processing parameters. However, the appearance is not affected by the cracks as they are in micro scale [70].
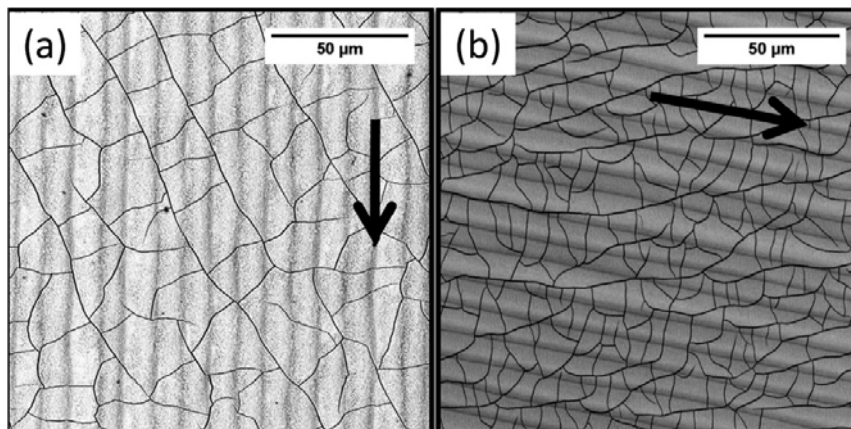
Figure 9 Micro Crack formation on TiO_2 resulted from post-solidification residual stress, along with the scanning direction of the laser path (parallel to the arrows). [87]

2.4 Fresnel zone plates (FZP)

A Diffractive Optical Element (DOE) is a device that divides and redirects the electromagnetic waves, thus modifying the reflected/transmitted wave fronts of the segments by controlling their phases [89]. This can be achieved through three main ways: by selectively varying heights of the device's surface, or its optical properties. The variation follows a specific predesigned pattern on the surface to provide the required optical performance. Fresnel zone plates (FZP's) are one good example of DOE, as they are a flat optical diffractive device whose main functionality is to focus the electromagnetic wave. An FZP consists of a central circle surrounded by a number of annulus zones; the areas of these zones are exactly the same. The geometrical dimensions of an FZP is determined by the functional focal length and the wavelength that it is designed for.

Photolithography is mostly used to fabricate an FZP [90, 91]; the method is based on exposing a photoresist to an ultraviolet light, then developing the photoresist followed by etching [90, 92-94]. However, the process requires a mask that contains the specific profile that wants to be generated. Figure 10 illustrates the photolithographic processing and etching of a DOE. Other fabrication methods of such high accuracy elements are direct writing on the photoresist film (by either laser or electron beam), and then developing and etching the film [95, 96]. The working principles of DOE's, their fabrication methods, and some key issues associated with those are explained in detail in Chapter four.
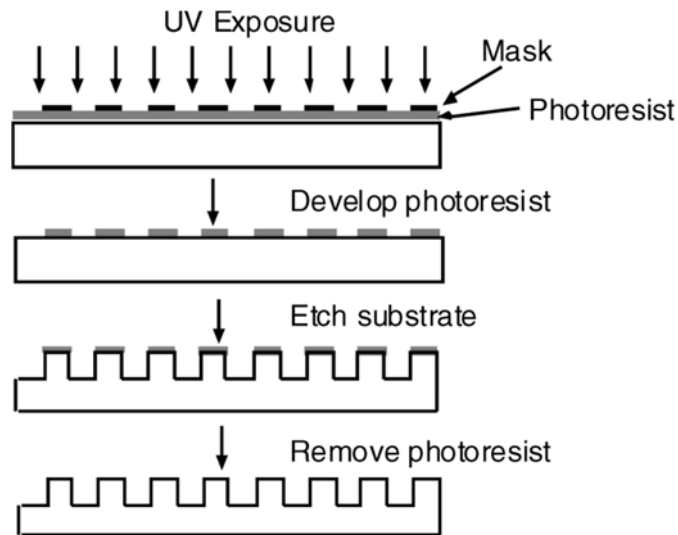
Figure 10 Fabrication of FZP by Photolithography [89]

2.5 Laser-induced oxygen reduction for colour erasing

Laser-induced oxygen reduction is a chemical process of oxygen loss from metal oxides. It is similar in principle but opposite to the oxidation process. It is a reversed process of the oxidation as it is based on extracting the oxygen from the substance rather than gaining it. Heating metal oxides in a low oxygen environment leads to the diffusion of the oxygen out to the atmosphere. The surface temperature should be high enough to melt the oxide to diffuse the oxygen back to the atmosphere as the reduction process is directly proportional to the temperature and to the low oxygen concentration [97].

Heating the substrate can be achieved either in a furnace or by using laser as a local heating source. Processing a material with laser in a low oxygen environment is not a new technique: it is used to eliminate the oxides during the processing of metals, to reduce oxygen from the oxides and to polish metal surfaces [98]. The laser-induced reduction of oxygen was used to alter the electric properties of oxides.

32

Otto et al. [97] treated a number of oxidic perovskites (such as $SrTiO_3$, $BaTiO_3$, and some ceramics) in a reducing atmosphere to locally increase the conductivity of the oxides by several folds of magnitude compared to the neighbouring unprocessed surface. They attributed the change in the conductivity to the vacancies and free electrons resulting from the reduction. They also show that the process is reversible; heating the oxides in a rich oxygen environment leads to a reduction of the conductivity. The same group of researchers conducted similar work on lanthanum-doped lead zirconium titanate (PLZT) ceramics and $YBa_2Cu_3O_7$ [99, 100]. They show that altering the laser power, scanning speed and the H_2 pressure leads to a change in the resistivity by five orders and this was attributed to the metallization of the oxide by reduction. Similarly, Shen et al. [101] conducted a study to locally cause a reversible altering of superconducting films to a semiconductor using laser-induced reduction.

The processing of titanium and titanium oxides in a controlled environment has been reported for different applications. Tsukamoto et al. [102] altered and restored the original conductivity of TiO_2 using femtosecond and CW; they attributed this change to the oxygen deficiency in titanium dioxide that reduced to form lower oxide (TiO) or pure titanium. Nanai et al. [103] processed Ti with laser in a pure nitrogen atmosphere to generate a thin film of TiN and they discovered that by annealing Ti in vacuum, a shiny surface is generated and reprocessing it in vacuum again does not change its structural or optical properties. The processing of titanium in nitrogen [104-106], an oxygen-nitrogen mixture [107], an oxygen-argon mixture [108], and the reprocessing of titanium oxide on titanium substrate to generate a thicker film [16] have also been reported.

As mentioned earlier, the generated colours on titanium surface result from the formation of a transparent thin layer of titanium oxide on the substrate. Employing laser-induced reduction could be a good tool to metalize the surface, thus erasing the colours.

Removing titanium oxides from the substrate is generally difficult to achieve through chemical etching, mechanical abrasion or other methods. This is so because the surface has high mechanical and chemical wear resistance (along with high corrosion resistance) and it is durable in different solutions [48]. This has been proven by Veiko et al. [81, 82] as they found that the film was not affected after they had abraded it for 5 minutes, immersed it in 5% citric acid for 40 minutes, given it an ultrasonic bath for 20 minutes, and soaked it for one hour in 200°C muffle furnace.

Daurelio et al. [109] used laser to remove layers of paint (de-painting), oxides (de-oxidation), rust (de-rusting), and grease, among other substances. It is worth stressing that the method is based on laser cleaning and laser polishing by thermal ablation, as the used fluence is very high and since the controlled environment is not essential.

Laser-induced reduction for erasing colours is totally different from laser polishing and laser cleaning. Laser polishing is a process that superficially melts the surface to improve the surface finish; it sometimes involves the use of inert gases or a vacuum chamber to prevent the oxidation process. On the other hand, laser cleaning is based on one or all of the following three mechanisms: evaporation processing (such as ablation), impact processing (such as shock cleaning), and vibration based processing [1]. To conclude, there are no existing methods of selectively erasing the oxide-based colours without removing the upper layer as in laser cleaning by ablation.

2.6 Laser-induced periodic surface structures

Processing materials with laser using fluence less or close to the ablation threshold of the material leads to formation of subwavelength periodic features called ripples or laser-induced periodic surface structures (LIPSS). It was discovered by Birnbaum [110] in 1965. When he was examining the damage caused by the interaction of ruby laser on different semiconductors, he noticed regular parallel straight lines. He suggested that their formation is a result of the intensity distribution caused by the diffraction effects at the focus of the lens. Since then, LIPSS gained considerable interest due to their multifunctional surface applications and the fact that they represent the smallest features that can be generated by light at the far field [111]. The other important property about LIPSS is that they can be generated on different types of materials (such as polymers, semiconductors, glasses and metals) [7, 112]. Surfaces covered with LIPSS show different surface properties; therefore they found applications in many mechanical and optical fields as they were used to alter the surface functional property, such as wetting properties [113] , tribological properties [114-116], optical properties as in colour marking [117-120], and other applications such as antibacterial and cell growth surfaces [121]. The interest generated by LIPSS has led to a significant growth in the number of publications in the last decade, reaching approximately 80 articles per year [7].

LIPSS periodicity is dependent on the wavelength of the laser as well as the material optical properties. LIPSS have a period of the same order of laser wavelength on metals [120] while it is much smaller on semiconductors and dielectrics ($\lambda/2$ [122] or smaller by one order [123, 124]). From many reported empirical studies, it is evident that the depth of LIPSS is nonlinearly dependent on laser fluence [125], and the value is reported to be between 130-220 nm [126].

The orientation of the LIPSS is directly correlated to the polarization of the laser and it is orthogonal to the electrical field vector of the laser. However, LIPSS parallel to the electrical field vector were also reported, especially on dielectrics [122, 127]. The fact that LIPSS orientation can be controlled has attracted the research community as an extra degree of freedom to modify the surface properties. The state of polarisation is usually controlled using wave plates [128-130] or diffractive optical elements, such as spatial light modulators (SLM) and liquid crystal polarisers [131-135].

The influence of the state of polarization on the laser processing has been reported for different aspects. In the interesting work of Jia et al. [136], they superimposed two pulses that have dissimilar wavelength and perpendicular polarization and they noticed that the orientation of the resulted LIPSS can be controlled by the energy of the lower fluence pulse. Cai et al. [137] generated polarization selective holograms in glass using femtosecond induced nano gratings written with different orientation. Beresna et al. [138] produced polarization dependant diffraction grating by controlling the orientation of the LIPSS. Coloured images based on LIPSS orientations imprinted by Dusser et al. [9] on metallic surface by generating pixels of LIPSS each with different orientation. Later Yao et al. [139] coded two symbols in one field (each written employing LIPSS) with different polarization vector. The symbols appear selectively based on the light incident angle. The work then was extended by Li et al. [118] by coding multiple patterns in one field which can be selectively displayed based on the incident angle. Xu Ji et al. [140] generated cross periodic LIPSS within the same spot, and they showed that the orientation of these cross-periodic structures is polarization dependant. Gregorcic et al. [141] superimposed two trains of pulses that have different vectors of polarization and they show that the orientation of the generated LIPSS depends on the polarization of the last train of pulses and that LIPSS can be overwritten. Lam

et al. [142] were able to control the orientation of LIPSS within the spot itself using SLM by generating spots containing predesigned orientations of LIPSS.

Controlling the state of polarization dynamically during the processing has also been reported. Nolte et al. [129] produced high aspect ratio holes with regular circularity exit by rotating the vector of polarization during the percussion drilling. Same good results but with helical drilling obtained by Fohl et al. [128]. Allegre et al. [131, 143] switched between S- and P-polarization in real time during the helical drilling and sheet metal cutting. Later Jim et al. [132] (from the same group) extended the work to include other states of polarization, radial and azimuthal, using spatial light modulator; they produced LIPSS related to the four states of polarization in real time. Graf et al. [144] dynamically rotated the polarization while scanning a line of LIPSS and they showed that higher rotation speed of the vector of polarization generates disordered structures similar to those obtained by circular polarization [144].

2.7 Summary

Although laser colour marking by oxidation of metallic surface has outdone other methods, there are several key issues related to this method. The colourising process is based on two laser strategies, either by scanning or by using masks. The former is limited by the relative large processing area (millimetre scale), while the latter is limited by the relatively long processing time to produce specific marks with high resolution. Therefore, a method is required to increase the resolution of the processed area to control the oxide film thickness in the minimum possible size, which is the beam size. The method is applicable on only few metals such as titanium and tantalum, which are relatively expensive. This has limited the applications of the method. The literature review revealed an additional limitation that there are no available erasing and rewriting methods rather than ablating the coloured surfaces. Having the ability to achieve that selectively, applicability of the method on different materials, and

37

the selectively erasing of colours could open the door for many other potential applications rather than only colour marking.

CHAPTER 3:

LASER INDUCED SINGLE SPOT OXIDATION OF TITANIUM

Authors Contributions

This chapter of the alternative thesis format is published in the journal of Applied Surface Science. I am the first author of this publication. The paper's detail and contributions of co-authors are outlined below.

Jwad, T.[1], Deng, S.[2], Butt, H.[*], & Dimov, S[**]. (2016) Laser induced single spot oxidation of titanium, Applied Surface Science, 387, 617-624.

[1] **Tahseen Jwad**: is the main author and he conceived the ideas of single spot oxidation method, designed the experiments, performed all necessary characterization, data analysis and process modelling/simulation work, and wrote the manuscript that was reviewed by the principal supervisor, **Prof. S. Dimov** ([**]), and the co-supervisor, **Dr. H. Butt** ([*]).

[2]Sunan Deng: contributed to the reflectance measurements.

CHAPTER 3: LASER INDUCED SINGLE SPOT OXIDATION OF TITANIUM

Abstract

Titanium oxides have a wide range of applications in industry, and they can be formed on pure titanium using different methods. Laser-induced oxidation is one of the most reliable methods due to its controllability and selectivity. Colour marking is one of the main applications of the oxidation process. However, the colourizing process based on laser scanning strategies is limited by the relatively large processing area in comparison to the beam size. Single spot oxidation of titanium substrates is proposed in this research in order to increase the oxidation resolution in the processed area and also to address the requirements of potential new applications. The method is applied to produce oxide films with different thicknesses and hence colours on titanium substrates. High resolution colour image is imprinted on a sheet of pure titanium by converting its pixels' colours into laser parameter settings. Optical and morphological periodic surface structures are also produced by an array of oxide spots and then analysed. Two colours have been coded into one field and the dependencies of the reflected colours on incident and azimuthal angles of the light are discussed. The findings are of interest to a range of application areas, as they can be used to imprint optical devices such as diffusers and Fresnel lenses on metallic surfaces as well as for colour marking.

Keywords: Laser-induced colorizing, titanium oxide, single spot oxidation, color patterning, color coding.

1. Introduction

Titanium (Ti) oxides have received considerable attention by the research community and industry in the last two decades due to their attractive optical and surface properties [1, 2]. In particular, their corrosion resistance, wear resistance, anti-galling properties, biological properties, high strength to weight ratio, good fatigue strength and aesthetic properties (permanent colours) [3], together with Ti mechanical properties [4] are very attractive for a wide range of applications, e.g. photocatalysis, gas sensing, medical implants, optical coatings [5], aerospace and parts identification [3].

Literature review shows that Ti oxide films can be generated by different methods such as heat treatment, immersion in hydrogen peroxide solutions, dipping in rutile and gelatine [6], passivation and anodizing [3]. Although some of these methods are similar and require an immersion of Ti samples into a chemical bath and then to apply DC power, the resulting thickness of the oxide films vary. Another important limitation is that the majority of these treatment methods are nonselective and the resulting oxide thickness is not totally controllable. In addition, high power and wet chemical bath are required, that make them hazardous processes [4].

It is therefore not surprising that oxidation of metals through laser processing is becoming attractive for applications requiring selectivity and high precision [7]. In particular, laser-induced oxidation can offer the following advantages over the other methods:

- Oxidation of pixels/spots with a resolution down to laser wavelength [8];
- High precision spatial-temporal control;
- Less processing time for relatively small processing areas;
- High repeatability.

Laser-induced colouring of metals can be achieved not only by creating thin films of oxide but also by generating laser-induced periodic surface structures (LIPSS). In particular, different colours were obtained on a range of materials by producing LIPSS employing lasers with pulse durations shorter than the electron-phonon relaxation time (one to tens of picoseconds [9]). LIPSS represents ripples that are usually perpendicular to the laser polarization and diffract light in different colours in the visible range depending on its incident angle. Such periodic surface structures find applications in optical coding [10] and image imprinting [11] and can be generated on a variety of materials such as metals [12-14] and semiconductors [15-17]. In this research only the laser-induced colouring of metals by forming a thin metal oxide layer with nanosecond pulse lasers is studied.

Laser-induced oxidation of different metals has been investigated by many research groups [18] in particular laser-induced colouring of Ti substrates, i.e. the composition and mechanism of laser-induced Ti oxides [5, 19, 20], the structures of Ti oxide films [2, 7], laser-induced colouring versus anodizing [4], and the dependence of colours on laser processing parameters [1, 20-22]. Applications of laser-induced oxidation of metals with its related colouring effects have been considered in jewellery and part identification [23-25]. However, the colourization process reported in the literature was carried out by laser scanning over a relatively large area as compared to the beam spot size. This has limited the applications of the process since the smallest fields of colours that can be produced are in millimetres scale. A comprehensive study of other potential applications has therefore not been carried out, apart from colour marking. The objective of this research is to develop a method to control the size of the oxidation area and its thickness on titanium substrates by laser-induced single spot oxidation and thus to imprint coloured image. By applying this approach the aim is to achieve a pixel resolution down to the beam spot size with high spatial control in the processed area.

2.   Experimental setup

A nanosecond (redENERGY G4 50W) laser from SPI Lasers is used in this research. With wavelength of 1064 nm and a 1 MHz maximum pulse repetition rate, it can be used for laser processing with 25 different pulse durations, from 15 to 220 ns. The beam delivery system used in this experimental study is shown in Figure 1. The 3D scanner (RhoThor RTA) from Newson Engineering can realise scanning speeds of up to 2.5 m/s and the spot size can be controlled down to a few microns in the focal plane with the integrated beam expander and 100 mm telecentric focusing lens. The beam delivery setup is mounted on a mechanical z stage, while the workpiece is horizontally mounted on a high precision stack-up of four mechanical stages (two rotary and two linear Aerotech stages). The beam quality (M^2), which represents the degree of variation of a beam from an ideal Gaussian beam, is better than 1.3. It means that the waist diameter is 30% larger than the ideal Gaussian beam (the beam being 1.3 times diffraction limited). The output energy is controlled by an energy attenuator and monitored by an inline power meter. Commercially pure (Grade 1) titanium substrates with a 0.7 mm thickness were used in all the experiments in a temperature-controlled environment (25 °C). Prior to laser processing, the samples were cleaned ultrasonically for 10 minutes in water and 10 minutes in acetone and dried with hot air. Alicona G5 Infinite Focus (IF) system is used to inspect the morphology of the processed Ti substrates, while the reflectivity measurements along the entire visible spectrum of wavelengths were performed using Ocean Optics USB2000+ Spectrometer with tungsten-filament lighting (CIE illuminant A) and Carl Zeiss Scope A1 optical microscope.
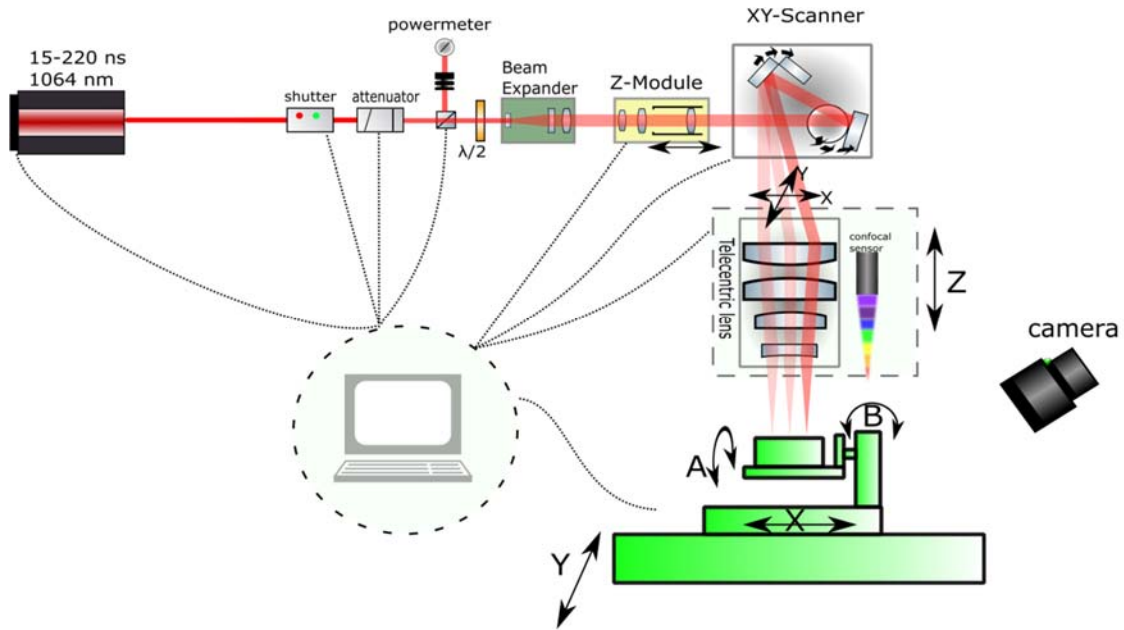
Fig. 1. Laser platform setup

3. Single spot oxidation method

A single spot oxidation method is proposed in this research for a higher resolution than that achievable by applying raster scanning strategies. In addition, by applying this method different topographies can be created on the surface and thus the reflected colours to dependent on the incident and azimuthal angles. Thus, the objective is to achieve a higher resolution down to the beam spot size with high spatial control in the processed area together with an angular dependence of the colours due diffraction effects.

A single spot of oxide is created on the substrate by a pre-defined number of pulses (a pulse-train processing) that have fluence below the ablation threshold of titanium. Then, the beam is re-positioned and the next pulse-train is delivered on the substrate and this is repeated until the area that has to be processed is fully covered. In this single spot oxidation method the colour coding is carried out by controlling the number of pulses and fluence, especially the cumulative fluence resulting from each pulse-train.

Initially, arrays of oxide fields were produced on a titanium substrate by applying the proposed single spot oxidation method. Each array included 10 x 10 square fields (2 mm x 2 mm each)

and each square contains (66 by 66) oxidation spots. For producing these arrays, the power is varied from 1% to 100% of the average power (50 W). The distances between any two successive spots in both X and Y directions were fixed at 30 μm while the beam spot size was 80 μm. Thus, the spots overlap. The pulse repetition rate was set to be either 1 MHz or 500 kHz, while the duration time of the pulse-trains was varied from 50 to 214 μs and thus to have trains with different number of pulses, i.e. from approximately 50 to 214 pulses per spot.

A range of colours were generated with the proposed method, i.e. silver, golden, violet, orange, blue, and light blue and their variations, that are the same as those reported in the literature which achieved by employing the raster scanning strategy. From the produced initial arrays of oxide fields, 15 fields of colours were selected to produce 6 x 6 mm fields for further analysis. They were selected to cover a wide range of cumulative fluences and colours but at the same time to minimise the time necessary to carry out the analysis. In particular, Figure 2 depicts these 15 colours, while their laser processing parameters are presented in Table 1. Again, the distances between the spots in both X and Y directions were fixed at 30 μm while the effective spot size is varying from 40 to 80 μm depending on the fluence. The spots' overlaps can be clearly seen in Figure 2.
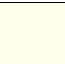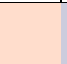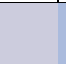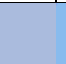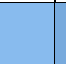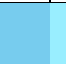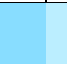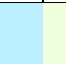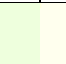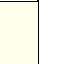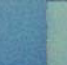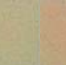
Figure 3 shows the dependency between the generated colours and cumulative fluence, Cumulative fluence is defined as the average fluence multiplied by the number of pulses and can be calculated as follows [20].

$$F = EN/A = P_{avg}N/AV \tag{1}$$

where: F is cumulative fluence, E - the pulse energy, N - the number of pulses, A - the beam spot area, P_{avg}-the average power, and V-the pulse repetition rate.

Three zones are identified in Figure 3 based on the cumulative fluence levels. In Zone A no colours can be generated because the pulse energy is too low and fluence is below the oxidation threshold ($\simeq 0.19$ J/cm^2) while in Zone C the ablation threshold is exceeded. The oxidation conditions are satisfied in Zone B, especially the cumulative fluence is below $\simeq$ 210 J/cm^2, and thus the colours are changing with the decrease of the cumulative fluence.

Table 1 Laser processing parameters, the L*a*b* values, RBG images, and pictures of 15 colours produced by single spot oxidation (sorted by their cumulative fluence)

sample	1	2	4	7	3	5	6	8	12	11	10	15	9	14	13
RGB image															
photo															
L*	97.49	94.27	91.17	87.61	89.77	79.15	73.02	68.92	67.77	73.19	84.32	80.07	90.2	95.43	97.37
a*	1.916	2.166	5.697	8.699	7.199	2.932	-2.43	-11.3	-13.34	-19.48	-22.21	-20.5	-19.08	-8.199	-4.121
b*	6.567	26.77	21.15	9.128	12	-8.210	-16.34	-30.5	-30.28	-28.28	-22.86	-22.7	-11.85	8.849	12.08
PRR (MHz)	1	1	0.5	1	0.5	0.5	0.5	1	1	1	1	0.5	1	1	1
N	50	50	50	75	50	50	50	100	150	150	150	75	150	214	214
BT(µs)	50	50	100	75	100	100	100	100	150	150	150	150	150	214	214
F (J/cm2)	32.13	46.96	64.26	70.44	74.15	84.04	93.93	98.87	103.8	118.6	133.4	140.8	148.3	180.1	203.4

Note: L*a*b* is CIELAB colour space; PRR - pulse repetition rate; N - number of pulses, BT - burst time, F - cumulative fluence

4. Results and discussion

In this section the results obtained by applying the single spot oxidation method are presented together with its potential applications.
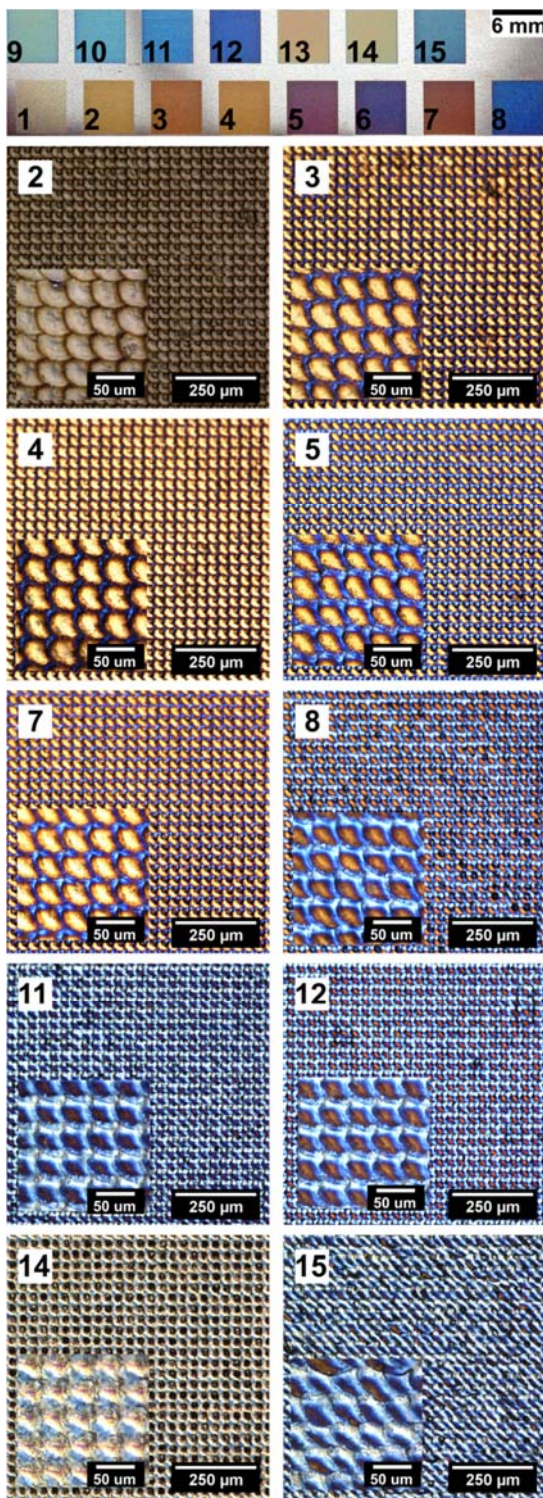
Fig. 2. Selected colours generated by single spot oxidation

Fig. 3. Dependency of the generated colours on the cumulative fluence

4.1 Colours parameters

The average three measurements of reflectance spectra of samples 2-15 are shown in Figure 4. They are clustered under three groups based on their cumulative fluence, i.e. 64-93, 98-148, and 180-203 J/cm^2, and their reflectance spectra are shown in Figure 4 (a), (b), and (c),

respectively while one reflectance curve from each group is given in Figure 4(d) to compare them.
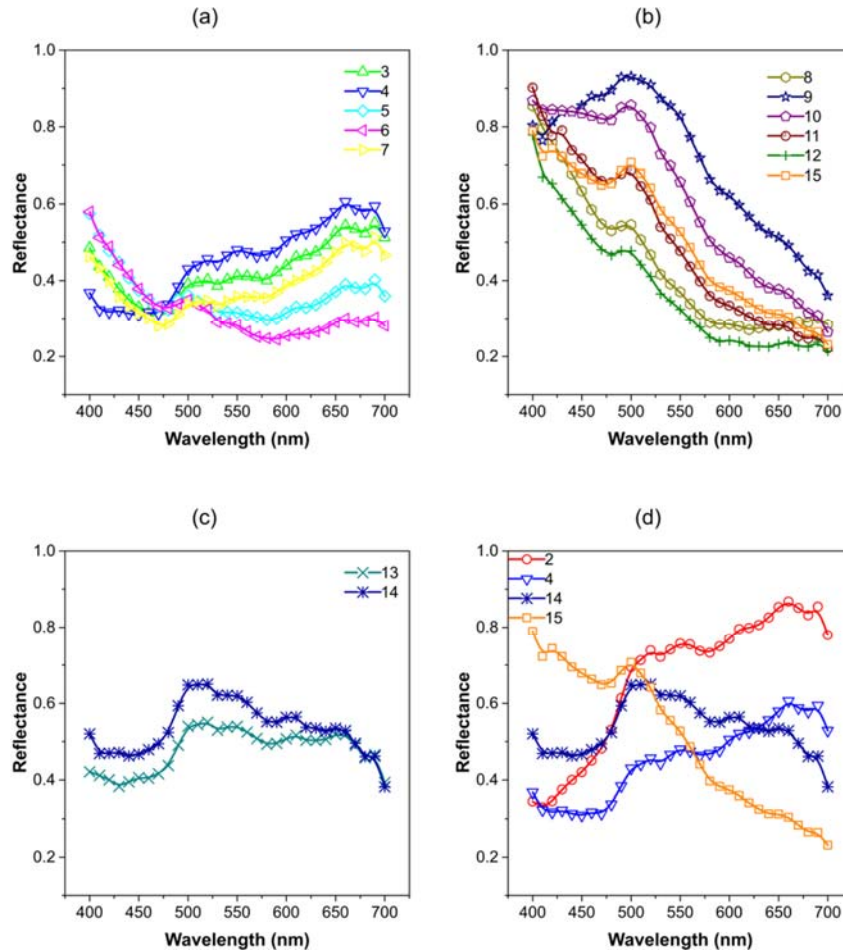
Fig. 4. Reflectance spectra of sample 2-15. For samples processed with cumulative fluence 64-93 (a), 98-148 (b) and 180-203 (c) J/cm^2, while (d) combines the reflectance results obtained with the three fluence ranges..

The Tristimulus values X, Y, and Z, which represent the amounts of the three primary colours, were calculated with Equations 2 to 4 by compensating the values of the colour matching functions ($\bar{x}$, $\bar{y}$, and $\bar{z}$), the illuminate spectral power distribution (S) and the measured reflectance data along the visible wavelength (360-830 nm) based on CIE 1931 [26].Then, the chromaticity coordinates x and y are calculated for each sample and then

projected on the CIE1931 two dimensional chromaticity diagram as depicted in Figure 5.

$$X = k \sum_{\lambda} R(\lambda)\, S(\lambda)\, \bar{x}(\lambda)\, \Delta\lambda \tag{2}$$

$$Y = k \sum_{\lambda} R(\lambda)\, S(\lambda)\, \bar{y}(\lambda)\, \Delta\lambda \tag{3}$$

$$Z = k \sum_{\lambda} R(\lambda)\, S(\lambda)\, \bar{z}(\lambda)\, \Delta\lambda \tag{4}$$

$$k = 100 / \sum_{\lambda} S(\lambda)\, \bar{y}(\lambda)\, \Delta\lambda \tag{5}$$

Where:

$R(\lambda)$ Is the reflectance factor,

$S(\lambda)$ - The relative spectral power of a CIE standard illuminant,

$\bar{x}(\lambda)$, $\bar{y}(\lambda)$, and $\bar{z}(\lambda)$ - The colour-matching functions of the CIE standard observers, and

k - The normalising constant
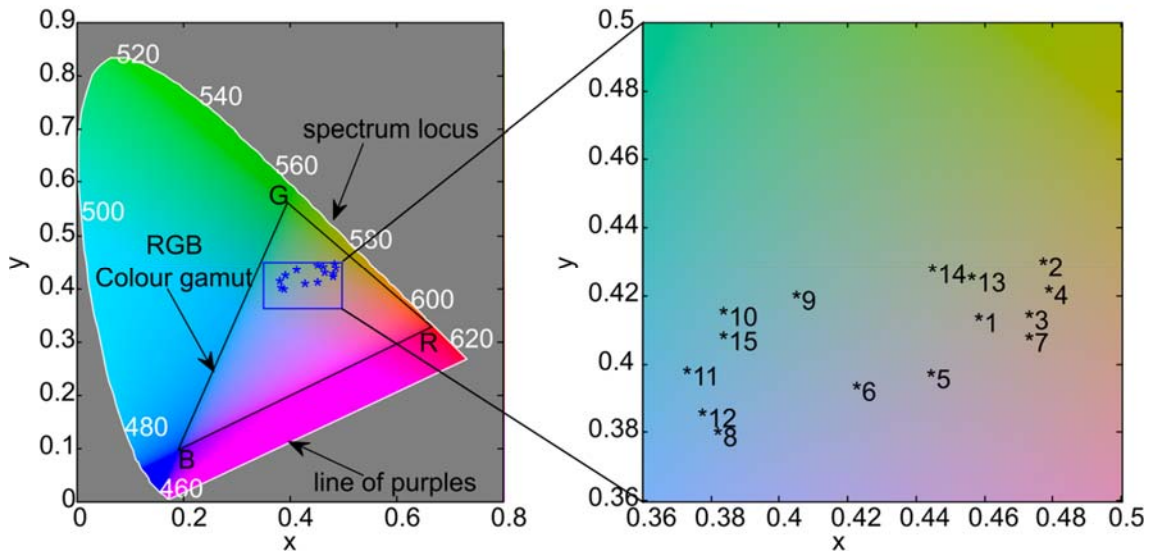
Fig. 5. The chromaticity of 15 samples projected over the CIE 1931 x-y colour space with CIE Illuminant A at Y-tristimulus value of 39 that is the average of Y for the 15 samples).

Note: Y is equal 100 for perfect white surface.

Although CIE1931 and its x-y chromaticity diagram have been used widely in colour industry, their representation in terms of the visual perception is non-uniform. Especially, equal distances in the x-y diagram does not represent an equal magnitude of change in colours [27]. Therefore, the Tristimulus values are converted into L*a*b* and thus to show the colour difference because CIELAB (L*a*b* colour space in CIE 1976) is a uniform colour space and it is recommended when differences in colours have to be represented [28]. The values of L*a*b*, their representations as RGB images, and the photos of all 15 samples are shown in Table 1, where they are ordered by their cumulative fluence.

4.2 Images imprinting

A selective oxidation was performed in order to control the oxide thickness of each spot on a Ti substrate. In particular, the single spot oxidation was used to produce pixels of thin oxide films. The films thicknesses and hence the colours are a function of beam spot size, burst time, pulse repetition rate and pulse energy. To assess the process capabilities and limitations, an image was imprinted on a titanium substrate. Each pixel of this image was produced with different laser settings, i.e. pulse energy, and thus the oxide thickness was varied. A programme was created in MATLAB to generate laser executable commands to carry out this selective oxidation process. In particular, the programme converts images into executable commands for the laser system. These commands contained the laser parameter settings for each pixel, i.e. power, pulse repetition rate, pulse-train time, and X & Y positions that were set based on the image greyscale map. The pixels were dots with a diameter equal to the beam spot size and thus a high resolution image was imprinted by varying the laser settings. The number of pixels per inch (PPI) can be varied and can go up to 25400/$\mathbf{d}$, where $\mathbf{d}$ is the beam diameter (μm) at the intersection plane with the workpiece. Ultimately, $\mathbf{d}$ can be reduced down to the laser

wavelength with the use of high quality focusing lens that has maximum Numerical Aperture (NA). Numerical aperture depends on the diameter of the focusing optic, its radius of curvature and the lens material. It is equal to $(n \sin \theta)$, where n is the refractive index of the lens and θ is the divergence of the focused beam (the angle between outer distance of the focused beam in the far-field and the beam axis) [29].

To create oxidation patterns on the substrate, two processing strategies were used. The first one was by irradiating the pixels one by one along each row and each column while the second one was a layer-based strategy where the pixels were clustered into one hundred groups (layers) based on their 8-bit representation in the grayscale image. In particular, the 8-bit greyscale image was scaled down from 0-255 to 1-100, where 1 to 100 corresponded to the used average power in percentages, while the pulse repetition rate and train time were kept the same in this experiment at 1 MHz and 0.4 ms, respectively (400 pulses per train). Thus, each layer was produced with different pulse energy and contained all pixels associated with a given group. To imprint an image on a substrate all the layers have to be irradiated one by one.

A 300 by 300 pixels' image of the Mona Liza was used to carry out imprinting trials figure 6 (f). The image was converted into 300 by 300 spots and the laser power for each of them was set from 1 to 100% depending on the pixel's 8-bit code. The beam diameter was selected to be 80 μm. Thus, the imprinting resolution (pixel density) achieved was 317 PPI while the overall size of the picture was 24 by 24 mm². The laser processing time for this image was more than 150 minutes when the first strategy (pixel by pixel processing) was applied. In this case most of the processing time was spent on executing a sequence of 300 by 300 pulse-trains with varying laser processing settings for each pixel. When the layer-based strategy was applied with the same laser settings the processing time was reduced more than seven times, down to less than 20 minutes. However, although the processing time was reduced, the imprinted picture

was distorted in some areas. These errors were due to the beam deflectors' dynamics effects when applying the layer-based approach that could be minimised by introducing machine-specific compensations in executing machining vectors [30]. Figure 6 (a-e) shows the image produced with the layer-based strategy on a titanium substrate when the built-in software tool for counteracting the dynamic effects was applied.
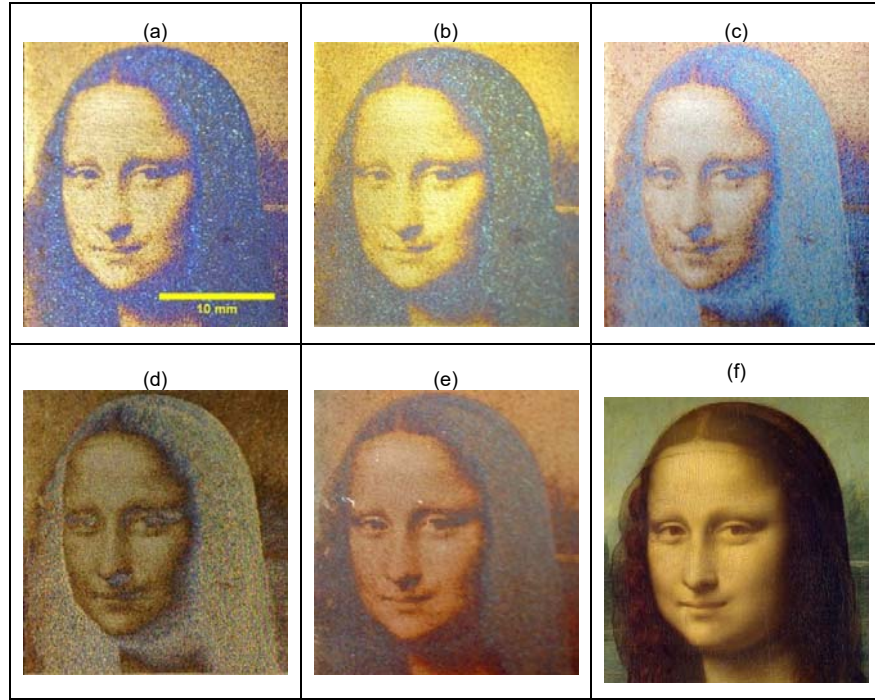
Fig. 6. Imprinted image shown in different incident and azimuthal angles. (a) Both normal, (b) different incident, (c –e) different azimuthal angles, while (f) is the original image.

This method of imprinting images with permanent colours on Ti substrate can be applied on other types of metals if their oxides have similar properties to Ti oxide such as niobium, tantalum, and chrome, or even on steel. Images in grey scale can be produced by applying this strategy on other types of materials, but then the imprinting mechanism is different. In particular, no oxidation spots are formed but craters are created by applying pulse energies with fluence higher than the ablation threshold. Craters with different depths can be generated by varying the pulse energy and thus to imprint images with different contrast.

4.3 The angular dependence of the reflected colours

The fields formed by spots of oxides (see Figure 2) reflect different colours when the viewing angle and/or the light incident angle are changed. Inspecting these arrays of single oxidation spots unveiled optical and topographical periodic surface structures because the spots forming them have different profiles/depths, due to the varying oxides' thickness, the beam Gaussian energy distribution and also the spots overlap. All these result in texturing effects on the surface as shown in Figure 2. These periodic surface structures can explain the different colours observed by varying the incident and azimuthal angles. The profile of these structures along a 150 µm line of fields 2 and 14 obtained with Alicona G5 system (FV) with 100x objective is given in Figure 7. The periodicity of these structures (peak to peak) is around 32 µm for all inspected samples and this reflects the used constant distance between any two successive spots in applying the proposed single spot oxidation method. At the same time the
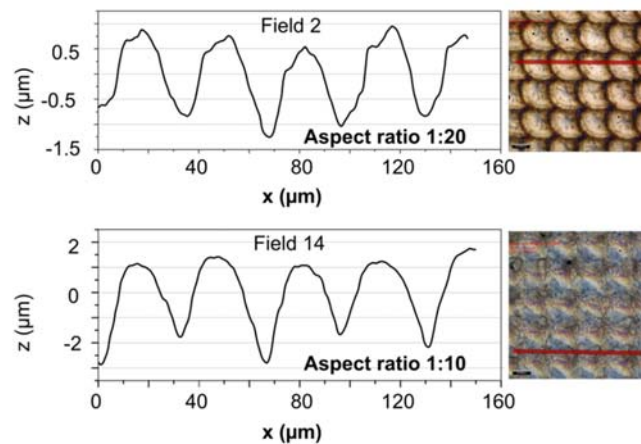
Fig. 7. The profiles of the periodic structures for Fields 2 and 14 in Figure 2, respectively

average amplitude between peaks and valleys is 1.1 to 4.3 µm for these two fields, respectively, that is in line with the different cumulative fluence, 46.96 and 180.1 J/cm^2, used for producing them.

As it was the case with the colours of single spot oxidation arrays, the reflected colours of the imprinted image are dependent on the incident and azimuthal angles, too. In particular, the hair colour of the imprinted image appears blue and black, golden, or light blue depending on the incident and azimuthal angles as shown Figure 6 (a-e). However, the difference here is that the respective area of the imprinted images contains hundreds of spots that were generated using different laser parameter settings and thus resulted in different oxides' topographies and colours. The colours originate from the thin film interference effect produced by the oxide layer while their angular dependence is due to the profile of the craters. As white light is projected on the oxide film in different incident angles due to the craters' profile, the interference is affected and leads to this angular dependency.
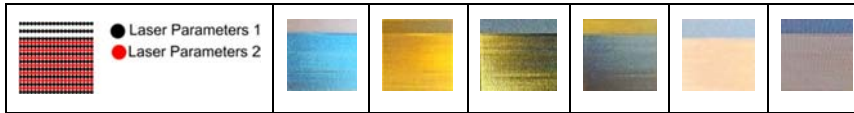
Fig. 8. One field coded with two colours using two different laser parameter settings, captured with different incident and azimuthal angles

To demonstrate potential applications of this angular dependency, two laser parameters were chosen to process a field of 10 mm by 10 mm on a Ti substrate. Single oxidation spots were generated on the substrate by using two different laser parameter settings for the odd and even lines of a field as shown in Figure 8. Note that 20% of the even rows (upper part of the field) have not been processed for the sake of comparison. This phenomena is of interest as it can be used for producing colour coded and colour dependent optical devices on metallic surfaces, such as flat Fresnel lenses, optical diffusers and holograms [31].

5. Conclusions

A method for single spot oxidation is proposed for colourizing/patterning titanium substrates. Different controllable colours were produced on the Ti substrate by generating arrays of single spot oxide films. High resolution images were imprinted to assess the capabilities and also to judge better about potential applications of the proposed method. The fields produced with arrays of single spot oxidations showed an angular dependence of the colours due diffraction effects. This was due to periodic topographies generated with the single spot processing strategy. The findings reported in this paper are of interest to a range of application areas, as they can be used to imprint optical devices such as diffusers and Fresnel lenses on metallic surfaces. Also, images with permanent colours can be imprinted on Ti or other substrates with a resolution up to $25400/\mathbf{d}$.

References

1. Skowronski, L., A.J. Antonczak, M. Trzcinski, L. Lazarek, T. Hiller, A. Bukaluk, and A.A. Wronkowska, *Optical properties of laser induced oxynitride films on titanium.* Applied Surface Science, 2014. **304**: p. 107-114.

2. Antonczak, A.J., L. Skowronski, M. Trzcinski, V.V. Kinzhybalo, L.K. Lazarek, and K.M. Abramski, *Laser-induced oxidation of titanium substrate: Analysis of the physicochemical structure of the surface and sub-surface layers.* Applied Surface Science, 2015. **325**: p. 217-226.

3. Puippe, J.C., *Surface treatments of titanium implants.* European Cells and Materials, 2003. **5**(1): p. 32-33.

4. del Pino, A.P., J.M. Fernandez-Pradas, P. Serra, and J.L. Morenza, *Coloring of titanium through laser oxidation: comparative study with anodizing.* Surface & Coatings Technology, 2004. **187**(1): p. 106-112.

5. del Pino, A.P., P. Serra, and J.L. Morenza, *Oxidation of titanium through Nd : YAG laser irradiation.* Applied Surface Science, 2002. **197**: p. 887-890.

6. Rohanizadeh, R., M. Al-Sadeq, and R.Z. LeGeros, *Preparation of different forms of titanium oxide on titanium surface: Effects on apatite deposition.* Journal of Biomedical Materials Research Part A, 2004. **71A**(2): p. 343-352.

7. Gyorgy, E., A.P. del Pino, P. Serra, and J.L. Morenza, *Structure formation on titanium during oxidation induced by cumulative pulsed Nd : YAG laser irradiation.* Applied Physics a-Materials Science & Processing, 2004. **78**(5): p. 765-770.

8. Boyd, I.W., *Laser processing of thin films and microstructures : oxidation, deposition, and etching of insulators*. Springer series in materials science. 1987, Berlin ; New York: Springer-Verlag. viii, 320 p.

9. Breitling, D., A. Ruf, and F. Dausinger, *Fundamental aspects in machining of metals with short and ultrashort laser pulses.* Photon Processing in Microelectronics and Photonics Iii, 2004. **5339**: p. 49-63.

10. Yao, J.W., C.Y. Zhang, H.Y. Liu, Q.F. Dai, L.J. Wu, S. Lan, A.V. Gopal, V.A. Trofimov, and T.M. Lysak, *Selective appearance of several laser-induced periodic surface structure patterns on a metal surface using structural colors produced by femtosecond laser pulses.* Applied Surface Science, 2012. **258**(19): p. 7625-7632.

11. Dusser, B., Z. Sagan, H. Soder, N. Faure, J.P. Colombier, M. Jourlin, and E. Audouard, *Controlled nanostructrures formation by ultra fast laser pulses for color marking.* Optics Express, 2010. **18**(3): p. 2913-2924.

12. Vorobyev, A.Y. and C.L. Guoa, *Colorizing metals with femtosecond laser pulses.* Applied Physics Letters, 2008. **92**(4).

13. Fan, P.X., M.L. Zhong, L. Li, P. Schmitz, C. Lin, J.Y. Long, and H.J. Zhang, *Angle-independent colorization of copper surfaces by simultaneous generation of picosecond-laser-induced nanostructures and redeposited nanoparticles.* Journal of Applied Physics, 2014. **115**(12).

14. de la Cruz, A.R., R. Lahoz, J. Siegel, G.F. de la Fuente, and J. Solis, *High speed inscription of uniform, large-area laser-induced periodic surface structures in Cr films using a high repetition rate fs laser.* Optics Letters, 2014. **39**(8): p. 2491-2494.

15. Zhang, C.Y., J.W. Yao, H.Y. Liu, Q.F. Dai, L.J. Wu, S. Lan, V.A. Trofimov, and T.M. Lysak, *Colorizing silicon surface with regular nanohole arrays induced by femtosecond laser pulses.* Optics Letters, 2012. **37**(6): p. 1106-1108.

16. Ionin, A.A., S.I. Kudryashov, S.V. Makarov, L.V. Seleznev, D.V. Sinitsyn, E.V. Golosov, O.A. Golosova, Y.R. Kolobov, and A.E. Ligachev, *Femtosecond laser color marking of metal and semiconductor surfaces.* Applied Physics a-Materials Science & Processing, 2012. **107**(2): p. 301-305.

17. Yang, H.D., X.H. Li, G.Q. Li, C. Wen, R. Qiu, W.H. Huang, and J.B. Wang, *Formation of colorized silicon by femtosecond laser pulses in different background gases.* Applied Physics a-Materials Science & Processing, 2011. **104**(2): p. 749-753.

18. Nanai, L., R. Vajtai, and T.F. George, *Laser-induced oxidation of metals: State of the art.* Thin Solid Films, 1997. **298**(1-2): p. 160-164.

19. del Pino, A.P., P. Serra, and J.L. Morenza, *Coloring of titanium by pulsed laser processing in air.* Thin Solid Films, 2002. **415**(1-2): p. 201-205.

20. Adams, D.P., R.D. Murphy, D.J. Saiz, D.A. Hirschfeld, M.A. Rodriguez, P.G. Kotula, and B.H. Jared, *Nanosecond pulsed laser irradiation of titanium: Oxide growth and effects on underlying metal.* Surface & Coatings Technology, 2014. **248**: p. 38-45.

21. Veiko, V., G. Odintsova, E. Ageev, Y. Karlagina, A. Loginov, A. Skuratova, and E. Gorbunova, *Controlled oxide films formation by nanosecond laser pulses for color marking.* Optics Express, 2014. **22**(20): p. 24342-24347.

22. Antonczak, A.J., B. Stepak, P.E. Koziol, and K.M. Abramski, *The influence of process parameters on the laser-induced coloring of titanium.* Applied Physics a-Materials Science & Processing, 2014. **115**(3): p. 1003-1013.

23. Rusconi, R. and J. Gold, *Color marking-High-contrast and decorative effects can be achieved in color on plastics and metals using ND: YAG or Nd: YVO4 lasers.* Industrial Laser Solutions-for Manufacturing, 2005. **20**(12): p. 16-19.

24. Hongyu, Z., *Laser-induced colours on metal surfaces*. 2001, SIMTech Technical Report PT/01/005/AM.

25. O'Hana, S., A.J. Pinkerton, K. Shoba, A.W. Gale, and L. Li, *Laser surface colouring of titanium for contemporary jewellery.* Surface Engineering, 2008. **24**(2): p. 147-153.

26. CIE, C., *Commission Internationale de l'Eclairage Proceedings, 1931*. 1932, Cambridge University Press Cambridge.

27. Westland, S. and C. Ripamonti, *Computational colour science using MATLAB*. 2004, Hoboken, NJ: J. Wiley. x, 207 p.

28. ISO/CIE, *2011. ISO 11664-4:2011(E)/CIE S 014-4/E:2007 Joint ISO/CIE Standard: Colorimetry — Part 4: CIE 1976 L*a*b* Colour Space. .*

29. Ion, J.C., *Laser processing of engineering materials : principles, procedure and industrial application*. 2005, Amsterdam ;: Boston : Elsevier/Butterworth-Heinemann. xviii, 556 p.

30. Penchev, P., S. Dimov, D. Bhaduri, S.L. Soo, and B. Crickboom, *Generic software tool for counteracting the dynamics effects of optical beam delivery systems.* Proceedings of the Institution of Mechanical Engineers, Part B: Journal of Engineering Manufacture, 2015: p. 0954405414565379.

31. Butt, H., Y. Montelongo, T. Butler, R. Rajesekharan, Q. Dai, S.G. Shiva-Reddy, T.D. Wilkinson, and G.A. Amaratunga, *Carbon nanotube based high resolution holograms.* Adv Mater, 2012. **24**(44): p. OP331-6.

CHAPTER 4:

FABRICATION OF TIO$_2$ THIN FILM BASED FRESNEL ZONE PLATES BY NANOSECOND LASER DIRECT WRITING

Authors Contributions

This chapter of the alternative thesis format is published in Journal of Micro and Nano-Manufacturing. I am the first author of this publication. The paper's detail and contributions of co-authors are outlined below.

Jwad, T.[1], Deng, S.[2], Butt, H.[*], & Dimov, S[**]. (2018) Fabrication of TiO2 Thin Film-Based Fresnel Zone Plates by Nanosecond Laser Direct Writing. Journal of Micro and Nano-Manufacturing, 6(1), 011001 (9 pages).

[1] **Tahseen Jwad**: is the main author and he conceived the ideas of using the oxide film as a phase shifter to produce optical devices on metallic surfaces. He designed the experiments together with their experimental setups, performed all necessary characterization, data analysis and process modelling/simulation work of the lenses, and wrote the manuscript that was reviewed by the principal supervisor, **Prof. S. Dimov** (**), and the co-supervisor, **Dr. H. Butt** (*).

[2] Sunan Deng: contributed to the assessment of the lenses' performance.

CHAPTER 4: FABRICATION OF TIO₂ THIN FILM-BASED FRESNEL ZONE PLATES BY NANOSECOND LASER DIRECT WRITING

Abstract

Fresnel zone plates (FZPs) have been gaining a significant attention by industry due to their compact design and light weight. Different fabrication methods have been reported and used for their manufacture but they are relatively expensive. This research proposes a new low-cost one-step fabrication method that utilises nanosecond laser selective oxidation of titanium coatings on glass substrates and thus to form TiO_2 nano-scale films with different thicknesses by controlling the laser fluence and the scanning speed. In this way phase-shifting FZPs were manufactured where the TiO_2 thin-films acted as a phase shifter for the reflected light while the gain in phase depended on the film thickness. A model was created to analyse the performance of such FZPs based on the scalar theory. Finally, phase-shifting FZPs were fabricated for different operating wavelengths by varying the film thickness and a measurement setup was built to compare experimental and theoretical results. A good agreement between these results was achieved and an FZP efficiency of 5.5% to 20.9% was obtained when varying the wavelength and the oxide thicknesses of the zones.

1.   Introduction

Diffractive optical elements (DOE's) have attracted a significant interest because they can be used as micro-scale optical elements [1], in particular due to their tiny size, simple design and very low weight [2]. This have widened their range of applications, i.e. in laser beam shaping, deflection, polarization, projection of coherent light, authenticity verification, lithography, and laser machining [3-5]. One type of such micro scale optical elements that has attracted a myriad of research interests are Fresnel Zone Plates (FZP) due to their applications in laser beam shaping, optical interconnection and imaging [2, 6], especially due to their compactness and focusing capabilities [7, 8].

Various fabrication techniques for FZPs have been reported in the literature. Photolithography is one of the most common fabrication methods [5, 9]. In its simplest form, the required pattern is written on a mask and then transferred onto a photoresist followed by developing, etching and photoresist removal steps to produce FZPs [5, 6, 10, 11]. Femtosecond Laser Direct Writing (FSLDW) is another common fabrication method, where patterns are produced directly on photoresist materials [1, 3] or inside transparent mediums such as fused silica [7, 8] and sapphire [12]. Other methods such as single point diamond turning and nanosecond laser ablation of thin film [13] has also been reported [4].

There are some advantages and also limitations associated with these fabrication techniques. In particular, the resolution of FZPs fabricated with photolithography can reach submicron scale, but it is a multi-step process with potential errors associated with them, i.e. errors related to the mask alignment. Also they are a relatively expensive and slow process [2, 5, 9]. At the same time, the single point diamond turning method is limited to the manufacture of only axis-symmetric FZPs [2, 14, 15]. FSLDW entails a high capital investment but 3D structures with resolutions down to sub-wavelength scale can be produced in one step [2, 7].

In this research, a new method is proposed to fabricate two-level phase-type FZPs using nanosecond lasers. It allows FZPs to be directly "written" onto substrates with titanium coatings. In particular, a nanometre scale thin film of titanium dioxide (TiO_2) is formed selectively on laser irradiated areas in air. This TiO_2 film is transparent to the visible light and leads to a phase shift when light propagates through the film until it is reflected at the TiO_2-Ti boundary or transmitted through the TiO_2 film on transparent substrates. The phase shift is dependent on the film thickness that is a function of the nanosecond laser fluence [16]. Thus, the thickness of the TiO_2 film can be varied at nanometre scale by controlling the laser fluence [17] and thus to fabricate cost-effective phase-type FZPs.

The advantages of the proposed method compared with other fabrication routes are:

- Direct write capabilities in a single step.

- The use of low cost nanosecond laser sources.

- The phase-type FZPs can be designed to work in both transmission and reflection modes.

- Multilevel FZP can be manufactured as the TiO_2 thickness can be controlled at nano scale.

The main limitation is the patterning resolution that can be achieved with this method as it is dependent on the beam spot size that theoretically can be of the same order as the laser wavelength. Whereas, sub-wavelength resolutions are possible with the FSLDW method employing two-photon polymerization [3]

The paper is structured as follows. The next section presents the theoretical considerations in designing two-level phase-type FZPs to work in a reflective mode together with a model for verifying the functionality of such FZP lenses. Then, the experimental setup and the process

design used to fabricate FZPs with the proposed method are outlined. Next, a set of two-level phase-type FZPs produced with different laser processing settings is analysed both in regards to the process capabilities and FZPs performance. Finally, conclusions are made about the capabilities of the proposed direct nanosecond laser writing method for producing FZP lenses.

2. Theoretical design and modelling

2.1 Geometrical design

FZPs are flat optical diffractive elements that can focus electromagnetic waves in a similar way to lenses. However, their focusing principles are based on diffraction and interference rather than refraction [18]. Fundamentally, there are two types of FZP lenses, amplitude and phase-shifting based ones. Figure 1(a-c) shows the different types of FZPs. This research proposes a fabrication method for phase-shifting FZPs which can have two- or more levels. In particular, two-level FZPs have a number of consecutive concentric binary zones. These altered zones are designed to change the phase of the reflected (or transmitted) electromagnetic waves by $2\pi/N$ as illustrated in figure 1(d), where N is the number of levels. In contrast to amplitude type FZP, these zones contribute to the light intensity at the focus instead of blocking it. Hence, the efficiency of the phase type FZPs is higher than that of the binary amplitude type. It is worth mentioning that both types of FZPs, amplitude and phase ones can work in reflection in addition to transmission mode when the transparent zones are replaced by reflection zones. The geometric dimensions of two level FZPs can be calculated as following [2, 18, 19].

$$r_m^2 + f^2 = (f + m\lambda/2)^2$$

$$r_m = \sqrt{m\lambda f + (m\lambda/2)^2} \qquad \simeq \sqrt{m\lambda f} \qquad \text{When } (m\lambda << f) \qquad (1)$$

where: r_m is the mth outer radius of the zones; m - zone number; f - the focal length; and λ - the wavelength.
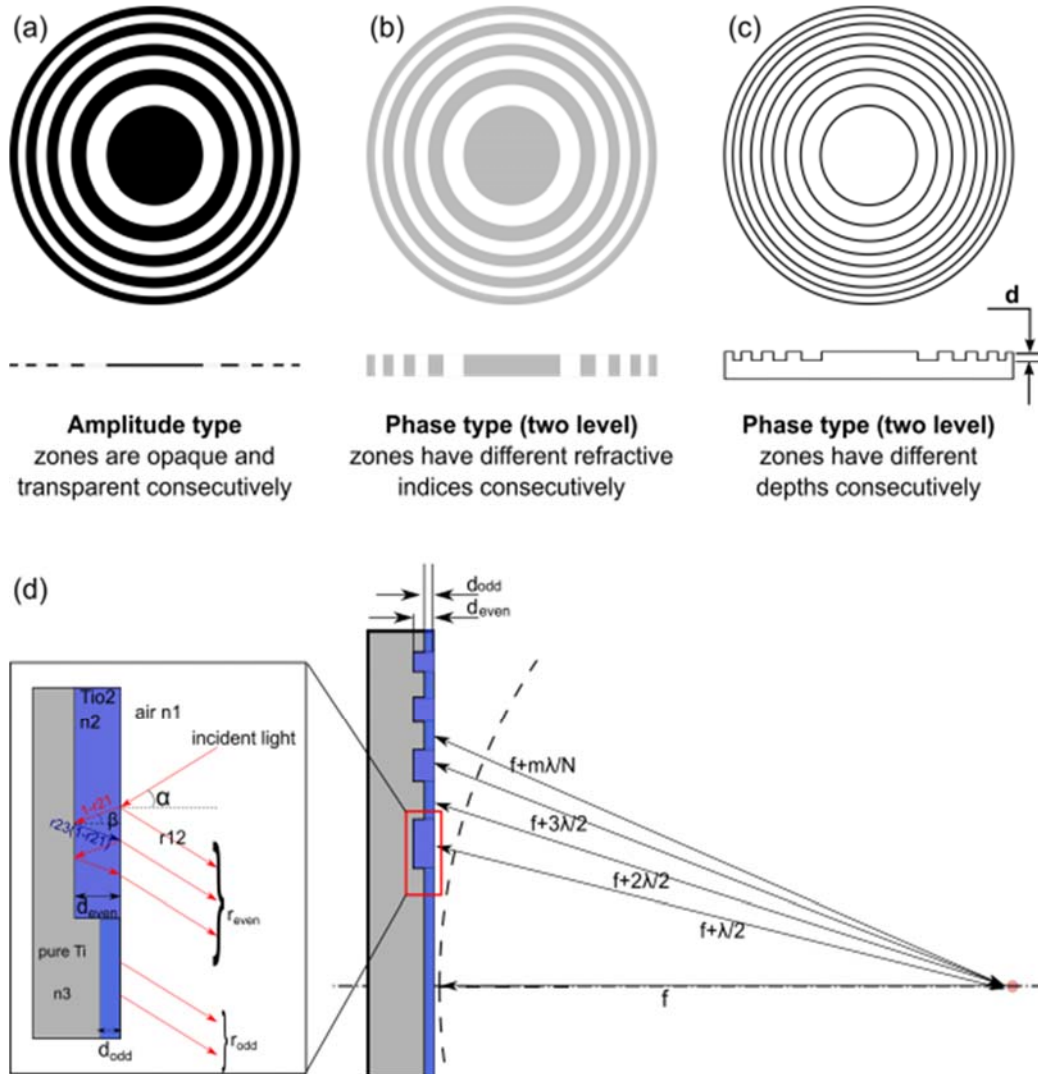
Fig. 1. FZP types: (a) amplitude type; (b) planner phase type; (c) phase type; (d) geometrical and optical design of the proposed FZP.

2.2 Oxide thickness of the zones

2.2.1 Thin film formation and light interference

As it has been stated earlier, the proposed fabrication method for FZPs employs a selective and controlled creation of a TiO$_2$ film by employing a nanosecond laser direct writing (NSLDW) process. Thus, it is important first to discuss the mechanism associated with the creation of such a film as a result of the nanosecond laser interaction with pure titanium. In particular, when lasers with long pulse duration (nanosecond or longer) interact with matter, heat is generated in the processed areas. This leads to localised heating of a Ti substrate surface and as a result a TiO$_2$ film is formed in a very controlled manner, i.e. through melting and solidification in air. However, the thickness of the laser affected region is minimal and it depends on the thermal diffusion length (L_h) [20]:

$$L_h \sim (4\, a\, \tau)^{1/2}$$

where: a is material thermal diffusivity and τ - the laser pulse duration. However, the thickness of the TiO$_2$ film formed on the surface is higher and depends on the cumulative fluence, i.e. on the pulse fluence and the number of pulses [21].

$$F_A = F\, N_p = \frac{\sqrt{2}EN_p}{A} = \frac{\sqrt{2}P_{Avg}N_p}{AV} = \frac{2\sqrt{2}P_{Avg}}{\pi w_0 S_p} = \frac{2\sqrt{2}EV}{\pi w_0 S_p} \tag{2}$$

where: F_A is the accumulated fluence; F - pulse fluence; N_p – the number of pulses; E - pulse energy; A – the effective area of pulse; P_{avg} - average laser power; V - pulse repetition rate; w_0 - the radius of the laser beam at the focal point; and S_p - the scanning speed.

The optical properties of the TiO₂ film formed on the surface are different than those of the substrate, especially the refractive index. This is of prime importance in designing a process for fabricating phase type FZPs employing nanosecond laser irradiation. In particular, due to this difference in the refractive index and since TiO₂ is a semi-transparent medium, thin film interference phenomena occur when the incident light is reflected at the boundary between the film and the Ti substrate. Therefore, the processed surfaces appear in different colours when it reflects white light depending on its thickness as show in Figure 2(a).
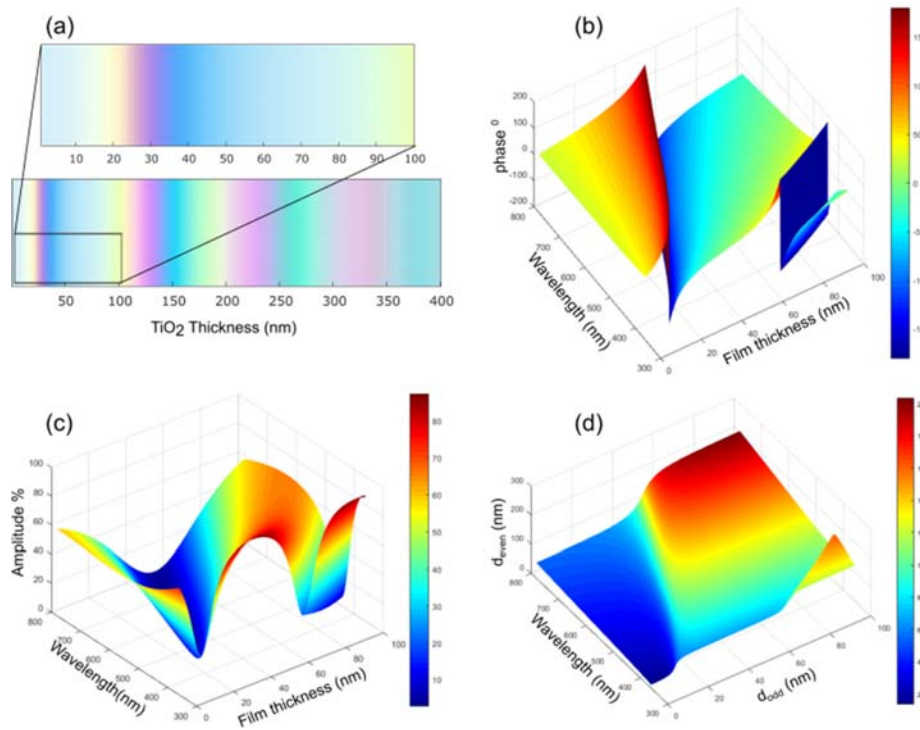
Fig. 2. Light interference in TiO₂ films on Ti substrates: (a) different colours of reflected white light from an Air-TiO₂-Ti system; (b) the phase shift vs. the TiO₂ thickness; (c) the amplitude (reflectance) vs. the TiO₂ thickness; and (d) the zone thickness leading to a (π) phase difference between consecutive zones for different film thicknesses and wavelengths.

For FZPs designed to work in reflective mode, the thin film interference phenomenon occurs when the out of phase rays of light reflected from the upper and lower boundaries of the film interfere. In particular, part of the incident electromagnetic wave is reflected from TiO₂

upper boundary (air-TiO$_2$) and undergoes a phase shift of π. While, the rest of the wave propagates through the thin film and is reflected at the TiO$_2$-Ti boundary. Therefore, it will be subjected to a change in its phase twice as it passes through the transparent film and is reflected back at the TiO$_2$-Ti boundary. The shifting angle depends on the refractive index, the light incident angle, wavelength, and the thickness of the film. Figure 2(b) shows the phase shift vs. the TiO$_2$ thickness throughout the entire visible spectrum of the electromagnetic waves.

As it is illustrated in Figure 1(d) the light subjected to a phase shift interferes with the light reflected from the upper boundary of the TiO$_2$ medium (air- TiO$_2$) and thus either constructive or destructive interference of different electromagnetic wavelengths occur. So, the phase delay caused by the TiO$_2$ film can be used to compensate the phase delay due to different distances from the FZP zones to the focal point as shown in Figure 1(d).

2.2.2 Thin film thickness difference between FZP zones

The design of FZPs to work in reflective mode as illustrated in Figure 1(d) requires the difference in paths lengths of the waves reflected from any two consecutive zones to the focal point of a lens to be equal to λ/N, where N is the number of levels of the lens. In other words, the reflected rays from any two consecutive zones have a phase difference of π in case of two-level FZPs when they reach the focus point. Thus, to avoid any destructive interference at the focus point such phase difference must be compensated by changing the thickness of the zone films, i.e. d_{odd} and/or d_{even}, and/or refractive index as illustrated in Figure 1(d). Since the refractive index of titanium dioxide is constant, only zones thickness can be varied. The thickness difference required between any consecutive zones can be determined by solving the equation below.

$$|\theta_{odd} - \theta_{even}| = 2\pi/N$$

$$\left| tan^{-1}\left(\frac{Im(r_{odd})}{Re(r_{odd})}\right) - tan^{-1}\left(\frac{Im(r_{even})}{Re(r_{even})}\right) \right| = 2\pi/N \tag{3}$$

where: θ_{odd} and θ_{even} are the phase of the reflected light from odd and even zones, respectively; r_{odd} and r_{even} – their reflection coefficients; and Re(r) and Im(r) - the real and imaginary parts of zones' reflection coefficient, respectively. The reflection coefficient of three mediums system [22], i.e. air-TiO$_2$-Ti in this research, can be calculated as follows:

$$r = \frac{r_{12} + r_{23}e^{i2\delta}}{1 + r_{12}\, r_{23}e^{i2\delta}}$$

where: r_{12}, and r_{23} - the reflection coefficients in any two mediums, i.e. air-TiO$_2$ and TiO$_2$-Ti respectively in this research as illustrated in Figure 1(d) and can be calculated using Fresnel's equations of reflection [22, 23], i.e. $r_{(ab)} = \frac{\tilde{n}_b - \tilde{n}_a}{\tilde{n}_b + \tilde{n}_a}$, where: $\tilde{n}_1, \tilde{n}_2,$ and $\tilde{n}_3$ are the refractive indices of air, TiO$_2$, and Ti for normal incident angle, respectively; δ - the phase gain per single penetration in TiO$_2$ film and is equal to $(2\pi\, d/\lambda)\sqrt{\tilde{n}_2{}^2 + sin^2\alpha}$ and $2\pi\, d\tilde{n}_2/\lambda$ at a normal incident angle where: d is the TiO$_2$ film thickness.

The amplitude (reflectance R) of the interfered electromagnetic waves is equal to $|r|^2$ and can be calculated as follows [22, 23] :

$$R = Re(r)^2 + Im(r)^2 \tag{4}$$

where: Re(r) and Im(r) are the real and imaginary parts of the system reflection coefficient, respectively.

To achieve the required phase difference between the consecutive zones, their thickness can be calculated by solving Equation 3. Figure 2(d) depicts the dependence between the thicknesses of the odd and even zones in achieving the required phase difference for the visible wavelengths. However, a simplified equation can be used to calculate approximately the difference, in particular [24] :

$$|d_{odd} - d_{even}| \approx \frac{\lambda}{2N\tilde{n}_2} \quad \approx \frac{\lambda}{4\tilde{n}_2} \quad \text{for two-level FZP (see Figure 1(d))} \tag{5}$$

Thin film thickness does not only affect the phase difference of the electromagnetic waves, but also its amplitude, which consequently affects the FZP efficiency as illustrated in Figure 2(c). The effect of reflectance of the zones on the diffraction efficiency is discussed in detail in section 2.3.

Different combinations of TiO_2 film thicknesses can lead to different reflectance in the zones and thus to different overall FZP efficiencies. Therefore, the amplitude should be considered in designing FZPs in order to achieve the required efficiency. Considering Equations 3, 5 and Figure 1(d), to achieve a higher efficiency the reflectance of even or odd zones have to be maximized by minimizing the thickness difference, e.g. by having a zero TiO_2 thickness for one of the zones, or by using shorter wavelength, as illustrated in Figure 2(c) and Figure 1(d).

2.3 Modelling

To verify the functionality of FZPs produced with the proposed NSLDW process, a model was created in MATLAB to map the intensity distribution along the axis of propagation and also the diffraction efficiency of the lens. The distribution of the diffracted light in the far field can be determined using Maxwell's equations. However, in practice it is impossible to get the exact solution for most of the cases [15]. Therefore, the scalar theory of diffraction is widely used for determining the far field solution of diffractive elements. By knowing the function of the FZP gratings, the light distribution can be calculated at any distance along the axis of propagation using the following equation [14, 15].

$$g(f_x, f_y) = \int_{-\infty}^{\infty} \int_{-\infty}^{\infty} u(x_0, y_0)\, e^{\left(-i2\pi[(f_x x_0) + (f_y y_0)]\right)}\, dx\, dy \tag{6}$$

$$f_x = {}^{x}\!/_{\lambda z}$$

$$f_y = {}^{y}\!/_{\lambda z}$$

where: $g(f_x, f_y)$ is the far field energy distribution and $u(x_0, y_0)$ - the initial light field of energy. The far field energy distribution then can be easily calculated by a simple two dimension Fourier transformation. Since Fresnel and Fraunhofer approximations have been applied to Rayleigh-Sommerfeld integral, Equation 6 is only applicable with the following assumptions.

1. The feature size of the gratings is large compared to the wavelength (a high period

to wavelength ratio).

2. The distance between the element and the focal plane is large compared to feature sizes and wavelength (far field).

Diffraction efficiency is an important factor in assessing the FZP performance. It is represented by the focusing intensity relative to the total incident intensity [15, 25]. The equation for the theoretical diffraction efficiency is derived based on the scalar theory as below [6]:

$$\eta = \text{sinc}^2(1/N) = \left\{ \frac{\sin(\pi/N)}{(\pi/N)} \right\}^2$$

(7)

As can be seen from Equation 7, the efficiency depends only on the number of levels (N), e.g. it is equal to 41, 81, and 95% for two-, four-, and eight-level FZPs, respectively [24]. However, Fresnel losses, i.e. reflections or absorption, are not taken into account in Equation 7 and this will lead to a difference between the theoretical efficiency and the measured value. Therefore, Fresnel losses should be counted in the equation to get the theoretical efficiency close to the measured value, in particular:

$$\eta = \left\{ \frac{\sin(\pi/N)}{(\pi/N)} \right\}^2 \left\{ \frac{(|r_1| + |r_2| + \cdots |r_N|)}{N} \right\}^2$$

(8)

where: r_N are Fresnel coefficients of N zones.

For a reflective mode FZP lens designed for operation with green light (532 nm) with zones' TiO$_2$ thicknesses of 31.5 and zero nm for odd and even zones, respectively, the theoretical amplitude and phase of the reflected light from the zones are shown in Figure 3(a) and Figure 3(b), respectively. While the theoretical intensity at the focal plane and the intensities distribution along the axis of propagation of the designed lens are depicted in Figure 3 (c, d). The focus and the sub-focus at (f/3, f/5, f/7... etc.) are clearly noticeable in Figure 3 (d). It is worth noting that the intensity profile along the propagation axis for any lens are identical if they have the same number of zones as defined in Equation 9 [26].

$$I(p) = \left(\frac{\sin(M\pi/p)}{\cos\left(\pi/2p\right)} \right)^2 \tag{9}$$

where: I is the intensity; M - the number of zones; p - a point along the propagation axis with respect to the focal length (z/f).

3. Experimental setup and fabrication

3.1 Laser processing and measurements setups

A reconfigurable laser micro processing platform was used to fabricate FZPs as shown in Figure 4 (a). The main component technologies of the platform are: the beam delivery sub-system, stack of five mechanical stages (three linear and two rotary stages) and laser sources. The laser source used in this research is redENERGY G4 50 W from SPI Lasers. The laser wavelength is 1064 nm while pulse repetition rates and pulse durations used were 1 MHz and 220 ns, respectively. The laser beam is non-polarized and the beam quality factor (M^2) is better

than 1.3 while the output energy is controlled by an energy attenuator and monitored by an inline power meter.

The beam delivery configuration used in this research included a 3D scanner (RhoThor RTA) from Newson Engineering and a 100 mm telecentric focusing lens that allowed scanning speeds up to 2.5 m/s to be achieved. Furthermore, the beam delivery sub-system included a beam expander to adjust the spot size, which was fixed at 30 μm in this research.
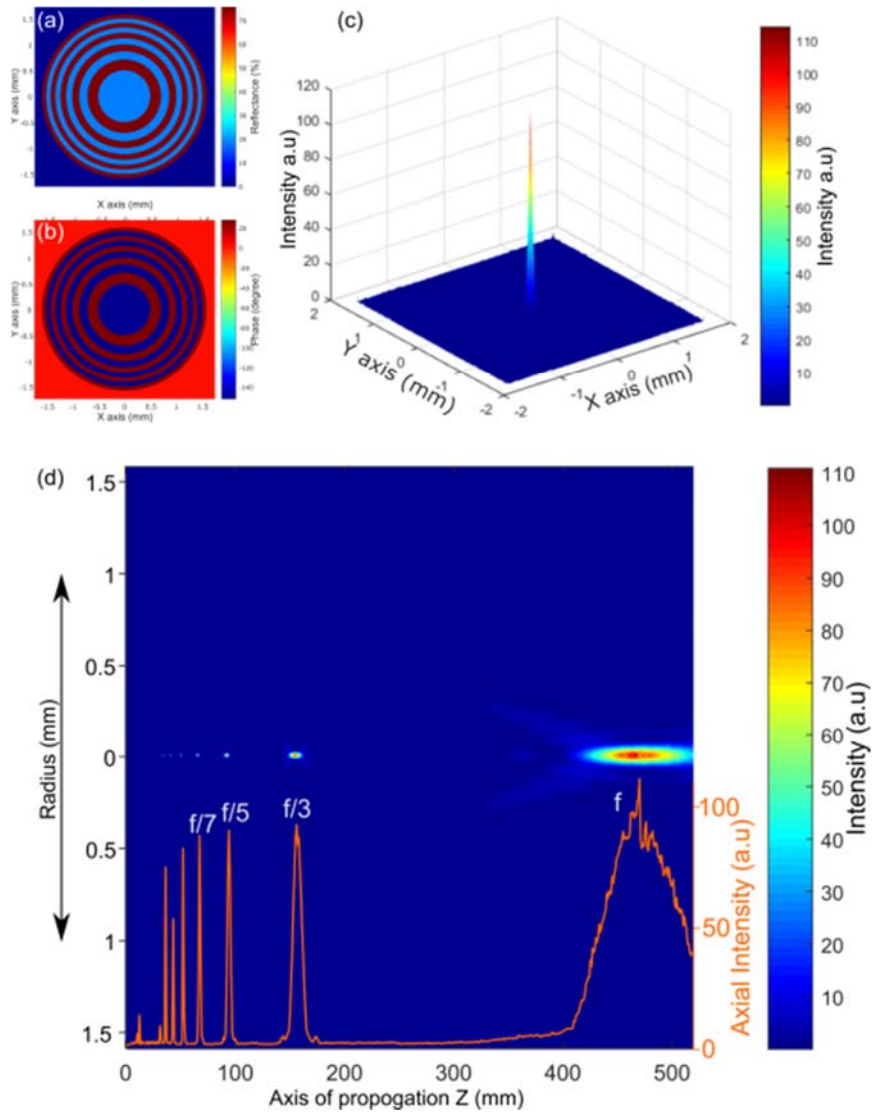
Fig. 3 Theoretical results of FZP designed for the green light: (a) zones' reflectance, (b) zones' phase, (c) intensity profile at the focal plane, and (d) intensity distribution and axial intensity along the axis of propagation (the focused intensity is in an arbitrary unit due to its dependency on the intensity of the incident beam).

Alicona G5 Infinite Focus (FV) system is used to inspect the fabricated FZPs. Reflectivity measurements for visible spectrum were performed using Ocean Optics USB2000+ Spectrometer and Carl Zeiss Scope A1 optical microscope. The FZP measurement setup consisted of two diode laser sources with different visible wavelengths (Red and Green), beam splitter, CCD, and powermeter (PM100D Thorlabs GmbH) as illustrated by Figure 4(b).
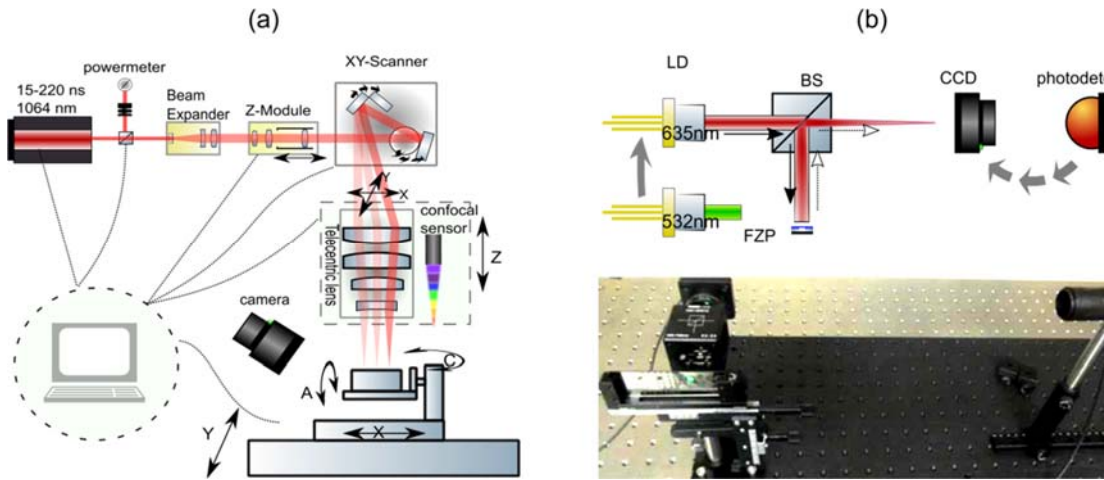
Fig. 4. Experimental setups: (a) the laser fabrication platform and (b) the optical measurement setup.

3.2. Substrate material and FZP design

A commercially available strip of glass was coated with pure Ti. Prior to the coating process, the 1 mm strip of glass was cleaned ultrasonically in water and then in acetone and finally dried with hot air. The Ti coating was sputtered on the glass substrate for 10 minutes. The thickness of the Ti coating was approximately 200 nm.

The FZP geometrical design is dictated by its specific application and depends on the wavelength of the electromagnetic waves, the focal length of the lens, and the radius of the first zone. In this research, the operating wavelength (λ) was selected to be 532 nm while the radius

of the first zone was 0.5 mm. Thus, the focal length (f) of this FZP design is 469.9 mm. The number of zones was chosen to be 10 and their radii were calculated using Equation 1. The TiO_2 thickness of even zones, d_{even}, was selected to be zero (pure Ti) while of odd zones, d_{odd}, was calculated to be 31.5 nm by solving Equation 3 and thus to have a phase difference of π.

3.3. FZP fabrication

The NSDLDW process was used to fabricate the FZP lens. Each zone was produced by scanning the laser beam over the substrate employing a circular hatching strategy. Pulse repetition rate and energy used were 1 MHz and 5.4 µJ, respectively, as stated in Section 3.1. With these laser settings, a laser spot size of 30 µm led to a fluence of 1.08 J/cm^2 per pulse. These laser parameters were selected to achieve a pulse fluence above titanium damage threshold of approximately 0.2 J/cm^2 [27]. The scanning speed was used to vary the cumulative fluence thus to control the TiO_2 thickness (see Equation 2).

Prior to the fabrication of FZP lenses, 10 mm by 10 mm fields as shown in Figure 5 (a) were produced on a substrate with Ti coating and thus to find the scanning speeds required to form TiO_2 films with required thickness. By measuring the reflectance spectra of these fields, their TiO_2 thickness was determined by comparing the measured reflectance spectra with the results obtained with the thickness-based model [23]. The required TiO_2 thickness of the odd zones of 31.5 nm was achieved with scanning speed of 400 mm/s or a cumulative fluence of 81 J/cm^2 calculated using Equation 2.

4. Results and discussion

Two-level phase-type FZPs for a range of operating wavelengths with different combinations of TiO_2 thicknesses were fabricated on substrates with Ti coating as shown in

Figure 5 (b, c). These FZP lenses were produced with different circular hatch distances, i.e. 30,
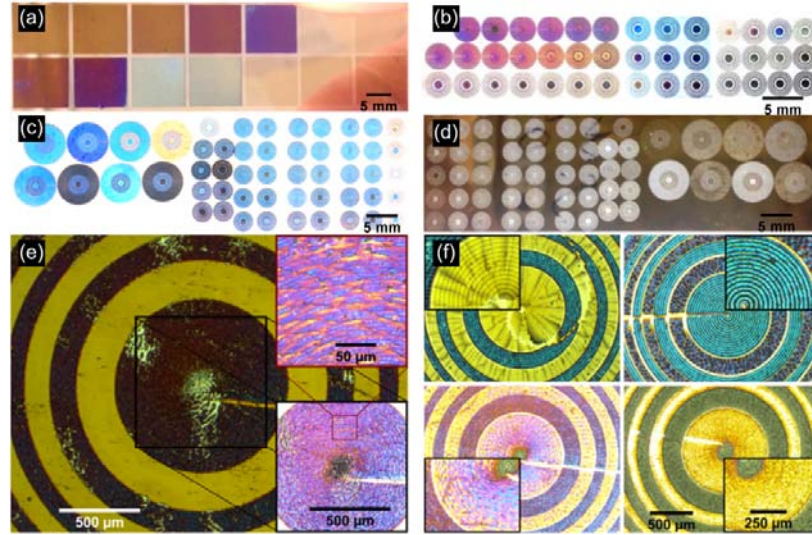
Fig. 5. FZPs fabricated with the direct nanosecond laser writing: (a) field maps of colours associated with different TiO_2 thicknesses; (b-c) lenses fabricated for a range of wavelengths with different combinations of TiO_2 thicknesses; (d) the back view of the sample shown in (c); (e) microscopic image of the FZP lens, which performance was analysed; (f) microscopic images of lenses with defects/shortcomings.

20, 10, and 5 µm. The inspection of fabricated FZPs revealed some issues with the used laser processing settings, i.e. the hatch distances, as higher hatch distances led to non-uniform TiO_2 thickness as depicted in the upper part of Figure 5 (f) while using lower hatch distances, less than 10 µm, led to uniform TiO_2 film (see the lower part of Figure 5 (f)). Other defects were also observed, such as cracks (see the upper left corner of Figure 5(f)), however they were minimised by using different combination of scanning speeds and pulse energies but with the same cumulative fluence of 81 J/cm^2 (Equation 2). Also, the centre of the lenses exhibited a small burn area, which was due to the accumulated heat as the lengths of the most internal circular pulse train tracks are very short compared to the outer ones and thus lead to a higher cumulative fluence, i.e exceeding 200 J/cm^2. Such shortcomings can be controlled by increasing the hatch distance in producing the zone at the centre and thus to reduce the cumulative fluence.

Furthermore, the starts and the ends of the scanned circles were either superimposed or did not overlap. These defects were due to the beam deflectors' dynamics effects, however they were minimised by employing build-in software tools to offset them [28]. However, it is worth stressing that these shortcomings did not affect the FZP's performance.

The FZP design outlined in Section 3.2 was used to fabricate a lens with the optimised laser settings, as it is shown in Figure 5 (e). The fabrication of this FZP lens took less than 4 sec., i.e. the processing speed was approximately $0.9 \text{ mm}^2/\text{s}$. The TiO_2 thicknesses of odd and even zones were determined by measuring the reflectance spectra of these fields as stated in Section 3.3 and they were approximately 31 and zero nm, respectively. The theoretical efficiency of a two-level FZP was approximately 40.52% when Fresnel losses were not considered (Equation 7) but it was reduced to 9.05% when they were taken into account (Equation 8). This drop of efficiency is due to the light absorption by titanium as well as the destructive light interference. The (Air-TiO_2-Ti) overall reflectivity of the odd and even zones was calculated to be 3.5% and 57%, respectively, by using Equation 4. This low reflectivity of 31 nm TiO_2 film is the result of the destructive interference as mentioned earlier.
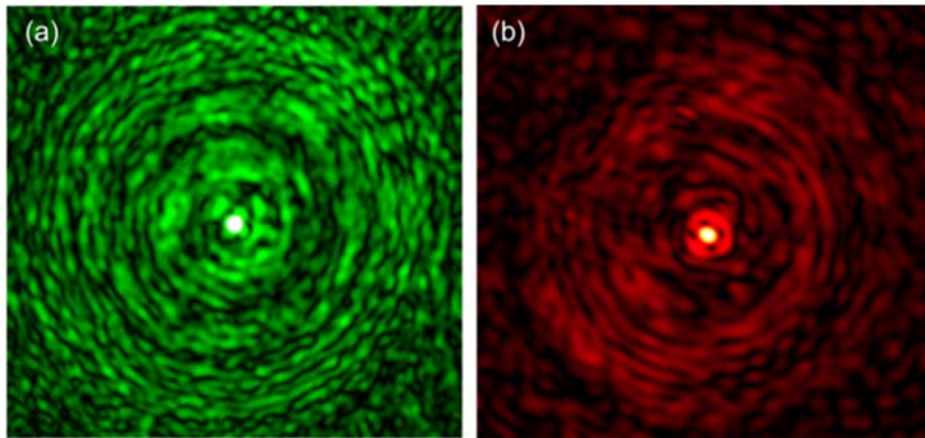

Fig. 6. Results obtained for the FZP lens: (a & b) at the focal planes for both green and red lights, respectively.

The efficiency is assessed in this research based on the ratio of the intensity at the focal spot to the intensity of incident light. Thus, the efficiency of a lens fabricated for the designated wavelength, i.e. 532 nm, was approximately 9.7%, which was higher than the theoretical value. This can be explained with the refractive indices used in calculations for Titanium and TiO_2 that were not measured but calculated employing the models reported in the literature [29, 30]. In addition, it is worth mentioning that the theoretical efficiency is very sensitive to the refractive indices' values and any small variations lead to noticeable changes in theoretical efficiency. For example, when the value of the TiO_2 refractive index at 532 nm used in the calculations was 2.78 instead of 2.66, the theoretical efficiency increases from 9.05% to 9.74%.

The focusing functionality of the fabricated lens for the green light (532 nm) was tested under red light (635 nm), too. Although the reflectance of odd and even zones was 9% and 57% for the 635 nm wavelength, respectively, which was higher than that obtained for the green light, the efficiency of the lens was less than half compared to that obtained for the green light. This is due to the fact that this FZP lens is designed for the green light, so using light with different wavelength lead to a destructive interference at the focal point. Figure 6 (a-b) shows images of the detected focus of the lens at the focal plane for the green and red lights, i.e. 469.9 and 393.7 mm, respectively. The focus of the lens can be clearly seen at the centre while there is also some low intensity light distribution around it. However, this low intensity can be ignored when it is compared with the intensity at the focus. This light distribution can be attributed to some inhomogeneity of the TiO_2 thickness at nano-scale due to small variation of cumulative fluence in processed areas that can be minimised by optimising the circular hatching strategy, i.e. its variables as hatch distance, scanning speed and pulse frequency together with pulse energy and duration.

The theoretical efficiency of FZPs that can be produced with the proposed NSLDW method for all visible wavelengths is shown in Figure 7 (a). As can be seen there, a range of efficiencies from 5.5% to 20.9% can be achieved depending on the wavelength and the combination of zones' TiO_2 thicknesses. For a lens designed for green light, the maximum efficiency that can be achieved is 9.9% while the minimum is 5.7% as depicted in Figure 7 (b). Due to the limitation of the available light sources in the experimental set-up used in this research, which are required to test lenses performance, FZPs with high efficiency (20.9 %) were not fabricated.
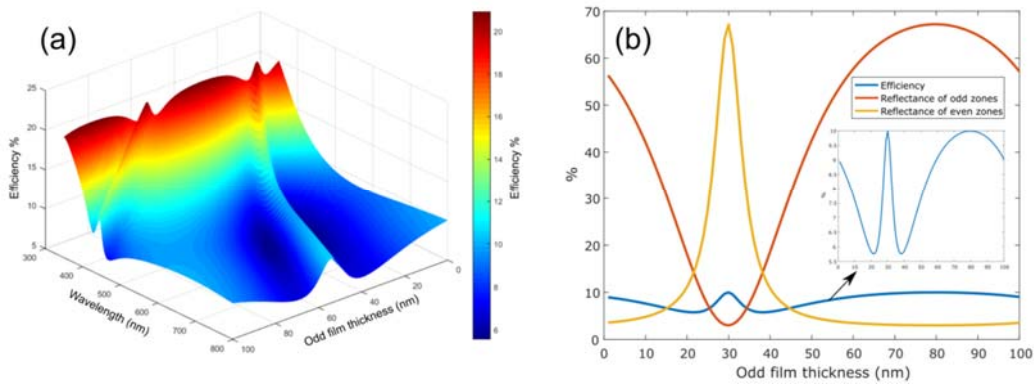
Fig. 7 Theoretical efficiency of FZPs when Fresnel losses are considered: (a) for the entire visible wavelength spectrum; and (b) the efficiency and zones' reflectance vs odd zones' TiO_2 thickness at wavelength of 532 nm.

5.   Conclusions

A NSLDW method is proposed for producing cost-effectively two-level phase-type FZPs with relatively high throughput on substrates with Ti coatings. It allows a controlled and selective formation of a TiO_2 thin film with a high resolution that acts as a phase shifter. In particular, the TiO_2 thickness can be controlled at nano-scale by varying the laser cumulative fluence. In addition, an analytic method is proposed for calculating the required TiO_2 thickness

differences between the FZP odd and even zones together with a model for validating the lenses' design. The performance of the two-level phase-type FZPs produced with the proposed method was analysed and the results showed a good agreement with the theoretical one. Based on the obtained results it can be concluded that FZPs with efficiencies in the range from 5.5% to 20.9% can be produced depending on the wavelength and the TiO_2 thickness combinations. In addition, the FZP lenses fabricated with the NSLDW method can work in both transmission and reflection modes. However, the Ti film thickness along with glass thickness and its refractive index should be taken into account in designing FZPs for the transmission mode.

Acknowledgments

References

1. Moebius, M., K. Vora, S. Kang, P. Munoz, G.L. Deng, and E. Mazur, *Direct Laser Writing of 3D Gratings and Diffraction Optics.* 2015 Conference on Lasers and Electro-Optics (Cleo), 2015.
2. Yu, Y.H., Z.N. Tian, T. Jiang, L.G. Niu, and B.R. Gao, *Fabrication of large-scale multilevel phase-type Fresnel zone plate arrays by femtosecond laser direct writing.* Optics Communications, 2016. **362**: p. 69-72.
3. Sohn, I.B., M.J. Ko, Y.S. Kim, and Y.C. Noh, *Direct femtosecond laser lithography for photoresist patterning.* Optical Engineering, 2009. **48**(2).
4. Falldorf, C., C. Dankwart, R. Glabe, B. Lunemann, C. von Kopylow, and R.B. Bergmann, *Holographic projection based on diamond-turned diffractive optical elements.* Applied Optics, 2009. **48**(30): p. 5782-5785.
5. Taghizadeh, M.R., P. Blair, B. Layet, I.M. Barton, A.J. Waddie, and N. Ross, *Design and fabrication of diffractive optical elements.* Microelectronic Engineering, 1997. **34**(3-4): p. 219-242.
6. Jahns, J. and S.J. Walker, *Two-dimensional array of diffractive microlenses fabricated by thin film deposition.* Appl Opt, 1990. **29**(7): p. 931-6.
7. Bricchi, E., J.D. Mills, P.G. Kazansky, B.G. Klappauf, and J.J. Baumberg, *Birefringent Fresnel zone plates in silica fabricated by femtosecond laser machining.* Optics Letters, 2002. **27**(24): p. 2200-2202.
8. Srisungsitthisunti, P., O.K. Ersoy, and X.F. Xu, *Volume Fresnel zone plates fabricated by femtosecond laser direct writing.* Applied Physics Letters, 2007. **90**(1).
9. Keskinbora, K., C. Grevent, U. Eigenthaler, M. Weigand, and G. Schutz, *Rapid prototyping of Fresnel zone plates via direct Ga(+) ion beam lithography for high-resolution X-ray imaging.* ACS Nano, 2013. **7**(11): p. 9788-97.
10. Rajasekharan, R., H. Butt, Q. Dai, T.D. Wilkinson, and G.A.J. Amaratunga, *Can Nanotubes Make a Lens Array?* Advanced Materials, 2012. **24**(23): p. Op170-Op173.
11. Moghimi, M.J., J. Fernandes, A. Kanhere, and H.R. Jiang, *Micro-Fresnel-Zone-Plate Array on Flexible Substrate for Large Field-of-View and Focus Scanning.* Scientific Reports, 2015. **5**.
12. Puisys, A. and D. Paipulas, *Integration of Fresnel Zone Plates in the Bulk of Sapphire Crystal by Femtosecond Laser Pulses.* Journal of Laser Micro Nanoengineering, 2015. **10**(1): p. 96-100.
13. Zhao, Q.C., A.K. Yetisen, A. Sabouri, S.H. Yun, and H. Butt, *Printable Nanophotonic Devices via Holographic Laser Ablation.* Acs Nano, 2015. **9**(9): p. 9062-9069.
14. O'Shea, D.C., T.J. Suleski, A.D. Kathman, and D.W. Prather, *Diffractive Optics: Design, Fabrication, and Test*. 2004.
15. Swanson, G.J., *Binary optics technology: theoretical limits on the diffraction efficiency of multilevel diffractive optical elements*. 1991, DTIC Document.
16. Jwad, T., S. Deng, H. Butt, and S. Dimov, *Laser induced single spot oxidation of titanium.* Applied Surface Science, 2016. **387**: p. 617-624.
17. Skowronski, L., A.J. Antonczak, M. Trzcinski, L. Lazarek, T. Hiller, A. Bukaluk, and A.A. Wronkowska, *Optical properties of laser induced oxynitride films on titanium.* Applied Surface Science, 2014. **304**: p. 107-114.
18. Wiltse, J.C., *The Fresnel Zone-Plate Lens.* Proceedings of the Society of Photo-Optical Instrumentation Engineers, 1985. **544**: p. 41-47.
19. Fang, Z.Y., C.F. Lin, R.M. Ma, S. Huang, and X. Zhu, *Planar Plasmonic Focusing and Optical Transport Using CdS Nanoribbon.* Acs Nano, 2010. **4**(1): p. 75-82.
20. Schaaf, P., *Laser processing of materials : fundamentals, applications and developments*. Springer series in materials science. 2010, Berlin ; London: Springer. xiv, 231 p.

21. Antonczak, A.J., B. Stepak, P.E. Koziol, and K.M. Abramski, *The influence of process parameters on the laser-induced coloring of titanium.* Applied Physics a-Materials Science & Processing, 2014. **115**(3): p. 1003-1013.
22. Stenzel, O., *The Physics of thin film optical spectra*. 2005: Springer.
23. Quinten, M., *A practical guide to optical metrology for thin films*. 2013, Weinheim, Germany: Wiley-VCH. xii, 211 p.
24. Guo, Y.J. and S.K. Barton, *Multilayer Phase Correcting Fresnel Zone Plate Reflector Antennas.* International Journal of Satellite Communications, 1993. **11**(2): p. 75-80.
25. Sanli, U.T., K. Keskinbora, C. Grevent, and G. Schutz, *Overview of the multilayer-Fresnel zone plate and the kinoform lens development at MPI for Intelligent Systems.* Euv and X-Ray Optics: Synergy between Laboratory and Space Iv, 2015. **9510**.
26. Hignette, O., J. Santamaria, and J. Bescos, *White-Light Diffraction Patterns of Amplitude and Phase Zone Plates.* Journal of Optics-Nouvelle Revue D Optique, 1979. **10**(5): p. 231-238.
27. Jwad, T., S.A. Deng, H. Butt, and S. DimovSchool, *Laser induced single spot oxidation of titanium.* Applied Surface Science, 2016. **387**: p. 617-624.
28. Penchev, P., S. Dimov, D. Bhaduri, S.L. Soo, and B. Crickboom, *Generic software tool for counteracting the dynamics effects of optical beam delivery systems.* Proceedings of the Institution of Mechanical Engineers, Part B: Journal of Engineering Manufacture, 2015: p. 0954405414565379.
29. Rakic, A.D., A.B. Djurisic, J.M. Elazar, and M.L. Majewski, *Optical properties of metallic films for vertical-cavity optoelectronic devices.* Applied Optics, 1998. **37**(22): p. 5271-5283.
30. Devore, J.R., *Refractive Indices of Rutile and Sphalerite.* Journal of the Optical Society of America, 1950. **40**(4): p. 266-266.

CHAPTER 5:

ERASING AND REWRITING OF TITANIUM OXIDE COLOUR MARKS USING LASER-INDUCED REDUCTION/OXIDATION

Authors Contributions

This chapter of the alternative thesis format is submitted in the journal of Applied Surface Science. I am the first author of this publication. The paper's detail and contributions of co-authors are outlined below.

Jwad, T.[1], Walker, M.[2], & Dimov, S. [**], 2018. Erasing and rewriting of titanium oxide colour marks using laser-induced reduction/oxidation. Applied Surface Science, 458, pp.849-854.

[1] **Tahseen Jwad**: is the main author and he conceived the ideas, designed the experiments together with their experimental setups, and wrote the manuscript that was reviewed by the principal supervisor, **Prof. S. Dimov** (**).

[2]Marc Walker: contributed with XPS measurements and their analysis.

CHAPTER 5: ERASING AND REWRITING OF TITANIUM OXIDE COLOUR MARKS USING LASER-INDUCED REDUCTION/OXIDATION

Abstract

Laser-induced oxidation of metallic surfaces such as titanium is used in many application areas for colour marking due to its selectivity, cleanness and processing speed. However, as the generated colours are permanent this reduces the flexibility and applicability of this laser processing technology. Therefore, a method is reported in this paper to erase selectively the oxide-based colours using laser-induced oxygen reduction. Especially, the colour marks are reprocessed in a low oxygen environment employing a nanosecond laser. A low fluence was used in order to diffuse oxygen out into the atmosphere and yield a lower form of metal oxides or a pure metal. Any cumulative fluence exceeding 25 J/cm^2 was sufficient to erase any laser-induced colours on titanium substrates. The XPS analysis revealed that all fields were mainly comprised of TiO_2 prior to erasing with only small contributions from Ti_2O_3 and TiO/TiN. Following the proposed laser-induced oxygen reduction, the relative concentration of TiO_2 decreased substantially while the overall amount of Ti in the near surface region increased. The results clearly show that the erasing of oxide-based colour marks is only due to oxygen diffusion back into the atmosphere and there were not any signs of laser ablation.

Keywords: nanosecond laser, Laser-induced reduction, metallization, titanium oxide, color erasing, color rewriting, color marking,

1. Introduction

Laser-induced oxidation of metals and semiconductors has gained a considerable attention by research community since it was reported for the first time in early 1970s [1]. One of the main advantages of laser-induced oxidation compared with other oxidation methods is the selectivity that differentiate and make this technology attractive for a range of applications [2, 3]. In particular, oxidation of titanium surfaces has many chemical, electrical, sensing, optical, tribological, and medical applications. This is due to the unique properties of titanium oxides compared to the substrate. One of the main applications of laser-induced oxidation of titanium is laser colour marking.

When pulsed (nanosecond or longer) or continuous wave (CW) lasers interact with a metal, a thin film of the metal oxides is formed due to melting and re-solidification of the substrate's material in air. The thickness of the generated film depends on used laser parameters, especially mainly on the accumulated fluence, and as result of the varying film thickness the surface can appear in different colours. This is due to the thin film interference phenomenon.

Generally, the oxidation of titanium leads to a number of stable Ti-O phases such as Ti_2O, TiO, Ti_2O_3, Ti_3O_5, and TiO_2. However, TiO_2 (rutile) is the main structure and is the most stable side product of the oxidized Ti substrate [1]. The formed film consists of multilayers of oxides as stated by Del pino et al. [4-6], and others [7-10]. In addition, it was reported that the oxygen concentration is depth dependent, in particular, decreases with the depth increase [11, 12]. Two main layers constitute the film, i.e. the first is a transparent TiO_2 with some Ti_2O_3 on top that is followed by lower forms of titanium oxides, such as TiO and Ti_2O. The surface colourization is attributed to the transparent top layer that is due to the thin film interference phenomenon mentioned above. At the same time, the underneath layer is opaque and has

metallic characteristics [6, 8], in particular its optical properties are very similar to those of pure titanium [13, 14].

Laser colour marking of titanium has been of interest to many industrial sectors, e.g. for aerospace, automotive, medical, optical and anti-counterfeit applications [15]. It is widely used to imprint product information, logos, and functional data on medical devices, implants, and surgical instruments [16, 17]. And, for this application area, it is critical the general surface properties of components, such as corrosion resistance and any performance characteristics [18, 19], to stay unaffected by the marking process. This is explicitly stated in ASTM F86 and F983 standards for permanent marking of implant components. In addition, the marking material should not be in anyway toxic. All these stringent requirements can be fulfilled by titanium dioxide that is the main side product on processed Ti substrates [1], i.e. it is nontoxic, biocompatible, and also exhibits negligible solubility in most solvents [20, 21].

Laser colour marking is one of the most flexible marking methods and this make the technology a very attractive proposition. However, as the generated colours are permanent this impacts its flexibility and applicability. Thus, capabilities to make such colour marks erasable and rewritable can broaden the application areas of this technology and can add one more advantage when compared with other methods.

Employing laser processing to remove paints (de-painting), oxides (de-oxidation), and rust (de-rusting) with different thicknesses was reported by Daurelio et al. [22], i.e. a very high fluence was applied to ablate paints and oxides. However, the oxides' removal in this case is performed by laser ablation and this leads to a range of negative side effects on the surfaces, e.g. changes in surface morphology and integrity, that affect the functional performance of processed parts. In another research, Veiko et al. [23, 24] demonstrated the high mechanical

and chemical wear resistance of titanium dioxides' thin films. In particular, neither the morphology nor the appearance were affected after treating the film by abrasion for 5 minutes, immersing it either in 5% citric acid for 40 minutes or in ultrasonic bath for 20 minutes, and soaking it for one hour in 200 °C muffle furnace.

Thus, colour surface marks induced on titanium surfaces by oxidation are very durable and cannot be erased by chemical treatments in various solutions [20, 21]. At the same time, any reprocessing of parts mechanically to remove such colour marks will affect their functionality and also will have cost implications. In addition, it is important to stress that neither chemical treatments nor mechanical processing can erase the Ti oxides selectively. Therefore, other methods for their selective removal should be sought.

In this paper, a method is presented for erasing colour marks on Ti substrates by laser processing in an oxygen controlled environment. In the next section, the methods and equipment used in the research are described and then the obtained results are presented and discussed. Finally, conclusions are made about the capabilities of the proposed method for metalizing transparent oxide layers and thus to achieve a metallic appearance.

2. Methods and equipment

In designing a method for removing colour marks in in the form of oxides on parts, it is important to take into account the specific requirements of various applications that can benefit from its implementation and also to have in-depth understanding of the laser-material interaction mechanism that should take place during the process. In particular, a method should be designed for erasing colour marks, i.e. laser-induced oxides, on titanium surfaces that should be able to "reverse" the oxidation mechanism in creating them. Especially, when

metals are heated in an oxygen rich environment, the oxygen reacts with their surface and free electrons are transferred from them into the adsorbed oxygen. As a result, ions are diffused through the native oxide layer to form thin oxide films [16, 25].

As was stated above, the proposed erasing method should be able to reverse the oxidation process and thus to reduce/remove the oxygen from such oxide layers and as a result to yield a lower form of metal oxides or a pure metal. To achieve this the surface should be heated in a low oxygen environment, i.e. vacuum or inert gas, so as to diffuse the oxygen out into the atmosphere. Especially, the applied laser fluence should be less than the damage threshold, but at the same time sufficiently high to heat the oxides to temperatures just below their melting point and thus to trigger the oxygen diffusion back into the atmosphere. Figure 1 illustrate the colorizing process and also the proposed method for erasing the laser-induced oxides.

Laser processing of materials in controlled environments have been used in different applications before. For example, it was applied to polish metal surfaces [26], nitride surfaces [27-30] and also to prevent the generation of oxides during laser cutting and texturing [31, 32]. In addition, laser processing in controlled environments was used to alter oxides' conductivity, in particular through a laser induced reduction (also known as laser induced metallization) that involved a controlled laser heating in inert gas atmosphere. In this way, the properties of different oxides' thin films were altered to become semiconductors, insulators or superconductors [33-37]. Thus, the proposed method should employ a similar laser-material interaction mechanism to perform so called laser-induced oxygen reduction.
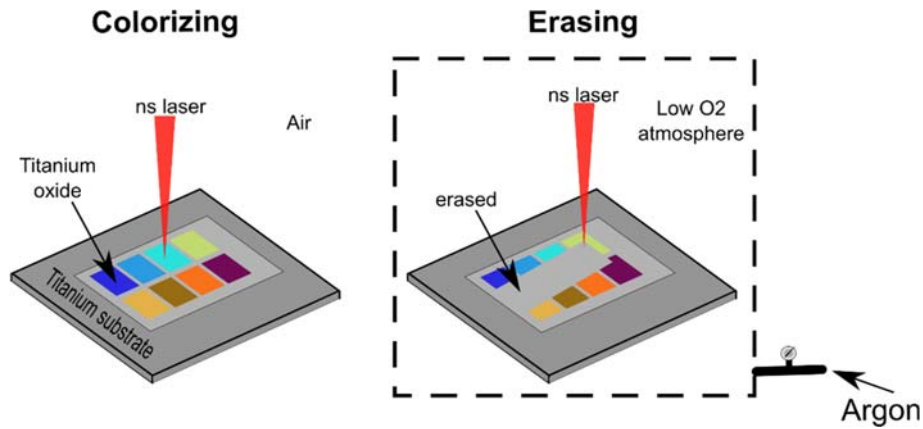
Fig. 1. Schematic sketches of laser colour marking and erasing by laser-induced oxidation and laser-induced oxygen reduction, respectively.

An experimental study was carried out to investigate the proposed method employing a nanosecond fibre laser source (redENERGY G4 50W) from SPI Lasers. With wavelength of 1064 nm and a 1 MHz maximum pulse repetition rate, it can be used for laser processing with 25 different pulse durations, from 15 to 220 ns. The experiments were performed on a reconfigurable laser micro processing platform with a 3D scanner (RhoThor RTA) from Newson Engineering and a 100 mm telecentric F-theta lens. The substrates were mounted horizontally on a high precision stack-up of mechanical stages from Aerotech. A specially designed chamber was employed to achieve a low oxygen atmosphere by purging the air and replace it with argon during the laser processing.

The substrates used in the experiments were 0.7 mm thickness sheets of commercially available pure titanium (Grade 1). The samples were cleaned ultrasonically in water and acetone and then dried with hot air prior to laser processing. The morphology of the processed Ti substrates was inspected using an Alicona G5 Infinite Focus (FV) system.

Compositional analysis of the surfaces of several samples was carried out using x-ray photoelectron spectroscopy (XPS) measurements conducted on a Kratos Axis Ultra DLD spectrometer at the University of Warwick Photoemission Facility. The samples were mounted on to a standard sample bar using electrically conductive carbon tape and loaded in to the instrument. XPS measurements were performed in the main analysis chamber, with the sample being illuminated using a monochromated Al Kα x-ray source. The measurements were conducted at room temperature and at a take-off angle of 90° with respect to the surface parallel. The core level spectra were recorded using a pass energy of 20 eV (resolution approx. 0.4 eV), from an analysis area of 300 μm by 700 μm. The spectrometer work function and binding energy scale of the spectrometer were calibrated using the Fermi edge and 3d5/2 peak recorded from a polycrystalline Ag sample prior to the commencement of the experiments. The data were analysed in the CasaXPS package, using Shirley backgrounds and mixed Gaussian-Lorentzian (Voigt) lineshapes. For compositional analysis, the analyser transmission function has been determined using clean metallic foils to determine the detection efficiency across the full binding energy range.

As stated earlier, the colours obtained through laser induced oxidation are dependent on the oxide thickness. In particular, the main colours that can be produced on titanium surfaces by increasing the film thickness range from golden through orange, purple, blue, light blue to greenish blue. Thus, to validate the proposed erasing method, fields with increasing film thickness were created that represented different colour grades producible through laser-induced oxidation. In particular, the colours are generated by scanning the laser over the 10×10 mm^2 fields employing a zig-zag hatching strategy with a 20 μm hatch distance. The laser pulse repetition rate and pulse energy used were 1 MHz and 19.8 μJ, respectively that were selected based on the result in another experimental study [3]. The laser spot diameter

was 60 µm and thus an average fluence of 0.351 J/cm^2 per pulse was used in all experimental

trials. The scanning speed was varied to process the fields and thus to produce TiO$_2$ with

varying thickness and hence colours. Especially, the scanning speed was varied from 360 to

80 mm/s and thus to achieve a cumulative fluence from 58 to 260 J/cm^2 as stated in Table 1.

The eight fields with varying colours on titanium substrates produced by laser-induced

oxidation in air with these process settings as shown in Fig2. (a).

Table 1: processed fields

Field number	1	2	3	4	5	6	7	8
colour								
Scanning speed (mm/s)	360	300	230	190	160	120	100	80
Cumulative fluence (J/cm^2)	58	70	91	110	131	175	210	260

3. Results and discussion

A set of experimental trials were performed to validate the proposed method for erasing

colour marks through laser-induced oxygen reduction. Especially, TiO$_2$ fields on Ti substrates

covering the whole range of colours in Table 1 were reprocessed in argon atmosphere with a

varying cumulative fluence from 12 to 210 J/cm^2. The laser-induced oxygen reduction

settings used in conducting these initial trials are given in Table 2. The efficiency of the

reduction process is directly proportional to the processing temperature and inversely

proportional to the oxygen concentration in the atmosphere [33]. Therefore, any processing of

colours, TiO$_2$ fields, with cumulative fluence of less than 20 J/cm^2 leads to altering the

colours' appearance but not to erasing them. At the same time, it was possible to erase all

Table 2. Laser-induced oxygen reduction parameters

Scanning speed (mm/s)	1750	1650	1550	1450	1350	1250	1150	1050	950	850	700	500	300	200	100
Pulse repetition rate (MHz)	1	1	1	1	1	1	1	1	1	1	1	1	1	1	1
Pulse's fluence (J/cm^2)	0.351	0.351	0.351	0.351	0.351	0.351	0.351	0.351	0.351	0.351	0.351	0.351	0.351	0.351	0.351
No of pulses*	34	36	38	41	44	48	52	57	63	70	85	120	200	300	600
Cumulative fluence (J/cm^2)	12	12.7	13.5	14.5	15.6	16.8	18.3	20	22	24.7	30	42.1	70.2	105.3	210.6
Effect	some colours were altered/ others were not effected				some altered/some erased			All colours were erased							

- The number of pulses per spot: is the ratio of (pulse repetition rate over the scanning speed) times the spot size.
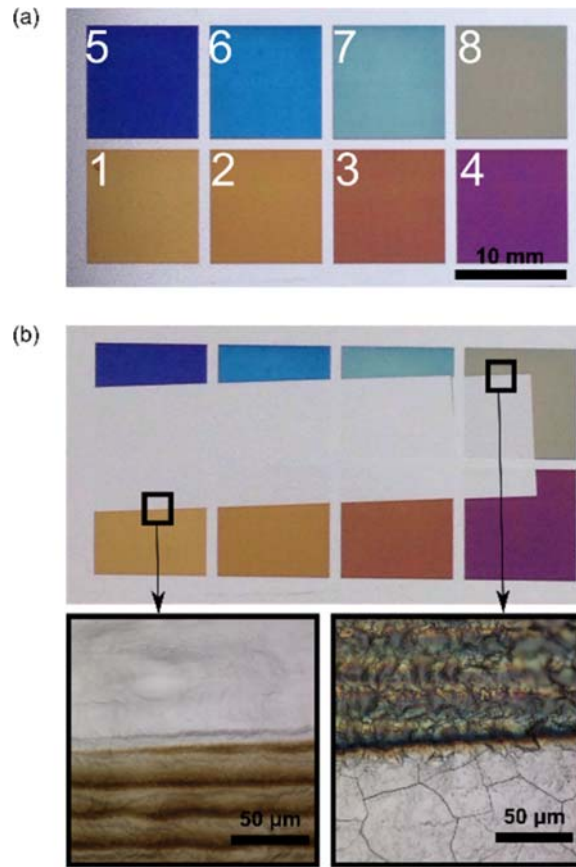
Fig. 2. Eight fields of colours generated on titanium substrate. (a) before erasing, (b) after erasing.

colours with their corresponding TiO$_2$ film thicknesses with any cumulative fluence exceeding 25 J/cm^2. The lowest cumulative fluence, i.e. 25 J/cm^2, was selected to investigate further the proposed method for erasing TiO$_2$ based colour marks in order to avoid any ablation and also to process the surface in the most efficient way. Figure 2 shows the processed fields of colours before and after being erased using accumulated fluence of 25 J/cm^2. There was no trace of colours left on the processed area of the substrate and its appearance was similar to that of as-received Ti substrates. However, the fields with the highest TiO$_2$ thickness, i.e. blue, light blue, greenish blue and yellowish blue, had some almost indistinguishable marks left after erasing them. These marks are colourless and they could be explained with the high

surface roughness that results after laser-induced oxidation with high fluence. Also, these almost indistinguishable marks could be considered as an evidence that the TiO_2 erasing process is the result of deoxidation by oxygen reduction rather than ablation as the as-received substrate roughness is not changed. In addition, it is important to stress that the pulse's fluence used was 0.35 J/cm^2 and it was much less than the ablation threshold of titanium, in particular approximately 1.17 J/cm^2 for the same laser pulse duration and wavelength [38].

Fig. 3. The three letters rewritten on the erased area of the colour marked fields

The objective of this research was not only to erase TiO_2 colour marks but also to develop a method that could be used to rewrite them on processed areas. Therefore, the acronym of the University (UOB) was rewritten over the erased area of the coloured field as shown in Figure 3. Especially, each of the letters in the acronym was produced with a different cumulative fluence, in particular 81, 120, and 220 J/cm^2, respectively.

The changes in the surface composition and film thicknesses were analysed employing XPS measurements prior to and after laser-induced oxygen reduction. Figure 4 depicts the Ti 2p

spectra acquired from Field 3 in Fig. 2 (a) before and after erasing the colour, respectively. The significant differences in the surface composition are clearly seen in the figure.

The binding energy of the Ti $2p_{3/2}$ component for each specific compound were analysed further. Prior to erasing, the spectrum is dominated by the contribution from TiO_2 at 459.3 eV [39]. A small contribution at 457.0 eV was also detected that could be due to a very small amount of Ti_2O_3 in the near-surface region. No contributions from Ti(II) at 455.5 eV or metallic Ti at 454.0 eV were observed within the sampling depth of Field 3. A similar Ti $2p$ spectra was obtained for Fields 2 and 4 before applying the laser-induced oxygen reduction (available in the supplementary information for the paper) and again the existence of a thick TiO_2 layer prior to erasing was detected on both fields.

After the erasing process (see Figure 4(b)), the Ti $2p$ spectrum revealed a reduction in the intensity of the TiO_2 components on all analysed fields along with increased contributions from multiple Ti oxidation states, namely TiO_2 (459.1 eV, 58.1 %), Ti_2O_3 (457.7 eV, 11.1 %), TiO/TiN (455.6 eV, 10.2 %) and metallic Ti (454.0 eV, 20.6 %). The metallic Ti $2p$ component was fitted using an asymmetric Lorentzian lineshape LA(1.2,5,8) that closely corresponds to the lineshape reported by Biesinger at al. [39]. Evidences of lower Ti oxidation states and metallic Ti in the spectrum suggests that the thickness of the TiO_2 film was reduced significantly and it was estimated to be approximately 2 nm after the erasing process (calculated using a thickogram [40]). Therefore, the erasing of the colours can be attributed fully to this significant reduction of the TiO_2 thickness after processing the area in Fig. 2 (b).
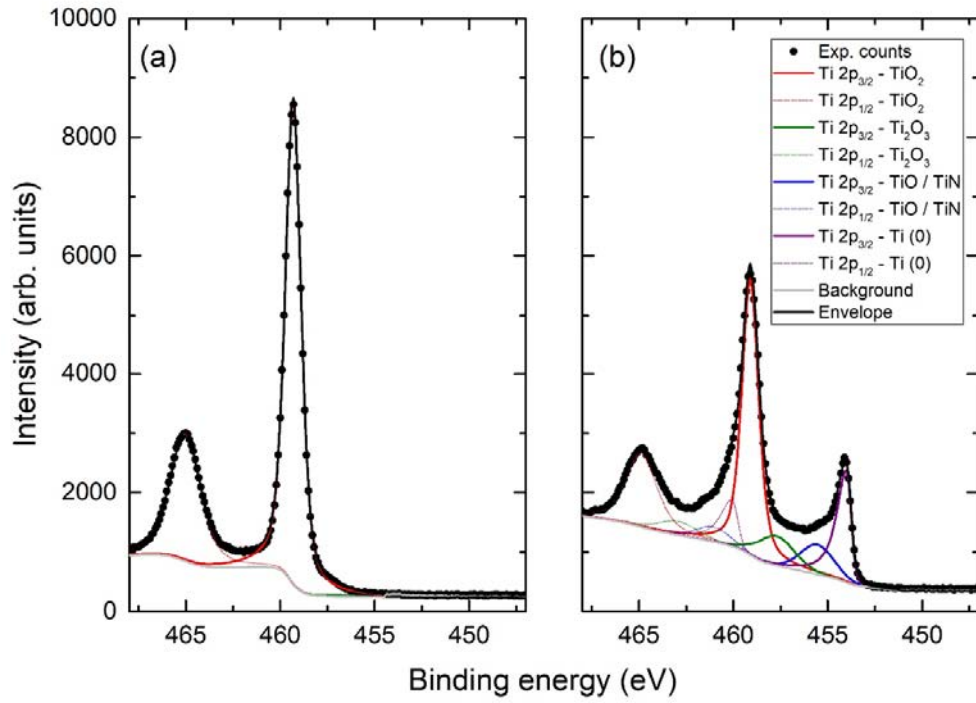
Fig. 4 Ti 2p XPS spectra obtained (a) before and (b) after the laser-induced oxygen reduction

.

Further evidences about the TiO_2 layer thickness reduction was found in the O 1s spectra shown in Figure 5 that was obtained again before and after the erasing process from Field 3 (see Fig. 2 (a)). The total elemental compositions obtained for Fields 2, 3 and 4 compared with that obtained after the processing of Field 3 (referred to as 3prime) are provided in Table 3. The TiO_2 contribution to the total detected O 1s intensity fell from 79 % to 62 % and the Ti:O ratio increased from 0.42:1 to 0.53:1, both clearly pointing to a thinning of the TiO_2 layer such that Ti atoms in lower oxidation states are now within the sampling depth in Field 3.
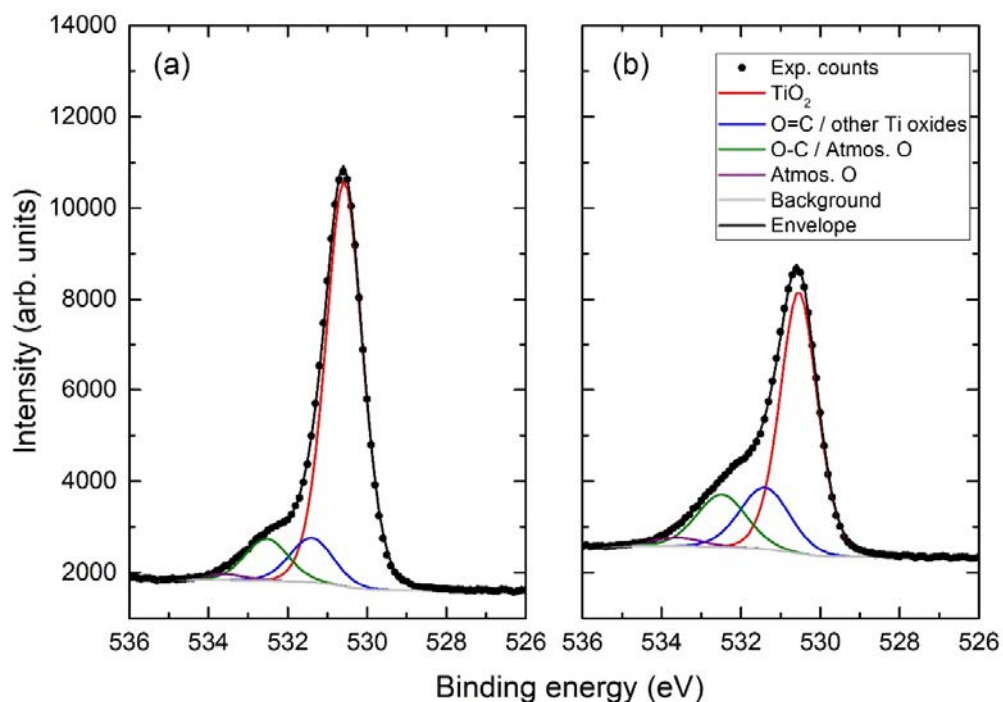
Fig. 5 O 1s XPS spectra obtained (a) before and (b) after the erasing process.

Table 3. Total elemental ratios derived from XPS measurements of Fields 2, 3, 4 and 3prime, accurate to +/- 2.0 %, together with the Ti:O ratio for them.

Sample	Ti	O	Ti:O	C	K	N	Zn	Ca	Na	Cl
2	15.8	39.6	0.4	40.1	0.3	1.6	0.7	0.7	1.2	0.2
3	18.1	43.5	0.42	35.6	0.2	1.5	0.3	0.4	0.5	0.0
4	16.6	40.9	0.41	35.3	1.4	1.2	0.3	0.5	2.9	1.0
3prime	20.3	38.6	0.53	37.5	0.0	3.3	0.1	0.1	0.1	0.0

The O 1s spectra obtained from Fields 2, 3, 4 and 3prime, available in the supplementary

information for the paper, clearly demonstrate the presence of substantial TiO_2 layers on the

surfaces of all of three fields prior to the erasing process. The relative intensity of TiO_2 in the

O 1s spectrum is significantly reduced for Field 3prime and thus the field exhibits a

significant thinning of the TiO_2 layer. The associated C $1s$ and N $1s$ spectra for Filed 3prime are also provided in the supplementary information to the paper and they confirm the presence of a small amount of TiN (at 396.6 eV to 397 eV in the N $1s$ spectra) and the formation of a small amount of TiC during the erasing process (282.1 eV in the C $1s$ spectrum). In addition, the downward shift in binding energy of the C-C/C-H component in the C $1s$ region, from 285.8 eV in Field 3 to 285.5 eV in Field 3prime, points again towards a thinning of the TiO_2 layer during the erasing process.

It should be noted that in the Ti $2p$ region, the contribution from TiN overlaps with TiO at a binding energy of 455.5 eV to 456 eV, and also the contribution from TiC in Field 3prime was too small to be resolved. Correlating the various XPS spectra and the atomic ratios provided in Table 3, there is a noticeable increase in the relative amount of N in Field 3prime. This suggests either the formation of TiN in the near surface region during erasing, or some small inclusions of TiN below the surface in Field 3 that are revealed during the erasing process. Of the three fields before applying the laser-induced oxygen reduction, Field 2 exhibits the most TiN and sub-oxide species, suggesting that this field has a thinner TiO_2 layer compared to Fields 3 and 4.

4. Conclusions

A method is proposed for selective erasing of oxide-based colour marks by laser-induced oxygen reduction. The colour marks can be reprocessed with a low fluence with a nanosecond laser in low oxygen environment and thus to diffuse oxygen out into the atmosphere and yield a lower form of metal oxides or a pure metal. Eight fields with different TiO_2 thicknesses with their corresponding colours were selectively processed to erase laser-induced colour marks.

Any cumulative fluence exceeding 25 J/cm^2 was sufficient to erase any laser-induced colours on the Ti substrates with only some almost indistinguishable marks left on fields with a higher TiO$_2$ thickness. These marks were colourless and were attributed to the high surface roughness that results after laser-induced oxidation with high fluence. The XPS analysis revealed that all fields were mainly comprised of TiO$_2$ prior to erasing with only small contributions from Ti$_2$O$_3$ and TiO/TiN. As a result of the proposed laser-induced oxygen reduction, the relative concentration of TiO$_2$ decreased substantially while and the overall amount of Ti in the near surface region increased. The results clearly show that the erasing of oxide-based colour marks is only due to oxygen diffusion back into the atmosphere and there were not any signs of laser ablation.

References

1. Boyd, I.W., *Laser processing of thin films and microstructures : oxidation, deposition, and etching of insulators*. Springer series in materials science. 1987, Berlin ; New York: Springer-Verlag. viii, 320 p.

2. Veiko, V., G. Kotov, M. Libenson, and M. Nikitin. *Thermochemical action of laser radiation*. in *Soviet Physics Doklady*. 1973.

3. Jwad, T., S.A. Deng, H. Butt, and S. DimovSchool, *Laser induced single spot oxidation of titanium.* Applied Surface Science, 2016. **387**: p. 617-624.

4. del Pino, A.P., P. Serra, and J.L. Morenza, *Coloring of titanium by pulsed laser processing in air.* Thin Solid Films, 2002. **415**(1-2): p. 201-205.

5. del Pino, A.P., P. Serra, and J.L. Morenza, *Oxidation of titanium through Nd : YAG laser irradiation.* Applied Surface Science, 2002. **197**: p. 887-890.

6. del Pino, A.P., P. Serra, and J.L. Morenza, *Laser surface processing of titanium in air: Influence of scan traces overlapping.* Journal of Laser Applications, 2003. **15**(2): p. 120-123.

7. Lavisse, L., J.M. Jouvard, L. Imhoff, O. Heintz, J. Korntheuer, C. Langlade, S. Bourgeois, and M.C.M. de Lucas, *Pulsed laser growth and characterization of thin films on titanium substrates.* Applied Surface Science, 2007. **253**(19): p. 8226-8230.

8. Adams, D.P., R.D. Murphy, D.J. Saiz, D.A. Hirschfeld, M.A. Rodriguez, P.G. Kotula, and B.H. Jared, *Nanosecond pulsed laser irradiation of titanium: Oxide growth and effects on underlying metal.* Surface & Coatings Technology, 2014. **248**: p. 38-45.

9. Ageev, E.I., Y.M. Andreeva, Y.Y. Karlagina, Y.R. Kolobov, S.S. Manokhin, G.V. Odintsova, A.A. Slobodov, and V.P. Veiko, *Composition analysis of oxide films formed on titanium surface under pulsed laser action by method of chemical thermodynamics.* Laser Physics, 2017. **27**(4).

10. Merlin, R. and T.A. Perry, *Growth of amorphous Ti2O3 layers by laser-induced oxidation.* Applied Physics Letters, 1984. **45**(8): p. 852-853.

11. Thuillard, M. and M. Vonallmen, *Laser-Produced Ti/Ti-Oxide Thin-Film Structures.* Applied Physics Letters, 1985. **47**(9): p. 936-938.

12. Akman, E. and E. Cerkezoglu, *Compositional and micro-scratch analyses of laser induced colored surface of titanium.* Optics and Lasers in Engineering, 2016. **84**: p. 37-43.

13. Johnson, P.B. and R.W. Christy, *Optical-Constants of Transition-Metals - Ti, V, Cr, Mn, Fe, Co, Ni, and Pd.* Physical Review B, 1974. **9**(12): p. 5056-5070.

14. Ordal, M.A., R.J. Bell, R.W. Alexander, L.A. Newquist, and M.R. Querry, *Optical-Properties of Al, Fe, Ti, Ta, W, and Mo at Submillimeter Wavelengths.* Applied Optics, 1988. **27**(6): p. 1203-1208.

15. Ion, J.C., *Laser processing of engineering materials : principles, procedure and industrial application*. 2005, Amsterdam ;: Boston : Elsevier/Butterworth-Heinemann. xviii, 556 p.

16. Bäuerle, D., *Laser processing and chemistry*. 4th ed. 2011: Springer Science & Business Media.

17. Brunette, D.M., *Titanium in medicine : material science, surface science, engineering, biological responses, and medical applications*. Engineering materials. 2001, Berlin ; New York: Springer. xiii, 1019 p.

18. *Standard Practice for Permanent Marking of Orthopaedic Implant Components*. 2013.

19. *Standard Practice for Surface Preparation and Marking of Metallic Surgical Implants*.

20. Abbott, A.P., G. Capper, D.L. Davies, K.J. McKenzie, and S.U. Obi, *Solubility of metal oxides in deep eutectic solvents based on choline chloride.* Journal of Chemical and Engineering Data, 2006. **51**(4): p. 1280-1282.

21. Hongyu, Z., *Laser-induced colours on metal surfaces*, in *SIMTech Technical Report PT/01/005/AM*. 2001.

22.   Daurelio, G., G. Chita, and M. Cinquepalmi, *New laser surface treatments: cleaning, de-rusting, de-oiling, de-painting, de-oxidizing and de-greasing.* Lasers in Material Processing, 1997. **3097**: p. 369-391.

23.   Veiko, V.P., E.A. Vlasova, A.S. Krivonosov, M.K. Moskvin, and G.V. Odintsova, *Laser decoration of precious metals.* Bulletin of the Russian Academy of Sciences: Physics, 2017. **81**(12): p. 1383-1386.

24.   Veiko, V., G. Odintsova, E. Vlasova, Y. Andreeva, A. Krivonosov, E. Ageev, and E. Gorbunova, *Laser coloration of titanium films: New development for jewelry and decoration.* Optics and Laser Technology, 2017. **93**: p. 9-13.

25.   Lugomer, S., *Laser technology : laser driven processes*. 1990, Englewood Cliffs, N.J.: Prentice Hall. xiv, 449 p.

26.   Kumstel, J. and B. Kirsch, *Polishing titanium- and nickel-based alloys using cw-laser radiation.* Lasers in Manufacturing (Lim 2013), 2013. **41**: p. 355-364.

27.   Nánai, L., I. Hevesi, B.S. Luk'yanchuk, E.M. Morozova, A.S. Rogachev, A.V. Simakhin, N.M. Sukonkhina, and G.A. Shafeev, *Characteristics of laser-heated titanium in a nitrogen atmosphere.* Acta Physica Hungarica, 1989. **65**(4): p. 405-409.

28.   Gyorgy, E., A.P. del Pino, P. Serra, and J.L. Morenza, *Surface nitridation of titanium by pulsed Nd : YAG laser irradiation.* Applied Surface Science, 2002. **186**(1-4): p. 130-134.

29.   Ohtsu, N., W. Saito, and M. Yamane, *Selectable surface nitridation of titanium using focused pulsed Nd:YAG laser irradiation with nitrogen gas blow.* Surface & Coatings Technology, 2014. **246**: p. 52-56.

30.   Ohtsu, N., K. Kodama, K. Kitagawa, and K. Wagatsuma, *Comparison of surface films formed on titanium by pulsed Nd:YAG laser irradiation at different powers and wavelengths in nitrogen atmosphere.* Applied Surface Science, 2010. **256**(14): p. 4522-4526.

31.   Shanjin, L. and W. Yang, *An investigation of pulsed laser cutting of titanium alloy sheet.* Optics and Lasers in Engineering, 2006. **44**(10): p. 1067-1077.

32.   Rao, B.T., R. Kaul, P. Tiwari, and A.K. Nath, *Inert gas cutting of titanium sheet with pulsed mode CO2 laser.* Optics and Lasers in Engineering, 2005. **43**(12): p. 1330-1348.

33.   Otto, J., R. Stumpe, and D. Bäuerle. *Laser Induced Reduction and Etching of Oxidic Perovskites*. 1984. Berlin, Heidelberg: Springer Berlin Heidelberg.

34.   Kapenieks, A., M. Eyett, and D. Bauerle, *Laser-Induced Surface Metallization of Ceramic Plzt.* Applied Physics a-Materials Science & Processing, 1986. **41**(4): p. 331-334.

35.   Liberts, G., M. Eyett, and D. Bauerle, *Laser-Induced Surface Reduction of the High-Tc Superconductor Yba2cu3o7-X.* Applied Physics a-Materials Science & Processing, 1988. **45**(4): p. 313-316.

36.   Shen, Y.Q., T. Freltoft, and P. Vase, *Laser Writing and Rewriting on Yba2cu3o7 Films.* Applied Physics Letters, 1991. **59**(11): p. 1365-1367.

37.   Tsukamoto, M., R. Nishii, Y. Muraki, T. Shinonaga, M. Yoshida, M. Takahashi, and N. Abe, *Rewriting of low electrical resistance lines on TiO2 film by writing and erasing with femtosecond and CW fiber lasers.* Applied Surface Science, 2014. **313**: p. 730-735.

38.   Gyorgy, E., A.P. del Pino, P. Serra, and J.L. Morenza, *Structure formation on titanium during oxidation induced by cumulative pulsed Nd : YAG laser irradiation.* Applied Physics a-Materials Science & Processing, 2004. **78**(5): p. 765-770.

39.   Biesinger, M.C., L.W.M. Lau, A.R. Gerson, and R.S.C. Smart, *Resolving surface chemical states in XPS analysis of first row transition metals, oxides and hydroxides: Sc, Ti, V, Cu and Zn.* Applied Surface Science, 2010. **257**(3): p. 887-898.

40.   Cumpson, P.J., *The Thickogram: a method for easy film thickness measurement in XPS.* Surface and Interface Analysis, 2000. **29**(6): p. 403-406.

Supplementary Information XPS
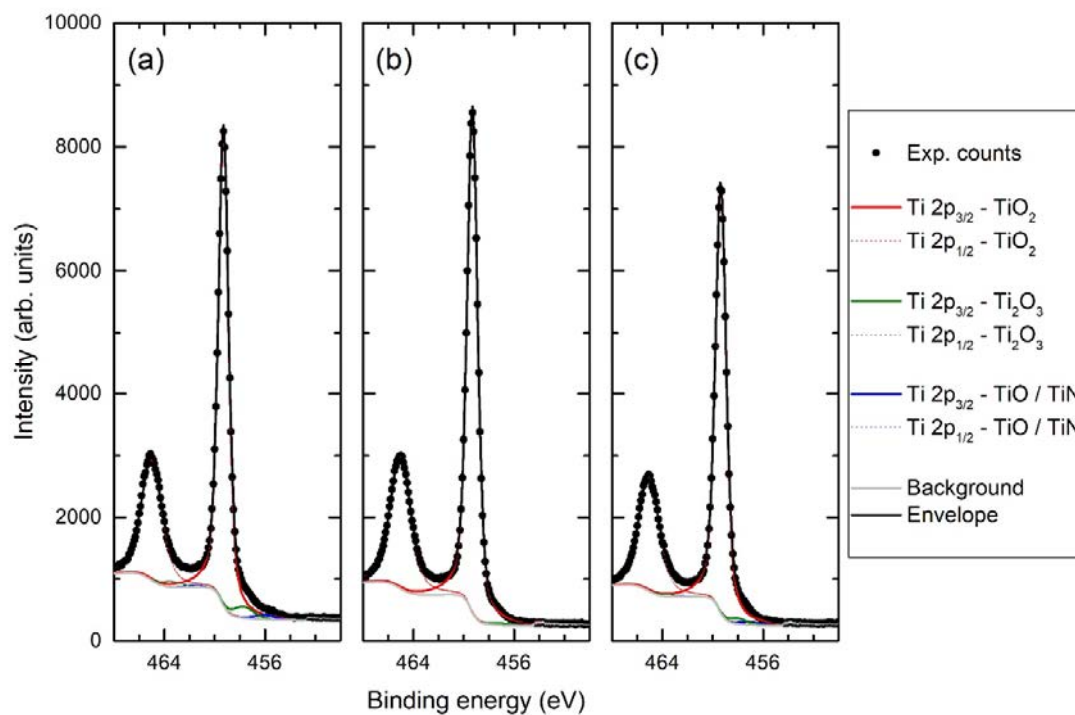
Fig. S1 – Ti 2*p* spectra from (a) sample 2, (b) sample 3 and (c) sample 4, all prior to the erasing process. A breakdown of the Ti 2*p* bonding environments is given in Table S1.

Table S1 – A breakdown of the percentage contributions to the Ti 2*p* spectra presented in Figures 4 and S1.

Sample	TiO$_2$	Ti$_2$O$_3$	TiO / TiN	Ti(0)
2	94.7	3.8	1.5	0
3	99.5	0.5	0	0
4	97.1	1.9	1	0
3prime	58.1	11.1	10.2	20.6
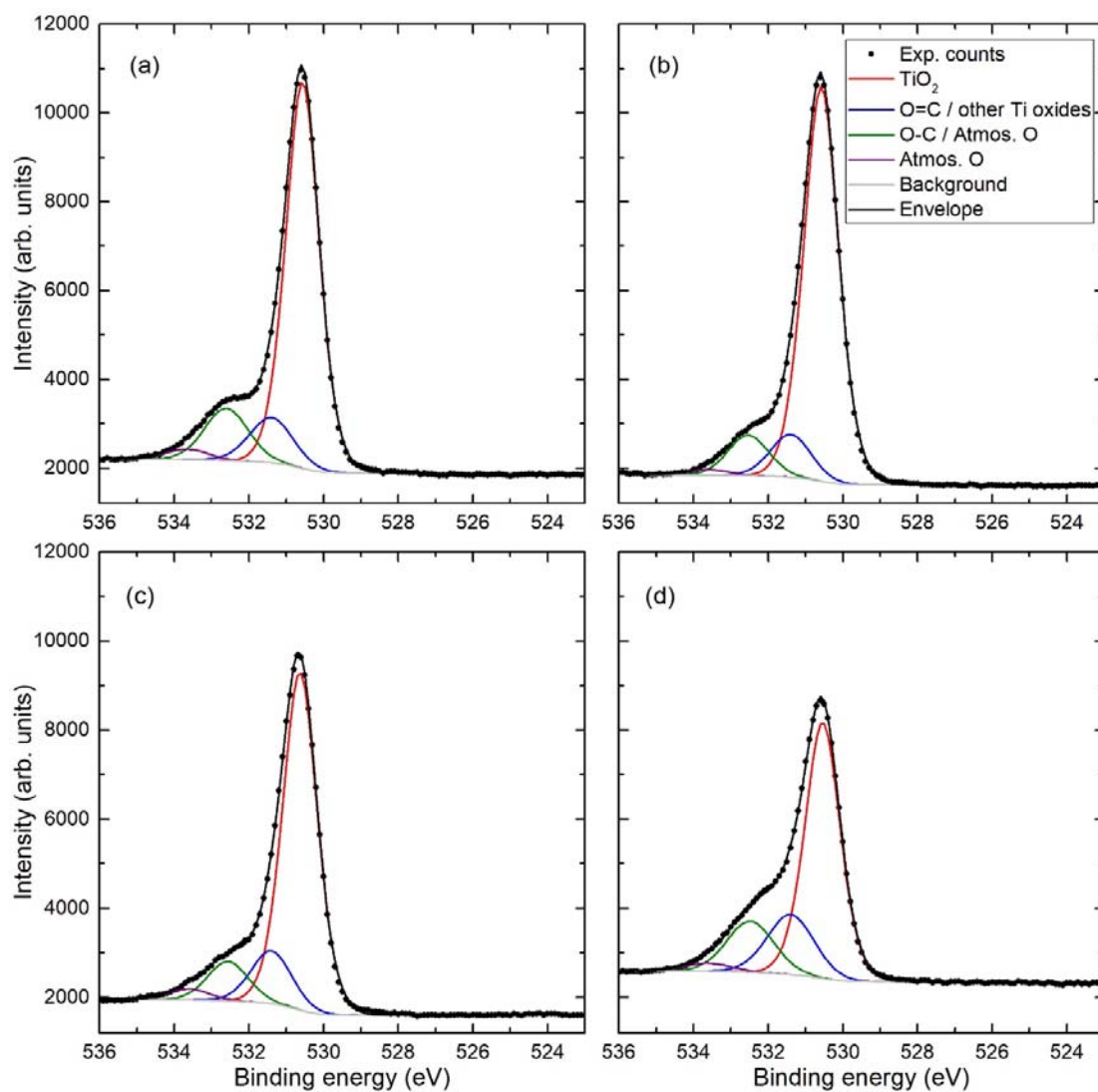
Figure S2 – O 1*s* spectra from (a) sample 2, (b) sample 3, (c) sample 4 and (d) sample 3prime. The data clearly show the reduction in the relative intensity of the TiO$_2$ component in sample 3prime, indicating that the TiO$_2$ layer on the surface has thinned during the erasing process.
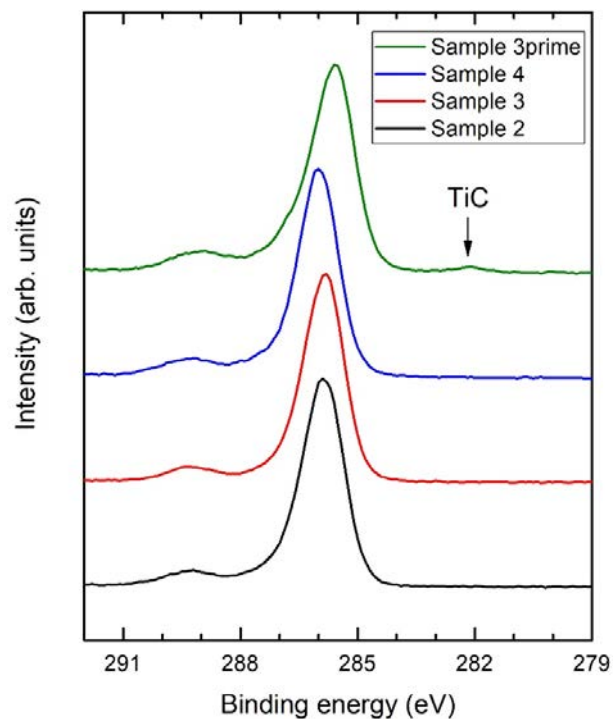
Figure S3 – C 1*s* spectra from samples 2, 3, 4 and 3prime. An additional feature at 282.1 eV was observed on sample 3prime, corresponding to a small amount of TiC in the near-surface region detected after erasing. The small downward shift in binding energy of the C-C/C-H component observed in sample 3prime is due to the thinning of the TiO_2 layer during the erasing process.
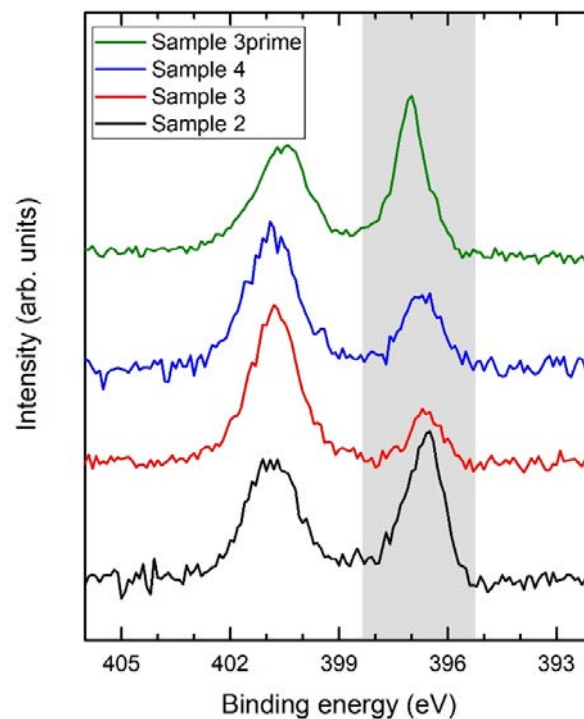
Figure S4 – N 1*s* spectra from samples 2, 3, 4 and 3prime. The area shaded in grey denotes the contribution to the spectrum from TiN. The increase in the intensity of this component between samples 3 and 3prime is due to the thinning of the TiO_2 layer during the erasing process.

CHAPTER 6:

LASER INDUCED RIPPLES' GRATINGS WITH ANGULAR PERIODICITY FOR FABRICATION OF DIFFRACTION HOLOGRAMS

Authors Contributions

This chapter of the alternative thesis format is published in Journal of Applied Surface Science. I am the first author of this publication. The paper's detail and contributions of co-authors are outlined below.

Jwad, T. [1], Penchev, P.[2], Nasrollahi, V.[3], & Dimov, S[**]. (2018) Laser induced ripples' gratings with angular periodicity for fabrication of diffraction holograms, Applied Surface Science, 453, 449-456.

[1] **Tahseen Jwad**: is the main author and he conceived the ideas, designed the experiments together with their experimental setups, process modelling/simulation work, and wrote the manuscript that was reviewed by the principal supervisor, **Prof. S. Dimov** (**).

[2]Pavel Penchev: contributed with the setting up of the beam delivery sub-system.

[3]Vahid Nasrollahi: contributed to the characterization work and the interpretation of obtained data.

CHAPTER 6: LASER INDUCED RIPPLES' GRATINGS WITH ANGULAR PERIODICITY FOR FABRICATION OF DIFFRACTION HOLOGRAMS

Abstract

Laser induced ripples (also known as Laser Induced Periodic Surface Structures, LIPSS) have gained considerable attention by both researchers and industry due to their surface functionalization applications. These ripples act as diffraction gratings for the visible light therefore it is widely used in some optical applications and colour marking. In this research, a method is proposed for producing diffractive patterns by varying the ripples' orientation along the beam path during the laser scanning and thus producing a pattern of ripples orientations. It was demonstrated that, by employing this method, it was possible to produce linear and radial pattern of gratings by changing the ripples' orientations following a given periodic function. As a result, smooth transitions of diffracted monochromatic light along the beam path were achieved, especially in diffracting colours from different locations when changing the azimuthal and incident angles of the incident white light. In addition, the reflection of polarized white light by such periodic gratings was investigated and it was shown that it was fully dependent on the ripples' orientations in respect to the light linear polarization vector.

Keywords: LIPSS, ripples, femtosecond laser, diffraction, selective reflection, polarization.

1. Introduction

Since laser induced ripples (also known as Laser Induced Periodic Surface Structures, LIPSS) were observed for the first time by Birnbaum [1] five decades ago, they attracted the interest of many researchers and industries due to their surface functionalization capabilities. LIPSS are considered the smallest structures that can be generated by using light in the far field [2] on most of the materials, e.g. metals, semiconductors, glasses and polymers [3, 4], and also in any environment, in particular in air, gases, liquids or vacuum [5, 6]. LIPSS have found applications in many fields including, but not limited to, brazing [7], modifying surfaces' wetting properties [8], improving surfaces' tribological performance [9-11], colour marking [12-16], inhibiting bacteria attachments and facilitating cell growth [17].

In general, LIPSS have three main characteristics: depth, periodicity and orientation. The capabilities to control them become very important in the effort to produce surfaces with given functional responses. Therefore, their formation mechanism has been investigated by many researchers in order to understand how the laser processing settings affect these three LIPSS characteristics and thus to meet the specific requirements of different applications. However, there is still no comprehensive understanding of this phenomenon [3, 4, 18] and the role of surface plasmon polaritions is still questionable [19]. From many reported empirical studies, it is evident that the LIPSS depth is nonlinearly dependent on laser fluence [20]. Regarding periodicity, LIPSS can have either low spatial frequency (LSFL) or high spatial frequency (HSFL). HSFL can be achieved using relatively low fluence [19, 21]. The periods of both LIPSS types are dependent on the laser wavelength (λ) [15]. For a normal beam incident angle, the LSFL period is approximately in the same order as λ, while for HSFL it is much smaller and depends on the material refractive index, typically $\lambda/2$ [22] or even smaller by one order of magnitude [23, 24]. In case of LSFL, an increase in the laser incident angle

leads to an increase of LIPSS period [25] (although some researchers have reported that the beam incident angle does not affect it [20]).

LIPSS orientation is dependent on the electric field vector of the laser polarization [20, 26]. Generally, their orientation is orthogonal to the linear polarization vector; however, LIPSS parallel to the polarization vector have been reported, too [18, 22]. Thus, the laser polarization state is very important and has a major impact on laser-matter interaction, especially on the absorbed laser energy that directly affects the damage threshold [27] and laser-matter interaction results, e.g., the width of the scanning lines [2, 28] and also the LIPSS orientation [2, 29] . Consequently, polarization state affects most of the laser-based processes such as, drilling [29-31], cutting [29, 32], welding [29] and texturing, e.g., the generation of complex surface structures [33]. Hence, the ability to control the polarization state during laser processing is important both for ablation and surface texturing applications [26].

The polarization state can be controlled employing different methods, such as using wave plates [30, 31, 34] or by employing diffractive optical elements, e.g. spatial light modulators (SLM) and liquid crystal polarizers [26, 35-38]. This control of the state of polarization is achieve by programming and modifying a specific pattern on the liquid crystal display which is controlled by means of an electric field. The effects of changing the polarization state were studied in the context of different laser processing applications, in particular, to control the orientation of nano gratings by superimposing two pulses [21]; to generate holograms inside glasses [39]; to produce polarization dependent diffraction gratings [40]; to imprint images on metallic surfaces [41]; to selectively control the appearance of two [42] or multiple symbols [13]; to generate HSFL and LSFL in one field [43]; to superimpose and overwrite LIPSS [19]; and also to generate LIPSS with different orientations within one spot using SLM [44]. Also, the influence of continuously altering the laser polarization state on drilling, sheet metal

cutting and texturing operations was reported [26, 30, 31, 33, 35, 45, 46]. Recently, Hermens et al. [38] reported a synchronized use of a liquid crystal polarizer, laser scanner and 5-axis stage to generate LIPSS with different orientations on freeform surfaces.

A method for producing a diffractive pattern on metallic surfaces by dynamically varying the laser electric field vector is reported in this paper. In particular, a method is proposed to continuously vary the orientation of the neighbouring LIPSS along the beam path by dynamically changing the orientation of a linear polarization vector during the scanning process. In this way, the LIPSS orientations within single spots or even within smaller areas (depending on the ratio between the polarization vector angular velocity and the scanning speed) were continuously varied to achieve smooth diffraction transitions along the beam path in the processed field. Then, to validate the method, linear and radial pattern of gratings were generated by following given periodic functions and scanning strategy.

2. Method

Before proceeding with the description of the proposed method, the LIPSS formation resulted from laser-matter interaction is discussed. LIPSS behaviour as a diffraction gratings when it shined with white light is also explained. In particular, when ultrashort pulsed laser with fluence close to the ablation threshold interact with metal substrates, periodic ripples are generated on the surface. The period, d, of these ripples is mainly dependent on the laser wavelength but also on laser incident angle and dielectric constants of both the medium and the substrate as shown in Equation 1 [25, 46].

$$d = \frac{\lambda}{Re\left(\sqrt{\dfrac{\varepsilon_d\ \varepsilon_m}{\varepsilon_d + \varepsilon_m}}\right)} \qquad \text{for normal incident angle} \qquad (1)$$

where: λ - laser wavelength, and ϵ_d and ϵ_m are the dielectric constants of the dielectric medium and the metal substrate, respectively.

Such ripples act as diffraction gratings when their periodicity is higher than the wavelength of the incident light. The diffraction order, angle and sensitivity are all dependent on the ripple periodicity and the light incident angle, as depicted in Fig.1. The functional dependence between them is as follows [47]:

$$m\lambda = d(\sin\theta_m - \sin\theta_{in}\cos\emptyset) \tag{2}$$

where: m is the diffraction order, θ_m - diffraction angle of the m_{th} order, θ_{in} - light incident angle, and ϕ - the azimuthal angle between the grating vector and the light incident vector in the grating plane.

Ripples diffract white light when the azimuthal angle of the incident light meets specific conditions. In particular, the light is diffracted when the projection of the incident light in the gratings plane is parallel to the LIPSS vector as illustrated in Figure 1. The intensity of the diffracted light depends on the azimuthal angle and it reaches its maximum when $\phi = 90°$ and drops down sinusoidally to its minimum at $\phi = 0°$. Thus, selectively diffractive patterns can be generated by controlling the rotation of the polarization vector of the laser and thus make the ripple orientation dependent on their position along the beam path. However, there should also be smooth transitions of ripples' orientations across the fields and therefore the angular rotational speed of the polarization vector should be synchronized with the beam scanning speed. In this way, any abrupt changes of ripples' orientation and discontinuities across the processing path can be avoided. As a result, depending on ripples' orientations, the processed

field diffracts the white light from some locations in the field but not from others when both the viewing and source angles are fixed.

Let us consider two cases of smooth light reflection across the processed fields by fixing the viewing angle. First, if the azimuthal angle of the light source varies, a smooth transition of diffracted/reflected light is achieved between neighbouring spots across the processed field. Another smooth transition of the diffracted/reflected light occurs when the incident angle of the source varies. Consequently, rainbow colours associated with the first order of diffraction appear one after another because of the varying incident angle that is followed by white light reflection with zero and -1 order diffractions, respectively. Hence, changes of incident or viewing angles lead to changes of the diffraction locations within the field and also in the diffracted colours.

As mentioned above, to generate LIPSS gratings with smooth transitions along the beam paths and thus across the processed fields, it is necessary to synchronize the angular speed of the polarization vector rotation with the beam scanning speed. The rest of the laser processing settings remain the same, in particular the scanning speed, scanning strategy, pulse repetition rate and pulse energy. It should be noted that the process settings that affect the scanning strategy (i.e., the beam scanning direction and hatch distance) also affect the resulting LIPSS gratings. The polarization vector rotation (i.e., the rotational speed of the $\lambda/2$ wave plate) could be constant, continuously varied (in particular by accelerating or decelerating it by any rate within one full revolution) or a combination of both; also, this could be implemented by setting specific time delays at every revolution or at a given number of them. Thus, by using any of the above process settings, a periodic function would be defined to repeat the LIPSS orientations at regular intervals. This function will have two variables, the ratio between the $\lambda/2$ wave plate angular speed and the beam scanning speed, and the hatch distance.
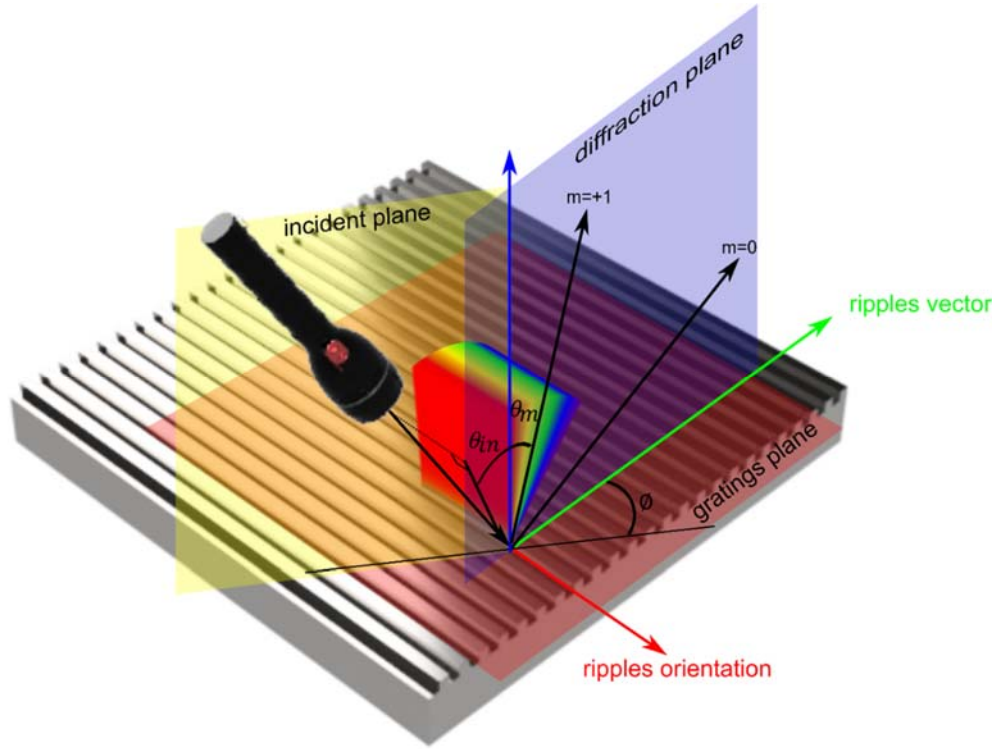
Fig. 1. Interaction of white light with diffraction gratings

A program in MATLAB was created to predict the resulting orientations along the beam path when one of these two variables is varied in the applied periodic function. The results are orientations' -matrices covering the processed field that can be depicted as images.

Since the resulting LIPSS grating is periodic, one of the variables driving this periodicity can be determined by applying the Fourier analysis. In particular, the consecutive LIPSS orientations along the beam path within the processed field would depend on the selected scanning strategy and could be represented as a vector. Then, the Fourier transform of the resulting vector can be computed to determine the respective Fourier series and periodic function. Ultimately, this function could be used to generate the digital signal that would control the $\lambda/2$ wave plate rotation.

3. Experimental setup

To experimentally validate the proposed method, a micro processing laser platform is used; an Yb-doped femtoseconds laser source from Amplitude Systemes with 310 fs pulse duration. A femtosecond source was selected as opposed to a nanosecond one since it is the common laser source for producing highly regular LIPSS without any thermal effect on substrate. A central wavelength of 1030 nm, maximum repetitions rate of 500 kHz, and maximum pulse energy of 10 µJ. The beam delivery sub-system includes a 3D scan head (RhoThor RTA) from Newson Engineering and a 100 mm telecentric focusing lens. In particular, the input beam diameter of 5 mm is focused to an irradiation spot size of 30 µm and maximum peak power of 32 MW.

A setup with a motorized polarizer was designed to rotate the λ/2 wave plate with a predefined angular speed. It was implemented employing a λ/2 wave polarizer, high-precision rotation mount from Thorlabs and a NEMA 17 stepper motor to drive the polarizer through a timing belt and pulleys. The motor has 200 steps per revolution (1.8° per step) and can be controlled for up to 6400 sub-steps/revolution using a controller (TB6600) from SODIAL(R). The control signals are generated by a C programme for a Raspberry-pi3 single board computer (SBC). Fig. 2 depicts the laser processing setup used in this research and a diagram showing the polarization control sub-system.
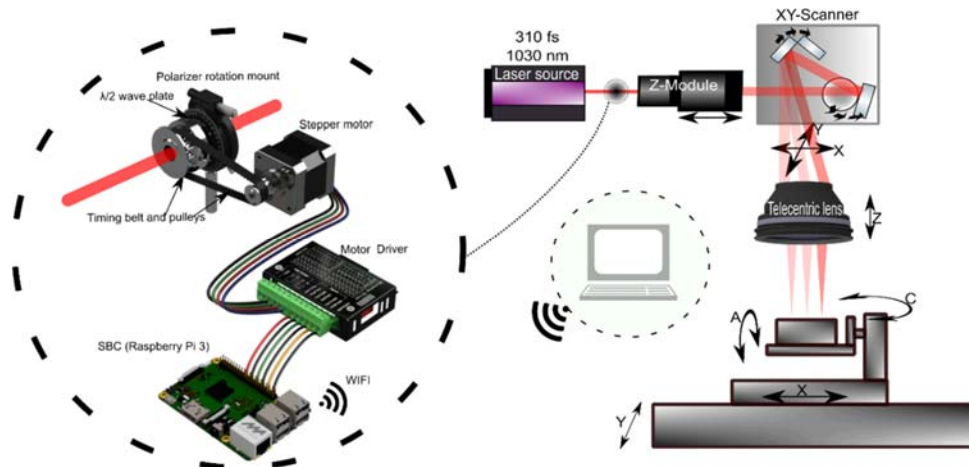

Fig. 2. The laser processing platform including the implemented motorized polarizer.

Mirror polished stainless steel grade 304 substrates were used. The samples were ultrasonically cleaned in water and acetone and dried with hot air prior to laser processing. The processed samples were analysed employing a focus variation microscope, Alicona G5 Infinite Focus system, and a scanning electron microscope, SEM JSM-6060. Images were captured using a Nikon D3300 camera.

3.1. Processing parameters

The most important factor affecting the ripples' generation is the laser fluence, which has to be close to the ablation threshold of the processed material. The other process settings that affect their generation are the pulse repetition rate, scanning speed and hatch distance. Some initial trials were performed to identify a suitable processing window to generate ripples' gratings on stainless steel 304 substrates. In particular, the following processing domain was identified: fluence in the range from 0.4 to 0.8 J/cm^2, number of pulses from 10 to 150 per spot, and hatch spacing in the range from 8 to 22 µm. The trials conducted showed that a higher fluence combined with a higher number of pulses and a smaller hatch distance led to darkening of the processed surface, while the opposite led to pale diffracted colours. A fluence of 0.56 J/cm^2 (a peak power of 13.5 MW) and 20 pulses per spot were found to be the best to produce colourful ripples' gratings and, therefore, they were used to produce all samples in this research.

To validate the proposed method for linear pattern of ripples' orientation, a number of 10 x 10 mm^2 fields were processed with a varying ratio between stepper motor rotation and beam scanning speeds (see Supplementary Fig. S1). All the fields were produced by applying a linear zigzag scanning strategy and the process settings used to produce one of them, (see Fig 3a) are discussed further in this section 4.1. In particular, the following process settings

were used to produce this field: a constant stepper motor speed of 7.8125 rev/sec achieved by sending control signals with 20 µs delays between them; and a scanning speed of 100 mm/s that resulted in a speed ratio of 28.125 °/mm. Consequently, the ripples' orientation was repeated periodically along the beam path at every 12.8 mm within this field. The laser pulse repetition rate was kept the same, 100 kHz, and thus to maintain the number of pulses per spot at 20. Another field with a linear pattern of ripples' orientation is selected to be presented to show the selective reflection of polarized white light in section 4.3, this field was produced with a stepper motor speed to scanning speed ratio of 159.8 °/mm along the beam path.

Another set of fields were produced but with a different processing strategy, in particular, with a circular hatching rather than the linear zigzag one. In this way, fields with a radial repetition of LIPSS orientations can be created (see Supplementary Fig. S2). One of these circular fields is shown in Fig 5a and is discussed further in this section 4.2. The diameter of the field is 10 mm and the circular hatch distance used is 12 µm. A constant stepper motor speed of 56.25 °/sec was applied to produce this field and this was achieved by setting a delay of 1 ms between the control signals. Laser scanning speed was set at 500 mm/sec, while the pulse repetition rate was 500 kHz. LIPSS orientations are repeated along the circular path at every 3200 mm. since the scanning speed is relatively high, the processing time for this circular field was approximately 13 sec only . Another field with a circular pattern of ripples' orientation is selected to be presented to show the selective reflection of polarized white light, this circular field was processed with a varying stepper motor speed to scanning speed ratio, especially starting with 159.8 °/mm and then decelerating it with a rate of 10 °/mm.

4. Results

Two sets of periodic patterns with linear and radial orientations were used to validate the proposed method and then to demonstrate a selective reflection of polarized white light in the sub-sections below.

4.1. Linear periodic ripples' gratings

The effects of changing azimuthal and incident angles are clearly depicted in Fig. 3a. With the change of the azimuthal angle the diffracted light is shifted from a given location to its neighboring one in both X and Y directions. This shift is due to the LIPSS orientation effect discussed in Section 2; in particular, the incident light is diffracted predominantly from LIPSS with grating vectors parallel to the light source in the LIPSS plane and not from those normal to it. The effect of the incident angle on the appearance of the field is also depicted in Fig 3a, where three different diffracted colours are shown together with the reflected white light (near to the zero order). The effect of changing the light incident angle can be seen in the supplementary video S1. It is worth noting that the used white light source has a high divergence; therefore, more than one colour is diffracted within the same viewing angle. The modelled distribution of the LIPSS orientations across this field (referred to as an orientations' matrix in Section 2) is shown in Figure 3b.
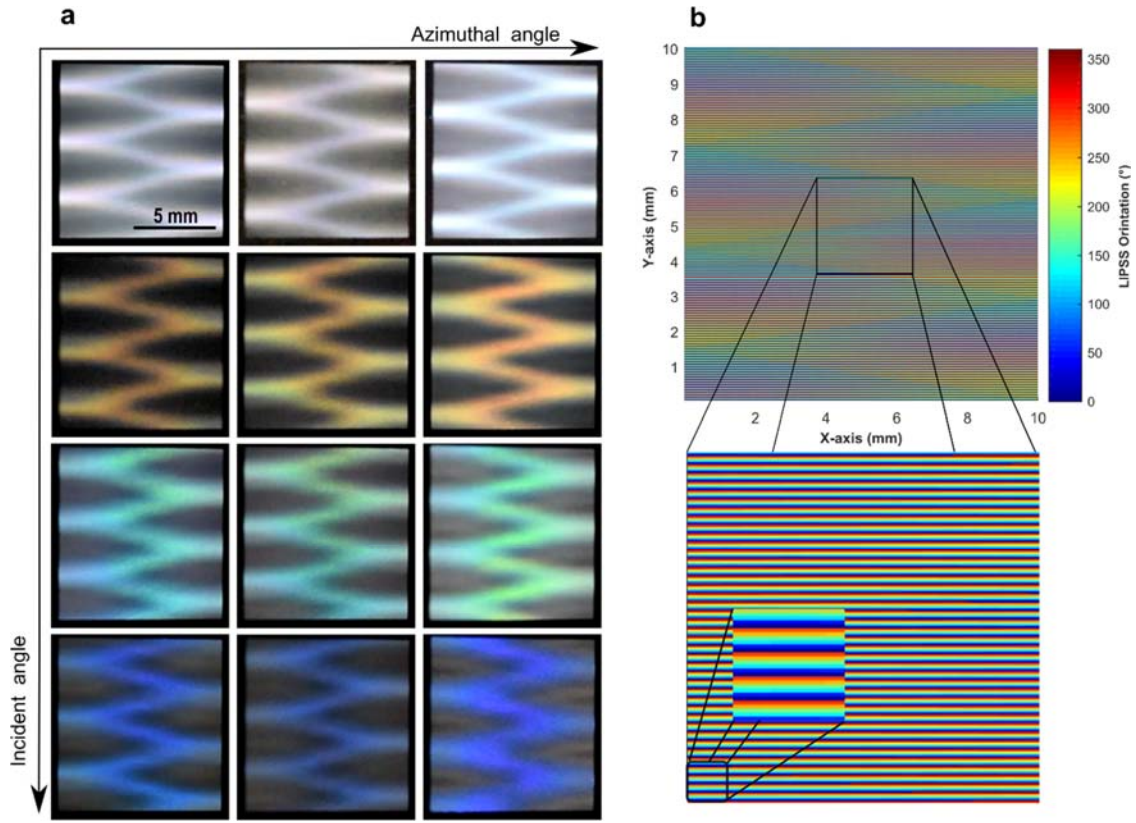
Fig. 3. A ripples' field with periodic orientations: (a) the effect of azimuthal and incident angles on the diffracted light from the processed field. (b) the modelled distribution of LIPSS orientations across the field.

An SEM image of an area of 66 x 48 μm² within the processed field showing the changing LIPSS orientations within this field of view is given in Fig. 4. The theoretical LIPSS period should be less than the laser wavelength, approximately 1 μm (see Equation 1 above). As expected, the measured period was approximately 810 nm. Thus, the LIPSS periodicity to wavelength ratio is approximately 0.78, close to reported ratios of 0.71 to 0.81 provided by other researchers [46]. This LIPSS periodicity of 810 nm leads to only first diffraction order of visible light wavelength spectrum (see Equation 2 above).

The overall processing time for producing the field was around 50 seconds and this could be reduced further by increasing the beam scanning and stepper motor rotational speeds or by employing a high-speed servomotor with a position feedback.
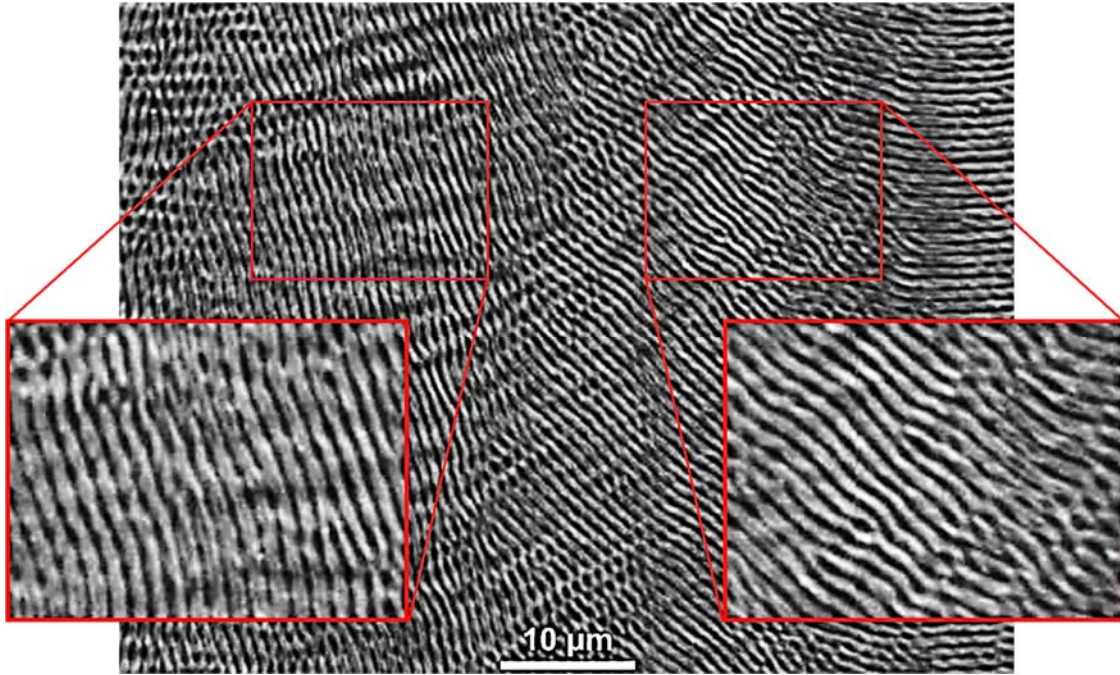
Fig. 4. A SEM image of the field shown in Fig. 3a that depicts different LIPSS orientations

4.2. Radial periodic ripples' gratings

The effects of changing the azimuthal and incident angles are depicted in Fig 5a, while Fig. 5b represents the modelled distribution of LIPSS orientations across the circular field. As it can be seen in Fig. 5a, the shifting of the diffracted light is radial rather than Cartesian. Although, the change in the polarization vector is periodic (a constant motor speed), the repetition of LIPSS orientations within the circle beam path is nonlinear. In particular, it is inversely proportional to the square of the circle radius and thus, with the increase of the radius, the frequency decreases. Also, the light diffracted from the field does not appear to be

symmetrical due to the fact that the circular scanning is not maintained across the field, in particular, it starts as circular at the field periphery and then transforms into an octagon at the centre. This can provide an additional effect to the diffractive pattern as shown in the figure. The effect of changing the source incident angles can be seen in the supplementary video S2.
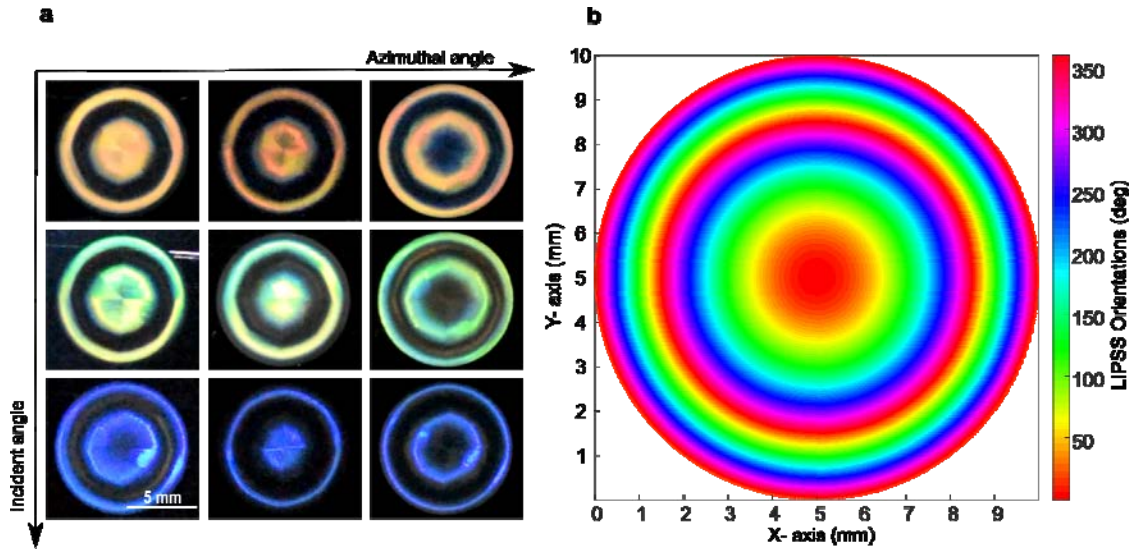
Fig. 5. A grating field with radial periodic ripples' orientations: (a) the effect of azimuthal and incident angles on the diffracted white light from the same processed field; (b) the modelled distribution of the ripples' orientations across the circular field.

4.3.   The effect of white light polarization

The fields produced employing the proposed method have another interesting optical property. In particular, they reflect the polarized white light depending on the relative orientations of different areas within the field with respect to the polarization vector. This behaviour is illustrated with the two fields in Fig. 6, one processed with a zigzag linear scanning strategy and the other with a circular one. The fields were viewed under the microscope using horizontal and vertical linear polarized light as shown in Fig. 6a and Fig. 6b, for the linear and in Fig. 6c and Fig. 6d for the circular, respectively. The change of the

polarization vector direction led to a change of the LIPSS grating reflection. This is due to the fact that the gratings only reflect light when their polarization vector is parallel to the gratings' vector. This effect is clearer in the centre of the second circular field in Fig. 6c and 6d; in particular, the change of the polarization vector led to reflection or no reflection at the centre.
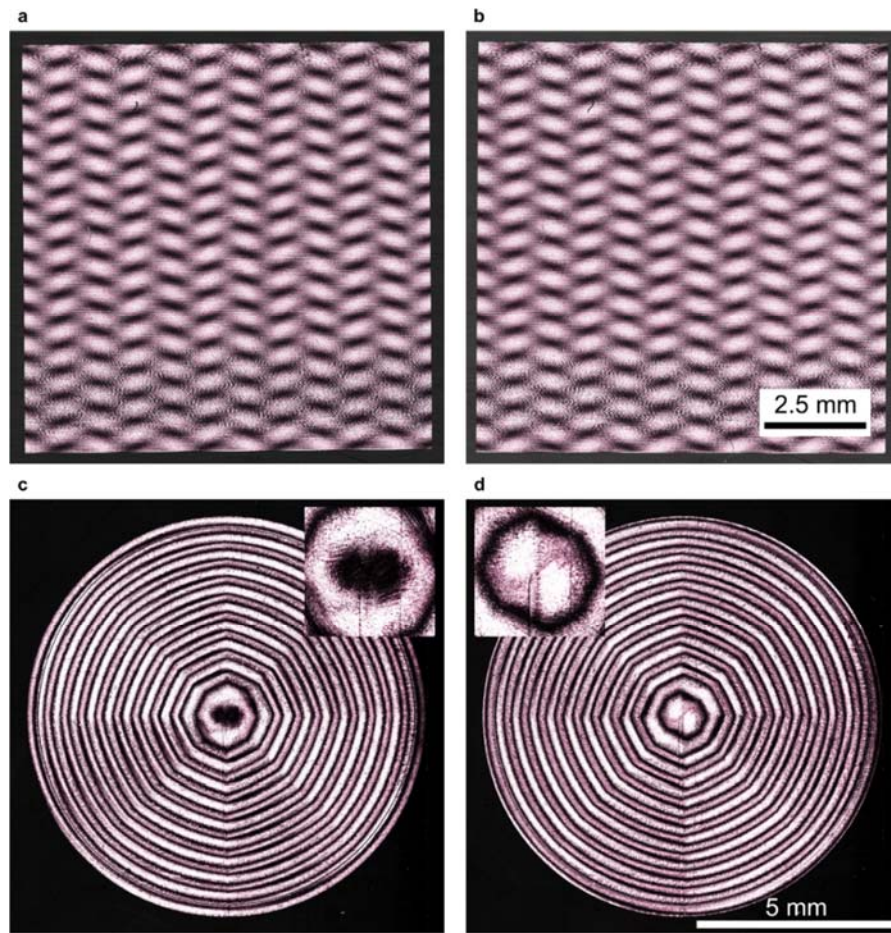
Fig. 6. The fields' reflection behaviour when interacting with a polarized white light: (a & b) a field processed with zigzag linear strategy reflecting vertical and horizontal linear polarized white light, respectively; (c & d) a field processed with a circular strategy reflecting vertical and horizontal linear polarized white light, respectively.

4.4.   Applications

The applications of surfaces with LIPSS gratings in which orientations are varied with a given periodic function are not limited to diffractive patterns and surface colour marking. Other possible applications that can be explored are the potential use of such gratings in micro fluidic systems for selective modification of wetting properties [48], in particular to create super hydrophobic tracks on surfaces and thus to direct the liquid flow along pre-defined paths. Another avenue to explore is the possibility to apply such periodic gratings in antibacterial applications [49] as some bacteria have the tendency to move along grooves. Thus, this could be inhibited by varying the LIPSS orientation with a predefined periodic function. In addition, cell migration surfaces can benefit from varied LIPSS orientations [17] and this can also be beneficial in aerodynamic and tribological applications.

Another aspect that is worth noting is that the LIPSS gratings produced with femtosecond lasers can be considered a cost-effective surface processing technology in the context of the application areas mentioned above. Bonse et al. [9] have calculated that the cost per unit area covered with LIPSS is approximately 0.1 €/cm^2. This considers the capital investment and maintenance costs associated with the use of state of the art femtosecond laser processing systems. Recently, Gnilitskyi et al. [50] reported that it was possible to produce highly regular LIPSS with a throughput 2.5 times' faster than that reported by Bonse et al. and thus the processing time and cost could be even lower. At the same time should be noted that the relative processing cost could be reduced further if the advantages and benefits of using such functionalized surfaces are taken into account in the context of specific applications. For example, the cost of using such LIPSS gratings for improving the tribological performance of products was calculated to go down to 0.002 €/ (cm^2 × %) as the friction reduction was approximately 50% [9].

5. Conclusions

A method for producing a diffractive pattern on metallic surfaces by using ripples' gratings is proposed in this research. Especially, gratings were generated where the LIPSS orientation was varied with a predefined periodic function. By applying the proposed method, linear and radial periodic ripples' gratings with angular periodicity were produced that exhibited a smooth diffraction of monochromatic light along beam path, especially reflecting different colours when changing the azimuthal and incident angles. In addition, the reflection of polarized white light by such gratings was investigated and it was shown that it was fully dependent on the LIPSS orientations in respect to the light linear polarization vector. In particular, the light was reflected only when the linear polarization vector was parallel to the LIPSS grating vector. The proposed method for producing periodic ripples' gratings could find applications in different areas, e.g. anti-counterfeiting, tribology, self-cleaning, bactericidal and cell growth enhancing surfaces, and optical applications.

References

1.   Birnbaum, M., *Semiconductor Surface Damage Produced by Ruby Lasers.* Journal of Applied Physics, 1965. **36**(11): p. 3688-&.

2.   Stankevic, V., G. Raciukaitis, F. Bragheri, X.W. Wang, E.G. Gamaly, R. Osellame, and S. Juodkazis, *Laser printed nano-gratings: orientation and period peculiarities.* Scientific Reports, 2017. **7**.

3.   Vorobyev, A.Y. and C.L. Guo, *Direct femtosecond laser surface nano/microstructuring and its applications.* Laser & Photonics Reviews, 2013. **7**(3): p. 385-407.

4.   Bonse, J., S. Hohm, S.V. Kirner, A. Rosenfeld, and J. Kruger, *Laser-Induced Periodic Surface Structures-A Scientific Evergreen.* Ieee Journal of Selected Topics in Quantum Electronics, 2017. **23**(3).

5.   Albu, C., A. Dinescu, M. Filipescu, M. Ulmeanu, and M. Zamfirescu, *Periodical structures induced by femtosecond laser on metals in air and liquid environments.* Applied Surface Science, 2013. **278**: p. 347-351.

6.   Yang, H.D., X.H. Li, G.Q. Li, C. Wen, R. Qiu, W.H. Huang, and J.B. Wang, *Formation of colorized silicon by femtosecond laser pulses in different background gases.* Applied Physics a-Materials Science & Processing, 2011. **104**(2): p. 749-753.

7.   Zhang, Y., G. Zou, L. Liu, A. Wu, Z. Sun, and Y.N. Zhou, *Vacuum brazing of alumina to stainless steel using femtosecond laser patterned periodic surface structure.* Materials Science and Engineering a-Structural Materials Properties Microstructure and Processing, 2016. **662**: p. 178-184.

8.   Long, J.Y., P.X. Fan, M.L. Zhong, H.J. Zhang, Y.D. Xie, and C. Lin, *Superhydrophobic and colorful copper surfaces fabricated by picosecond laser induced periodic nanostructures.* Applied Surface Science, 2014. **311**: p. 461-467.

9.   Bonse, J., R. Koter, M. Hartelt, D. Spaltmann, S. Pentzien, S. Hohm, A. Rosenfeld, and J. Kruger, *Tribological performance of femtosecond laser-induced periodic surface structures on titanium and a high toughness bearing steel.* Applied Surface Science, 2015. **336**: p. 21-27.

10.   Bonse, J., S. Hohm, R. Koter, M. Hartelt, D. Spaltmann, S. Pentzien, A. Rosenfeld, and J. Kruger, *Tribological performance of sub-100-nm femtosecond laser-induced periodic surface structures on titanium.* Applied Surface Science, 2016. **374**: p. 190-196.

11.   Bonse, J., R. Koter, M. Hartelt, D. Spaltmann, S. Pentzien, S. Hohm, A. Rosenfeld, and J. Kruger, *Femtosecond laser-induced periodic surface structures on steel and titanium alloy for tribological applications.* Applied Physics a-Materials Science & Processing, 2014. **117**(1): p. 103-110.

12.   Ou, Z.G., M. Huang, and F.L. Zhao, *Colorizing pure copper surface by ultrafast laser-induced near-subwavelength ripples.* Optics Express, 2014. **22**(14): p. 17254-17265.

13.   Li, J.W., G.Q. Li, Y.L. Hu, C.C. Zhang, X.H. Li, J.R. Chu, and W.H. Huang, *Selective display of multiple patterns encoded,with different oriented ripples using femtosecond laser.* Optics and Laser Technology, 2015. **71**: p. 85-88.

14.   Vorobyev, A.Y. and C.L. Guoa, *Colorizing metals with femtosecond laser pulses.* Applied Physics Letters, 2008. **92**(4).

15.   Li, G.Q., J.W. Li, Y.L. Hu, C.C. Zhang, X.H. Li, J.R. Chu, and W.H. Huang, *Femtosecond laser color marking stainless steel surface with different wavelengths.* Applied Physics a-Materials Science & Processing, 2015. **118**(4): p. 1189-1196.

16.   Li, G.Q., J.W. Li, Y.L. Hu, C.C. Zhang, X.H. Li, J.R. Chu, and W.H. Huang, *Realization of diverse displays for multiple color patterns on metal surfaces.* Applied Surface Science, 2014. **316**: p. 451-455.

17.   Martinez-Calderon, M., M. Manso-Silvan, A. Rodriguez, M. Gomez-Aranzadi, J.P. Garcia-Ruiz, S.M. Olaizola, and R.J. Martin-Palma, *Surface micro- and nano-texturing of stainless steel by femtosecond laser for the control of cell migration.* Scientific Reports, 2016. **6**.

18.   Buividas, R., M. Mikutis, and S. Juodkazis, *Surface and bulk structuring of materials by ripples with long and short laser pulses: Recent advances.* Progress in Quantum Electronics, 2014. **38**(3): p. 119-156.

19.   Gregorcic, P., M. Sedlacek, B. Podgornik, and J. Reif, *Formation of laser-induced periodic surface structures (LIPSS) on tool steel by multiple picosecond laser pulses of different polarizations.* Applied Surface Science, 2016. **387**: p. 698-706.

20.   Tan, B. and K. Venkatakrishnan, *A femtosecond laser-induced periodical surface structure on crystalline silicon.* Journal of Micromechanics and Microengineering, 2006. **16**(5): p. 1080-1085.

21.   Jia, T.Q., H.X. Chen, M. Huang, F.L. Zhao, J.R. Qiu, R.X. Li, Z.Z. Xu, X.K. He, J. Zhang, and H. Kuroda, *Formation of nanogratings on the surface of a ZnSe crystal irradiated by femtosecond laser pulses.* Physical Review B, 2005. **72**(12).

22.   Bonse, J., J. Kruger, S. Hohm, and A. Rosenfeld, *Femtosecond laser-induced periodic surface structures.* Journal of Laser Applications, 2012. **24**(4).

23.   Sugioka, K. and Y. Cheng, *Ultrafast lasers-reliable tools for advanced materials processing.* Light-Science & Applications, 2014. **3**.

24.   Sakabe, S., M. Hashida, S. Tokita, S. Namba, and K. Okamuro, *Mechanism for self-formation of periodic grating structures on a metal surface by a femtosecond laser pulse.* Physical Review B, 2009. **79**(3).

25.   Ionin, A.A., S.I. Kudryashov, S.V. Makarov, L.V. Seleznev, D.V. Sinitsyn, E.V. Golosov, O.A. Golosova, Y.R. Kolobov, and A.E. Ligachev, *Femtosecond laser color marking of metal and semiconductor surfaces.* Applied Physics a-Materials Science & Processing, 2012. **107**(2): p. 301-305.

26.   Jin, Y., O.J. Allegre, W. Perrie, K. Abrams, J. Ouyang, E. Fearon, S.P. Edwardson, and G. Dearden, *Dynamic modulation of spatially structured polarization fields for real-time control of ultrafast laser-material interactions.* Optics Express, 2013. **21**(21): p. 25333-25343.

27.   Venkatakrishnan, K., B. Tan, P. Stanley, and N.R. Sivakumar, *The effect of polarization on ultrashort pulsed laser ablation of thin metal films.* Journal of Applied Physics, 2002. **92**(3): p. 1604-1607.

28.   Han, W.N., L. Jiang, X.W. Li, P.J. Liu, L. Xu, and Y.F. Lu, *Continuous modulations of femtosecond laser-induced periodic surface structures and scanned line-widths on silicon by polarization changes.* Optics Express, 2013. **21**(13): p. 15505-15513.

29.   Weber, R., A. Michalowski, M. Abdou-Ahmed, V. Onuseit, V. Rominger, M. Kraus, and T. Graf, *Effects of Radial and Tangential Polarization in Laser Material Processing.* Lasers in Manufacturing 2011: Proceedings of the Sixth International Wlt Conference on Lasers in Manufacturing, Vol 12, Pt A, 2011. **12**: p. 21-30.

30.   Nolte, S., C. Momma, G. Kamlage, A. Ostendorf, C. Fallnich, F. von Alvensleben, and H. Welling, *Polarization effects in ultrashort-pulse laser drilling.* Applied Physics a-Materials Science & Processing, 1999. **68**(5): p. 563-567.

31.   Fohl, C., D. Breitling, and F. Dausinger, *Precise drilling of steel with ultrashort pulsed solid-state lasers.* Laser Processing of Advanced Materials and Laser Microtechnologies, 2003. **5121**: p. 271-279.

32.   Niziev, V.G. and A.V. Nesterov, *Influence of beam polarization on laser cutting efficiency.* Journal of Physics D-Applied Physics, 1999. **32**(13): p. 1455-1461.

33.   Skoulas, E., A. Manousaki, C. Fotakis, and E. Stratakis, *Biomimetic surface structuring using cylindrical vector femtosecond laser beams.* Scientific Reports, 2017. **7**.

34.   Hahne, S., B.F. Johnston, and M.J. Withford, *Pulse-to-pulse polarization-switching method for high-repetition-rate lasers.* Applied Optics, 2007. **46**(6): p. 954-958.

35.   Allegre, O.J., Y. Jin, W. Perrie, J. Ouyang, E. Fearon, S.P. Edwardson, and G. Dearden, *Complete wavefront and polarization control for ultrashort-pulse laser microprocessing.* Optics Express, 2013. **21**(18): p. 21198-21207.

36.   Cai, M.Q., P.P. Li, D. Feng, Y. Pan, S.X. Qian, Y.N. Li, C.H. Tu, and H.T. Wang, *Microstructures fabricated by dynamically controlled femtosecond patterned vector optical fields.* Optics Letters, 2016. **41**(7): p. 1474-1477.

37.   Hasegawa, S. and Y. Hayasaki, *Holographic Vector Wave Femtosecond Laser Processing.* International Journal of Optomechatronics, 2014. **8**(2): p. 73-88.

38.   Hermens, U., M. Pothen, K. Winands, K. Arntz, and F. Klocke, *Automated polarization control for the precise alignment of laser-induced self-organized nanostructures.* Optics and Lasers in Engineering, 2018. **101**: p. 44-50.

39.   Cai, W.J., A.R. Libertun, and R. Piestun, *Polarization selective computer-generated holograms realized in glass by femtosecond laser induced nanogratings.* Optics Express, 2006. **14**(9): p. 3785-3791.

40.   Beresna, M. and P.G. Kazansky, *Polarization Diffraction Grating Produced by Femtosecond Laser Nanostructuring in Glass.* 2010 Conference on Lasers and Electro-Optics (Cleo) and Quantum Electronics and Laser Science Conference (Qels), 2010.

41.   Dusser, B., Z. Sagan, H. Soder, N. Faure, J.P. Colombier, M. Jourlin, and E. Audouard, *Controlled nanostructrures formation by ultra fast laser pulses for color marking.* Optics Express, 2010. **18**(3): p. 2913-2924.

42.   Yao, J.W., C.Y. Zhang, H.Y. Liu, Q.F. Dai, L.J. Wu, S. Lan, A.V. Gopal, V.A. Trofimov, and T.M. Lysak, *Selective appearance of several laser-induced periodic surface structure patterns on a metal surface using structural colors produced by femtosecond laser pulses.* Applied Surface Science, 2012. **258**(19): p. 7625-7632.

43.   Ji, X., L. Jiang, X.W. Li, W.N. Han, Y. Liu, A.D. Wang, and Y.F. Lu, *Femtosecond laser-induced cross-periodic structures on a crystalline silicon surface under low pulse number irradiation.* Applied Surface Science, 2015. **326**: p. 216-221.

44.   Lam, B., J. Zhang, and C. Guo, *Generation of continuously rotating polarization by combining cross-polarizations and its application in surface structuring.* Optics Letters, 2017. **42**(15): p. 2870-2873.

45.   Allegre, O.J., W. Perrie, K. Bauchert, D. Liu, S.P. Edwardson, G. Dearden, and K.G. Watkins, *Real-time control of polarisation in ultra-short-pulse laser micro-machining.* Applied Physics a-Materials Science & Processing, 2012. **107**(2): p. 445-454.

46.   Graf', S. and F.A. Muller, *Polarisation-dependent generation of fs-laser induced periodic surface structures.* Applied Surface Science, 2015. **331**: p. 150-155.

47.   Hecht, E., *Optics*. 4th ed. 2002, Reading, Mass.: Addison-Wesley. vi, 698 p.

48.   Wu, B., M. Zhou, J. Li, X. Ye, G. Li, and L. Cai, *Superhydrophobic surfaces fabricated by microstructuring of stainless steel using a femtosecond laser.* Applied Surface Science, 2009. **256**(1): p. 61-66.

49.   Cunha, A., A.M. Elie, L. Plawinski, A.P. Serro, A.M.B. Rego, A. Almeida, M.C. Urdaci, M.C. Durrieu, and R. Vilar, *Femtosecond laser surface texturing of titanium as a method to reduce the adhesion of Staphylococcus aureus and biofilm formation.* Applied Surface Science, 2016. **360**: p. 485-493.

50.   Gnilitskyi, I., T.J. Derrien, Y. Levy, N.M. Bulgakova, T. Mocek, and L. Orazi, *High-speed manufacturing of highly regular femtosecond laser-induced periodic surface structures: physical origin of regularity.* Sci Rep, 2017. **7**(1): p. 8485.
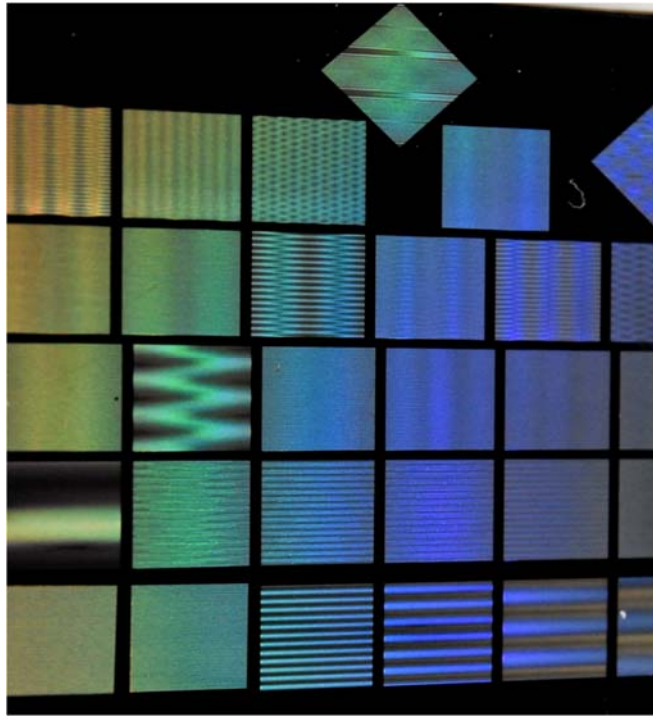
Figure S1. Fields of linear periodic pattern of ripples orientations processed with different stepper motor rotation to beam scanning speeds ratios.


Figure S2. Fields of radial periodic pattern of ripples orientations processed with different stepper motor rotation to beam scanning speed ratios.

CHAPTER 7 : CONTRIBUTIONS, CONCLUSIONS AND FUTURE WORK

This chapter presents the main contributions and conclusions reached in the research reported in the thesis. Suggestions for future work are also discussed.

7.1   Contributions

1. The colourization process, based on laser-induced oxidation, reported in the literature was carried out by laser scanning over a relatively large area as compared to the beam spot size. This has limited the applications of the process since the smallest fields of colours that can be produced are in millimetres scale. One of the novel aspects of this research is developing a method to control the size of the oxidation area and its thickness on titanium substrates. A single spot oxidation method is proposed to achieve this goal; it is based on irradiating substrates with the required accumulative fluence, i.e. fluence and number of pulses, spot by spot and thus to imprint colour images on titanium surfaces. By applying this approach, a pixel resolution down to the beam spot size with high spatial control in the processed area can be achieved. The proposed method could open the door to other potential applications, e.g. diffusers, that have not been explored so far due to resolution limitation of existing laser-induced oxidation methods.

2. Laser induced oxidation for colour marking of some specific metals, such as titanium and stainless steel, has been reported. This has limited the practical applications for this selective colour marking technology as it cannot be achieved on other materials. A method is proposed to apply the laser-induced oxidation for colour marking of any material by sputtering substrates with a thin film of titanium that then are processed

selectively with a nanosecond laser for direct writing applications with high spatial resolution.

To benefit from the proposed technology and the transparency of titanium dioxide, a method is proposed for direct writing diffraction optical devices on glass substrates. In particular, the fabrication of two-level phase-type FZPs with a nanosecond laser is demonstrated by creating titanium dioxide patterns on glass substrates with a thickness controlled at nano scale and thus to achieve the required phase delay based on the lens functional parameters. A model is created to determine the required thickness of FZP titanium dioxide zones based on its operational parameters.

3. A laser-induced oxygen reduction method is proposed for erasing selectively colour marks generated by laser-induced oxidation and thus to extend the flexibility and broaden the use of this technology. The method is based on reprocessing laser-induced titanium dioxides in low oxygen environment and this way to convert them into either lower oxides or into titanium for a potential follow up rewriting. It is important to stress that the removal of titanium dioxides is achieved without ablating the substrates.

4. LIPSS can be used as diffraction gratings since their periodicity is within the range of the visible light wavelength and their orientation is polarization dependant. These specific characteristics were utilised to develop a method for real time control of LIPSS orientation along the beam scanning path. Especially, a laser processing setup with a motorized polarizer and its controller for following a predefined speed function was designed and implemented to enable the synchronization of the $\lambda/2$ wave plate rotation with the laser scanning speed along the beam path. By employing the proposed method it is possible to generate LIPSS with smooth variations in their orientations along the scanning path and thus to create linear and circular pattern with different periods. In this

way, smooth transitions of diffracted light can be achieved from different locations within the processed fields and different rainbow colour effects observed when changing the viewing angles. The method was applied successfully to fabricate diffraction holograms.

7.2   Conclusions

1. A method is proposed to increase the spatial resolution of laser-induced oxidation process for colorizing and patterning titanium substrates. It employs a spot by spot or raster strategy instead of a commonly used scanning or vector one for large area processing to perform a single spot oxidation of titanium substrates. It was found that the required accumulative fluence to produce identical colours by both strategies were the same. The method was successfully applied for imprinting high resolution colour images on titanium substrates that required distinct colours to be produced on neighbouring spots by different accumulative fluence.

2. Since the machine's controllers commonly support the execution of vector-based processing strategies, a program was developed in MATLAB for implementing a raster processing approach that is necessary for performing a spot by spot colour imprinting. As the machine time is relatively high in raster compared with vector processing. Therefore the proposed spot by spot approach was modified into a layer-based one by grouping together the pixels that required the same laser parameters and thus to execute their processing more efficiently with a single command.

3. Due to the Gaussian distribution of the laser pulse energy, a beam size periodic structures appear on the processed substrates that lead to an angular dependence of

the colours due to diffraction and interference effects. These combined effects result in an additional effect as the observed colours become dependent on the viewing angle. These findings could be of interest to a range of applications as the proposed method could be used to imprint optical devices, e.g. for producing diffusers and oxides-based sensors. Furthermore, the resolution of the proposed method could be increased further by reducing the beam spot diameter with the use of high quality focusing lenses also by reducing the focal distance.

4. A method is proposed to extend the application area of laser-induced oxidation to colour marking of materials other than titanium. The method requires a thin film of titanium to be spattered on substrates before the follow up laser processing. For example, by applying a 200 nm thin film of pure titanium on glass substrates it is possible to imprint the same colours as those produced on titanium substrates. Thicker coatings do not affect the resulting colours, however a film thinner than 90 nm is not sufficient as it is just removed when subjected to laser irradiation.

5. A nanosecond laser direct writing (NSLDW) method is proposed to fabricate cost-effectively two-level phase-type FZPs with relatively high throughput on titanium coated substrates. The selectively created thin film of titanium dioxide acts as a phase shifter that is functionally dependent on film thickness, refractive index, and the light's wavelength. By varying the laser cumulative fluence the thickness of the film can be controlled at nano-scale and thus to tailor its phase delay and produce phase type FZP. In addition, an analytical method is proposed to determine the required titanium dioxide thickness difference between the FZP zones together with a validation model of the lenses' design.

6. The performance of two-level phase-type FZPs produced with proposed method was analysed and the results showed a good agreement with the theoretical predictions. In particular, efficiencies in the range of 5.5% to 20.9% can be achieved depending on the functional wavelength, as compared to the amplitude type FZP that has a theoretical efficiency of 10.1%. In addition, transmission mode FZP lenses can be fabricated, too, employing the proposed NSLDW method. However, the titanium film thickness along with glass thickness and its refractive index should be taken into account in designing transmission mode FZPs.

7. A method for erasing and or rewriting colour marks produced by laser-induced oxidation is presented. The method employs laser-induced oxygen reduction to metalize oxides or to convert them into lower oxides which usually have metallic characteristics. This can be achieved by reprocessing the induced colour marks with a nanosecond laser in a low oxygen environment and thus to diffuse the oxygen out into the atmosphere. The efficiency of the process depends on the built up substrate temperature and the oxygen concentration in surrounding environment. However, very low laser fluence was used to reprocess the colour marks in an argon inert gas chamber. It was possible to erase colour marks with different oxide thicknesses completely and as a result the reprocessed areas had a metallic appearance, similar to that of virgin substrates. The XPS analysis revealed that all fields were mainly comprised of TiO_2 prior to erasing with only small contributions from Ti_2O_3 and TiO/TiN. As a result of the proposed laser-induced oxygen reduction, the relative concentration of TiO_2 decreased substantially while the overall amount of Ti in the near surface region increased. The results clearly show that the erasing of oxide-based

47

colour marks is only due to oxygen diffusion back into the atmosphere and there were not any signs of laser ablation.

8. A method is proposed to generate diffraction holograms on metallic surfaces by smoothly varying the LIPSS orientation between two neighbouring spots. The LIPSS orientation is varied following a predefined periodic function by changing the laser polarization vector during the scanning. By applying the proposed method and also by changing the scanning strategies, linear and radial periodic ripples' gratings with angular periodicity were produced. The processed fields exhibited a smooth change in light diffraction along the linear and circular scanning paths when the viewing and/or the light incident angles were varied. Thus, different rainbow colours are diffracted from different locations in the field when changing the azimuthal and incident angles. In addition, these fields show polarization dependant reflection of white light, especially reflecting light only from areas where LIPSS direction vector is parallel to the polarization vector.

9. The proposed method for producing periodic ripples' orientations could find different applications, e.g. in anti-counterfeiting, tribology, self-cleaning, bactericidal and cell growth enhancing and optics.

7.3 Future work

- To reduce laser spot size by using high quality focusing lenses or lenses with smaller focal distances and thus to investigate the limits in increasing the imprinting resolution of the proposed single spot oxidation method. In addition, the use of a tophat beam energy profile should be investigated in order to carry out imprinting with a homogenous oxide thickness. Then, the performance of optical devices produced with Gaussian and tophat beams should be compared and analysed.

- To study the effects of the titanium coating thickness on glass substrates together with the laser processing parameters on the generated colours. Then to use higher quality focusing lenses or lenses with smaller focal distances to reduce the beam spot size and thus to investigate the capability of the proposed method for producing multi-level FZPs and other diffraction optical devices.

- To systematically study the effects of oxygen concentration and laser parameters on the laser-induced reduction technology when processing different oxide thicknesses and also to investigate the feasibility of processing surfaces with anodized colour effects.

- To design and implement a laser processing setup for attaining a higher polarization rotation speed while synchronizing it with higher speed beam deflectors and thus to achieve high spatial resolution changes of LIPSS orientation in a short time. This could be realized by using a stepper motor with higher speed or using servomotor with a feedback system to control the angular positions.

List of Refrences

1. Steen, W.M. and J. Mazumder, *Laser Material Processing, 4th Edition.* Laser Material Processing, 4th Edition, 2010: p. 1-558.
2. Kusinski, J., S. Kac, A. Kopia, A. Radziszewska, M. Rozmus-Gornikowska, B. Major, L. Major, J. Marczak, and A. Lisiecki, *Laser modification of the materials surface layer - a review paper.* Bulletin of the Polish Academy of Sciences-Technical Sciences, 2012. **60**(4): p. 711-728.
3. Ion, J.C., *Laser processing of engineering materials : principles, procedure and industrial application.* 2005, Amsterdam ;: Boston : Elsevier/Butterworth-Heinemann. xviii, 556 p.
4. Tian, Y.S., C.Z. Chen, S.T. Li, and Q.H. Huo, *Research progress on laser surface modification of titanium alloys.* Applied Surface Science, 2005. **242**(1-2): p. 177-184.
5. Chen, J., J. Shao, and H. Zhao. *Investigation on the mechanism of laser colorful marking.* in *Photonics and Optoelectronics Meetings (POEM) 2009: Industry Lasers and Applications.* 2009. International Society for Optics and Photonics.
6. Skowronski, L., A.J. Antonczak, M. Trzcinski, L. Lazarek, T. Hiller, A. Bukaluk, and A.A. Wronkowska, *Optical properties of laser induced oxynitride films on titanium.* Applied Surface Science, 2014. **304**: p. 107-114.
7. Bonse, J., S. Hohm, S.V. Kirner, A. Rosenfeld, and J. Kruger, *Laser-Induced Periodic Surface Structures-A Scientific Evergreen.* Ieee Journal of Selected Topics in Quantum Electronics, 2017. **23**(3).
8. Li, G.Q., J.W. Li, Y.L. Hu, C.C. Zhang, X.H. Li, J.R. Chu, and W.H. Huang, *Realization of diverse displays for multiple color patterns on metal surfaces.* Applied Surface Science, 2014. **316**: p. 451-455.
9. Dusser, B., Z. Sagan, H. Soder, N. Faure, J.P. Colombier, M. Jourlin, and E. Audouard, *Controlled nanostructrures formation by ultra fast laser pulses for color marking.* Optics Express, 2010. **18**(3): p. 2913-2924.
10. Maiman, T.H., *Optical and Microwave-Optical Experiments in Ruby.* Physical Review Letters, 1960. **4**(11): p. 564-566.
11. Maiman, T.H., *Stimulated Optical Radiation in Ruby.* Nature, 1960. **187**(4736): p. 493-494.
12. Bäuerle, D., *Laser processing and chemistry.* 4th ed. 2011: Springer Science & Business Media.
13. Breitling, D., A. Ruf, and F. Dausinger, *Fundamental aspects in machining of metals with short and ultrashort laser pulses.* Photon Processing in Microelectronics and Photonics Iii, 2004. **5339**: p. 49-63.
14. Mukherjee, S., S. Dhara, and P. Saha, *Laser surface remelting of Ti and its alloys for improving surface biocompatibility of orthopaedic implants.* Materials Technology, 2018. **33**(2): p. 106-118.
15. Boyd, I.W., *Laser processing of thin films and microstructures : oxidation, deposition, and etching of insulators.* Springer series in materials science. 1987, Berlin ; New York: Springer-Verlag. viii, 320 p.
16. Antonczak, A.J., L. Skowronski, M. Trzcinski, V.V. Kinzhybalo, L.K. Lazarek, and K.M. Abramski, *Laser-induced oxidation of titanium substrate: Analysis of the physicochemical structure of the surface and sub-surface layers.* Applied Surface Science, 2015. **325**: p. 217-226.
17. Jwad, T., S.A. Deng, H. Butt, and S. DimovSchool, *Laser induced single spot oxidation of titanium.* Applied Surface Science, 2016. **387**: p. 617-624.
18. Lugomer, S., *Laser technology : laser driven processes.* 1990, Englewood Cliffs, N.J.: Prentice Hall. xiv, 449 p.

19. Veiko, V., G. Kotov, M. Libenson, and M. Nikitin. *Thermochemical action of laser radiation*. in *Soviet Physics Doklady*. 1973.

20. Asmus, J. and F. Baker, *Record of the Tenth Symposium on Electron.* Ion, and Laser Beam Technology, Gaithersburg, MD, 1969: p. 241.

21. Arzuov, M.I., A.I. Barchukov, F.V. Bunkin, I.K. Vitalii, and A.A. Lyubin, *Violent surface oxidation of metals and associated phenomena resulting from continuous irradiation with CO 2 laser radiation.* Soviet Journal of Quantum Electronics, 1975. **5**(8): p. 931.

22. Arzuov, M.I., F.V. Bunkin, N.A. Kirichenko, V.I. Konov, and B.S. Lukyanchuk, *Dynamic Method of Measuring Optical and Diffusion Constants of Oxide-Films.* Jetp Letters, 1978. **27**(4): p. 214-218.

23. Arzuov, M.I., A.I. Barchukov, F.V. Bunkin, N.A. Kirichenko, I.K. Vitalii, and B.S. Luk'yanchuk, *Influence of interference effects in oxide films on the kinetics of laser heating of metals.* Soviet Journal of Quantum Electronics, 1979. **9**(3): p. 281.

24. Bunkin, F.V., N.A. Kirichenko, I.K. Vitalii, and B.S. Luk'yanchuk, *Interference effects in laser heating of metals in an oxidizing medium.* Soviet Journal of Quantum Electronics, 1980. **10**(7): p. 891.

25. Arzuov, M.I., A.I. Barchukov, F.V. Bunkin, N.A. Kirichenko, V.I. Konov, and B.S. Lukyanchuk, *Some Features of Laser-Heating of Oxidable Metals in the Air under Oblique Radiation Incidence.* Kvantovaya Elektronika, 1979. **6**(10): p. 2232-2236.

26. Metev, S.M., S.K. Savtchenko, and K.V. Stamenov, *Pattern Generation by Laser-Induced Oxidation of Thin Metal-Films.* Journal of Physics D-Applied Physics, 1980. **13**(4): p. L75-&.

27. Joshi, V.A., *Titanium alloys : an atlas of structures and fracture features*. 2006, Boca Raton: CRC/Taylor & Francis. 227 p.

28. Liu, X.Y., P.K. Chu, and C.X. Ding, *Surface modification of titanium, titanium alloys, and related materials for biomedical applications.* Materials Science & Engineering R-Reports, 2004. **47**(3-4): p. 49-121.

29. Lütjering, G. and J.C. Williams, *Titanium*. 2nd ed. Engineering materials and processes,. 2007, Berlin ; New York: Springer. xii, 442 p.

30. Chen, X. and S.S. Mao, *Titanium dioxide nanomaterials: Synthesis, properties, modifications, and applications.* Chemical Reviews, 2007. **107**(7): p. 2891-2959.

31. Puippe, J.C., *Surface treatments of titanium implants.* European Cells and Materials, 2003. **5**(1): p. 32-33.

32. Hongyu, Z., *Laser-induced colours on metal surfaces*. 2001, SIMTech Technical Report PT/01/005/AM.

33. Castellote, M. and N. Bengtsson, *Principles of TiO2 Photocatalysis*, in *Applications of Titanium Dioxide Photocatalysis to Construction Materials: State-of-the-Art Report of the RILEM Technical Committee 194-TDP*, Y. Ohama and D. Van Gemert, Editors. 2011, Springer Netherlands: Dordrecht. p. 5-10.

34. Eranna, G., B.C. Joshi, D.P. Runthala, and R.P. Gupta, *Oxide materials for development of integrated gas sensors - A comprehensive review.* Critical Reviews in Solid State and Materials Sciences, 2004. **29**(3-4): p. 111-188.

35. del Pino, A.P., P. Serra, and J.L. Morenza, *Oxidation of titanium through Nd : YAG laser irradiation.* Applied Surface Science, 2002. **197**: p. 887-890.

36. del Pino, A.P., J.M. Fernandez-Pradas, P. Serra, and J.L. Morenza, *Coloring of titanium through laser oxidation: comparative study with anodizing.* Surface & Coatings Technology, 2004. **187**(1): p. 106-112.

37. Akimov, A., A. Gagarin, V. Dagurov, V. Markin, and S. Pudkov, *Composition of an oxide film formed after pulsed heating of metal.* Sov. Phys. Tech. Phys, 1980. **25**: p. 1439.

38. Thuillard, M. and M. Vonallmen, *Laser-Produced Ti/Ti-Oxide Thin-Film Structures.* Applied Physics Letters, 1985. **47**(9): p. 936-938.

39. Strakovskii, L.G., *Ignition of Titanium by Means of Co2-Laser Radiation.* Combustion Explosion and Shock Waves, 1982. **18**(5): p. 579-582.

40. Lerner, E.J., *Laser marking systems strive for color and speed.* Laser Focus World, 1999. **35**(10): p. 123-+.

41. Brunette, D.M., *Titanium in medicine : material science, surface science, engineering, biological responses, and medical applications*. Engineering materials. 2001, Berlin ; New York: Springer. xiii, 1019 p.

42. *Standard Practice for Permanent Marking of Orthopaedic Implant Components*. 2013.

43. *Standard Practice for Surface Preparation and Marking of Metallic Surgical Implants*.

44. Abbott, A.P., G. Capper, D.L. Davies, K.J. McKenzie, and S.U. Obi, *Solubility of metal oxides in deep eutectic solvents based on choline chloride.* Journal of Chemical and Engineering Data, 2006. **51**(4): p. 1280-1282.

45. Carey, A., W. Steen, and D. Watkins. *Laser-surface ornamentation*. in *ICALEO'98*. 1998.

46. Langlade, C., A.B. Vannes, J.M. Krafft, and J.R. Martin, *Surface modification and tribological behaviour of titanium and titanium alloys after YAG-laser treatments.* Surface & Coatings Technology, 1998. **100**(1-3): p. 383-387.

47. Zheng, H.Y. and G.C. Lim, *Singapore Patent Application No. 200001597-4*. 2000.

48. Hongyu, Z., *Laser-induced colours on metal surfaces*, in *SIMTech Technical Report PT/01/005/AM*. 2001.

49. Zheng, H.Y. and G.C. Lim, *Process for laser marking metal surfaces*. 2003, Google Patents.

50. Zheng, H.Y., G.C. Lim, X.C. Wang, J.L. Tan, and J. Hilfiker, *Process study for laser-induced surface coloration.* Journal of Laser Applications, 2002. **14**(4): p. 215-220.

51. Rusconi, R. and J. Gold, *Color marking-High-contrast and decorative effects can be achieved in color on plastics and metals using ND: YAG or Nd: YVO4 lasers.* Industrial Laser Solutions-for Manufacturing, 2005. **20**(12): p. 16-19.

52. O'Hana, S., A.J. Pinkerton, K. Shoba, A.W. Gale, and L. Li, *Laser surface colouring of titanium for contemporary jewellery.* Surface Engineering, 2008. **24**(2): p. 147-153.

53. Crespo-Monteiro, N., N. Destouches, E. Gamet, L. Bois, F. Chassagneux, L. Nadar, and F. Vocanson, *Role of silver nanoparticles in the laser-induced reversible colour-marking and controlled crystallization of mesoporous titania films.* Plasmonics: Metallic Nanostructures and Their Optical Properties Ix, 2011. **8096**.

54. Antonczak, A.J., B. Stepak, P.E. Koziol, and K.M. Abramski, *The influence of process parameters on the laser-induced coloring of titanium.* Applied Physics a-Materials Science & Processing, 2014. **115**(3): p. 1003-1013.

55. Veiko, V., G. Odintsova, E. Ageev, Y. Karlagina, A. Loginov, A. Skuratova, and E. Gorbunova, *Controlled oxide films formation by nanosecond laser pulses for color marking.* Optics Express, 2014. **22**(20): p. 24342-24347.

56. Schuöcker, D., *Handbook of the Eurolaser Academy*. Vol. 2. 1998: Springer Science & Business Media.

57. Burgess, A. and K. Feng, *Color laser marking: A new marking and decorating alternative for olefins.* International Conference on Additives for Polyolefins, 1998: p. 185-191.

58. Quinten, M., *A practical guide to optical metrology for thin films*. 2013, Weinheim, Germany: Wiley-VCH. xii, 211 p.

59. Rancourt, J.D., *Optical thin films : user handbook*. 1996, Bellingham, Wash., USA: SPIE Optical Engineering Press. xii, 289 p.

60. Hecht, E., *Optics, 4th.* International edition, Addison-Wesley, San Francisco, 2002. **3**: p. 2.

61. Stenzel, O., *The Physics of thin film optical spectra*. 2005: Springer.

62. Lavisse, L., D. Grevey, C. Langlade, and B. Vannes, *The early stage of the laser-induced oxidation of titanium substrates.* Applied Surface Science, 2002. **186**(1-4): p. 150-155.

63.   del Pino, A.P., P. Serra, and J.L. Morenza, *Coloring of titanium by pulsed laser processing in air.* Thin Solid Films, 2002. **415**(1-2): p. 201-205.

64.   Adams, D.P., R.D. Murphy, D.J. Saiz, D.A. Hirschfeld, M.A. Rodriguez, P.G. Kotula, and B.H. Jared, *Nanosecond pulsed laser irradiation of titanium: Oxide growth and effects on underlying metal.* Surface & Coatings Technology, 2014. **248**: p. 38-45.

65.   Brihmat-Hamadi, F., E.H. Amara, and H. Kellou, *Characterization of Titanium Oxide Layers Formation Produced by Nanosecond Laser Coloration.* Metallurgical and Materials Transactions B-Process Metallurgy and Materials Processing Science, 2017. **48**(3): p. 1439-1449.

66.   Brihmat-Hamadi, F., E.H. Amara, L. Lavisse, J.M. Jouvard, E. Cicala, and H. Kellou, *Surface laser marking optimization using an experimental design approach.* Applied Physics a-Materials Science & Processing, 2017. **123**(4).

67.   del Pino, A.P., P. Serra, and J.L. Morenza, *Laser surface processing of titanium in air: Influence of scan traces overlapping.* Journal of Laser Applications, 2003. **15**(2): p. 120-123.

68.   Merlin, R. and T.A. Perry, *Growth of amorphous Ti2O3 layers by laser-induced oxidation.* Applied Physics Letters, 1984. **45**(8): p. 852-853.

69.   Jerkiewicz, G., H. Strzelecki, and A. Wieckowski, *A new procedure of formation of multicolor passive films on titanium: Compositional depth profile analysis.* Langmuir, 1996. **12**(4): p. 1005-1010.

70.   Akman, E. and E. Cerkezoglu, *Compositional and micro-scratch analyses of laser induced colored surface of titanium.* Optics and Lasers in Engineering, 2016. **84**: p. 37-43.

71.   Lavisse, L., J.M. Jouvard, L. Imhoff, O. Heintz, J. Korntheuer, C. Langlade, S. Bourgeois, and M.C.M. de Lucas, *Pulsed laser growth and characterization of thin films on titanium substrates.* Applied Surface Science, 2007. **253**(19): p. 8226-8230.

72.   Lawrence, S.K., D.P. Adams, D.F. Bahr, and N.R. Moody, *Deformation and fracture of a mudflat-cracked laser-fabricated oxide on Ti.* Journal of Materials Science, 2013. **48**(11): p. 4050-4058.

73.   Ageev, E.I., Y.M. Andreeva, Y.Y. Karlagina, Y.R. Kolobov, S.S. Manokhin, G.V. Odintsova, A.A. Slobodov, and V.P. Veiko, *Composition analysis of oxide films formed on titanium surface under pulsed laser action by method of chemical thermodynamics.* Laser Physics, 2017. **27**(4).

74.   Denker, S.P., *Electronic Properties of Titanium Monoxide.* Journal of Applied Physics, 1966. **37**(1): p. 142-&.

75.   Johnson, P.B. and R.W. Christy, *Optical-Constants of Transition-Metals - Ti, V, Cr, Mn, Fe, Co, Ni, and Pd.* Physical Review B, 1974. **9**(12): p. 5056-5070.

76.   Ordal, M.A., R.J. Bell, R.W. Alexander, L.A. Newquist, and M.R. Querry, *Optical-Properties of Al, Fe, Ti, Ta, W, and Mo at Submillimeter Wavelengths.* Applied Optics, 1988. **27**(6): p. 1203-1208.

77.   Devore, J.R., *Refractive Indices of Rutile and Sphalerite.* Journal of the Optical Society of America, 1951. **41**(6): p. 416-419.

78.   Siefke, T., S. Kroker, K. Pfeiffer, O. Puffky, K. Dietrich, D. Franta, I. Ohlidal, A. Szeghalmi, E.B. Kley, and A. Tunnermann, *Materials Pushing the Application Limits of Wire Grid Polarizers further into the Deep Ultraviolet Spectral Range.* Advanced Optical Materials, 2016. **4**(11): p. 1780-1786.

79.   Skowronski, L., A.A. Wachowiak, and A. Grabowski, *Characterization of optical and microstructural properties of semitransparent TiO2/Ti/glass interference decorative coatings.* Applied Surface Science, 2016. **388**: p. 731-740.

80.   Skowronski, L., M. Trzcinski, A.J. Antonczak, P. Domanowski, M. Kustra, W. Wachowiak, M.K. Naparty, T. Hiller, A. Bukaluk, and A.A. Wronkowska, *Characterisation of coloured TiOx/Ti/glass systems.* Applied Surface Science, 2014. **322**: p. 209-214.

81.	Veiko, V.P., E.A. Vlasova, A.S. Krivonosov, M.K. Moskvin, and G.V. Odintsova, *Laser decoration of precious metals.* Bulletin of the Russian Academy of Sciences: Physics, 2017. **81**(12): p. 1383-1386.

82.	Veiko, V., G. Odintsova, E. Vlasova, Y. Andreeva, A. Krivonosov, E. Ageev, and E. Gorbunova, *Laser coloration of titanium films: New development for jewelry and decoration.* Optics and Laser Technology, 2017. **93**: p. 9-13.

83.	Lecka, K.M., M.R. Wojcik, and A.J. Antonczak, *Laser-Induced Color Marking of Titanium: A Modeling Study of the Interference Effect and the Impact of Protective Coating.* Mathematical Problems in Engineering, 2017.

84.	Ocana, R. and A. Calatayud, *Laser-induced coloring on small titanium surfaces.* Laser Assisted Net Shape Engineering 9 International Conference on Photonic Technologies Proceedings of the Lane 2016, 2016. **83**: p. 225-232.

85.	Gyorgy, E., A.P. del Pino, P. Serra, and J.L. Morenza, *Structure formation on titanium during oxidation induced by cumulative pulsed Nd : YAG laser irradiation.* Applied Physics a-Materials Science & Processing, 2004. **78**(5): p. 765-770.

86.	Lavisse, L., M.C. Sahour, J.M. Jouvard, G. Pillon, M.C.M. de Lucas, S. Bourgeois, and D. Grevey, *Growth of titanium oxynitride layers by short pulsed Nd:YAG laser treatment of Ti plates: Influence of the cumulated laser fluence.* Applied Surface Science, 2009. **255**(10): p. 5515-5518.

87.	Espejo, H.M. and D.F. Bahr, *Substrate cracking in Ti-6Al-4V driven by pulsed laser irradiation and oxidation.* Surface & Coatings Technology, 2017. **322**: p. 46-50.

88.	Pan, A.F., W.J. Wang, X.S. Mei, B.X. Zheng, and Z.X. YanState, *Cracks growth behaviors of commercial pure titanium under nanosecond laser irradiation for formation of nanostructure-covered microstructures (with sub-5-mu m).* Applied Surface Science, 2016. **387**: p. 1046-1053.

89.	O'Shea, D.C., T.J. Suleski, A.D. Kathman, and D.W. Prather, *Diffractive Optics: Design, Fabrication, and Test*. 2004.

90.	Taghizadeh, M.R., P. Blair, B. Layet, I.M. Barton, A.J. Waddie, and N. Ross, *Design and fabrication of diffractive optical elements.* Microelectronic Engineering, 1997. **34**(3-4): p. 219-242.

91.	Keskinbora, K., C. Grevent, U. Eigenthaler, M. Weigand, and G. Schutz, *Rapid prototyping of Fresnel zone plates via direct Ga(+) ion beam lithography for high-resolution X-ray imaging.* ACS Nano, 2013. **7**(11): p. 9788-97.

92.	Jahns, J. and S.J. Walker, *Two-dimensional array of diffractive microlenses fabricated by thin film deposition.* Appl Opt, 1990. **29**(7): p. 931-6.

93.	Rajasekharan, R., H. Butt, Q. Dai, T.D. Wilkinson, and G.A.J. Amaratunga, *Can Nanotubes Make a Lens Array?* Advanced Materials, 2012. **24**(23): p. Op170-Op173.

94.	Moghimi, M.J., J. Fernandes, A. Kanhere, and H.R. Jiang, *Micro-Fresnel-Zone-Plate Array on Flexible Substrate for Large Field-of-View and Focus Scanning.* Scientific Reports, 2015. **5**.

95.	Moebius, M., K. Vora, S. Kang, P. Munoz, G.L. Deng, and E. Mazur, *Direct Laser Writing of 3D Gratings and Diffraction Optics.* 2015 Conference on Lasers and Electro-Optics (Cleo), 2015.

96.	Sohn, I.B., M.J. Ko, Y.S. Kim, and Y.C. Noh, *Direct femtosecond laser lithography for photoresist patterning.* Optical Engineering, 2009. **48**(2).

97.	Otto, J., R. Stumpe, and D. Bäuerle. *Laser Induced Reduction and Etching of Oxidic Perovskites*. 1984. Berlin, Heidelberg: Springer Berlin Heidelberg.

98.	Kumstel, J. and B. Kirsch, *Polishing titanium- and nickel-based alloys using cw-laser radiation.* Lasers in Manufacturing (Lim 2013), 2013. **41**: p. 355-364.

99.	Kapenieks, A., M. Eyett, and D. Bauerle, *Laser-Induced Surface Metallization of Ceramic Plzt.* Applied Physics a-Materials Science & Processing, 1986. **41**(4): p. 331-334.

100. Liberts, G., M. Eyett, and D. Bauerle, *Laser-Induced Surface Reduction of the High-Tc Superconductor Yba2cu3o7-X.* Applied Physics a-Materials Science & Processing, 1988. **45**(4): p. 313-316.
101. Shen, Y.Q., T. Freltoft, and P. Vase, *Laser Writing and Rewriting on Yba2cu3o7 Films.* Applied Physics Letters, 1991. **59**(11): p. 1365-1367.
102. Tsukamoto, M., R. Nishii, Y. Muraki, T. Shinonaga, M. Yoshida, M. Takahashi, and N. Abe, *Rewriting of low electrical resistance lines on TiO2 film by writing and erasing with femtosecond and CW fiber lasers.* Applied Surface Science, 2014. **313**: p. 730-735.
103. Nánai, L., I. Hevesi, B.S. Luk'yanchuk, E.M. Morozova, A.S. Rogachev, A.V. Simakhin, N.M. Sukonkhina, and G.A. Shafeev, *Characteristics of laser-heated titanium in a nitrogen atmosphere.* Acta Physica Hungarica, 1989. **65**(4): p. 405-409.
104. Gyorgy, E., A.P. del Pino, P. Serra, and J.L. Morenza, *Surface nitridation of titanium by pulsed Nd : YAG laser irradiation.* Applied Surface Science, 2002. **186**(1-4): p. 130-134.
105. Ohtsu, N., W. Saito, and M. Yamane, *Selectable surface nitridation of titanium using focused pulsed Nd:YAG laser irradiation with nitrogen gas blow.* Surface & Coatings Technology, 2014. **246**: p. 52-56.
106. Ohtsu, N., K. Kodama, K. Kitagawa, and K. Wagatsuma, *Comparison of surface films formed on titanium by pulsed Nd:YAG laser irradiation at different powers and wavelengths in nitrogen atmosphere.* Applied Surface Science, 2010. **256**(14): p. 4522-4526.
107. Yilbas, B.S., H. Ali, and C. Karatas, *[INVITED] Laser gas assisted treatment of Ti-alloy: Analysis of surface characteristics.* Optics and Laser Technology, 2016. **78**: p. 159-166.
108. Khafaji, N.Y., A.G. Demir, L. Vitali, D. Fustinoni, A. Niro, B. Previtali, and Z.A. Taha, *Optical characterization of laser coloured processing atmospheres titanium under different processing atmospheres.* Surface & Coatings Technology, 2017. **321**: p. 156-163.
109. Daurelio, G., G. Chita, and M. Cinquepalmi, *New laser surface treatments: cleaning, de-rusting, de-oiling, de-painting, de-oxidizing and de-greasing.* Lasers in Material Processing, 1997. **3097**: p. 369-391.
110. Birnbaum, M., *Semiconductor Surface Damage Produced by Ruby Lasers.* Journal of Applied Physics, 1965. **36**(11): p. 3688-&.
111. Stankevic, V., G. Raciukaitis, F. Bragheri, X.W. Wang, E.G. Gamaly, R. Osellame, and S. Juodkazis, *Laser printed nano-gratings: orientation and period peculiarities.* Scientific Reports, 2017. **7**.
112. Vorobyev, A.Y. and C.L. Guo, *Direct femtosecond laser surface nano/microstructuring and its applications.* Laser & Photonics Reviews, 2013. **7**(3): p. 385-407.
113. Long, J.Y., P.X. Fan, M.L. Zhong, H.J. Zhang, Y.D. Xie, and C. Lin, *Superhydrophobic and colorful copper surfaces fabricated by picosecond laser induced periodic nanostructures.* Applied Surface Science, 2014. **311**: p. 461-467.
114. Bonse, J., R. Koter, M. Hartelt, D. Spaltmann, S. Pentzien, S. Hohm, A. Rosenfeld, and J. Kruger, *Tribological performance of femtosecond laser-induced periodic surface structures on titanium and a high toughness bearing steel.* Applied Surface Science, 2015. **336**: p. 21-27.
115. Bonse, J., S. Hohm, R. Koter, M. Hartelt, D. Spaltmann, S. Pentzien, A. Rosenfeld, and J. Kruger, *Tribological performance of sub-100-nm femtosecond laser-induced periodic surface structures on titanium.* Applied Surface Science, 2016. **374**: p. 190-196.
116. Bonse, J., R. Koter, M. Hartelt, D. Spaltmann, S. Pentzien, S. Hohm, A. Rosenfeld, and J. Kruger, *Femtosecond laser-induced periodic surface structures on steel and titanium alloy for tribological applications.* Applied Physics a-Materials Science & Processing, 2014. **117**(1): p. 103-110.
117. Ou, Z.G., M. Huang, and F.L. Zhao, *Colorizing pure copper surface by ultrafast laser-induced near-subwavelength ripples.* Optics Express, 2014. **22**(14): p. 17254-17265.

118. Li, J.W., G.Q. Li, Y.L. Hu, C.C. Zhang, X.H. Li, J.R. Chu, and W.H. Huang, *Selective display of multiple patterns encoded,with different oriented ripples using femtosecond laser.* Optics and Laser Technology, 2015. **71**: p. 85-88.

119. Vorobyev, A.Y. and C.L. Guoa, *Colorizing metals with femtosecond laser pulses.* Applied Physics Letters, 2008. **92**(4).

120. Li, G.Q., J.W. Li, Y.L. Hu, C.C. Zhang, X.H. Li, J.R. Chu, and W.H. Huang, *Femtosecond laser color marking stainless steel surface with different wavelengths.* Applied Physics a-Materials Science & Processing, 2015. **118**(4): p. 1189-1196.

121. Martinez-Calderon, M., M. Manso-Silvan, A. Rodriguez, M. Gomez-Aranzadi, J.P. Garcia-Ruiz, S.M. Olaizola, and R.J. Martin-Palma, *Surface micro- and nano-texturing of stainless steel by femtosecond laser for the control of cell migration.* Scientific Reports, 2016. **6**.

122. Bonse, J., J. Kruger, S. Hohm, and A. Rosenfeld, *Femtosecond laser-induced periodic surface structures.* Journal of Laser Applications, 2012. **24**(4).

123. Sugioka, K. and Y. Cheng, *Ultrafast lasers-reliable tools for advanced materials processing.* Light-Science & Applications, 2014. **3**.

124. Sakabe, S., M. Hashida, S. Tokita, S. Namba, and K. Okamuro, *Mechanism for self-formation of periodic grating structures on a metal surface by a femtosecond laser pulse.* Physical Review B, 2009. **79**(3).

125. Tan, B. and K. Venkatakrishnan, *A femtosecond laser-induced periodical surface structure on crystalline silicon.* Journal of Micromechanics and Microengineering, 2006. **16**(5): p. 1080-1085.

126. Gecys, P., A. Vinciunas, M. Gedvilas, A. Kasparaitis, R. Lazdinas, and G. Raciukaitis, *Ripple Formation by Femtosecond Laser Pulses for Enhanced Absorptance of Stainless Steel.* Journal of Laser Micro Nanoengineering, 2015. **10**(2): p. 129-133.

127. Buividas, R., M. Mikutis, and S. Juodkazis, *Surface and bulk structuring of materials by ripples with long and short laser pulses: Recent advances.* Progress in Quantum Electronics, 2014. **38**(3): p. 119-156.

128. Fohl, C., D. Breitling, and F. Dausinger, *Precise drilling of steel with ultrashort pulsed solid-state lasers.* Laser Processing of Advanced Materials and Laser Microtechnologies, 2003. **5121**: p. 271-279.

129. Nolte, S., C. Momma, G. Kamlage, A. Ostendorf, C. Fallnich, F. von Alvensleben, and H. Welling, *Polarization effects in ultrashort-pulse laser drilling.* Applied Physics a-Materials Science & Processing, 1999. **68**(5): p. 563-567.

130. Hahne, S., B.F. Johnston, and M.J. Withford, *Pulse-to-pulse polarization-switching method for high-repetition-rate lasers.* Applied Optics, 2007. **46**(6): p. 954-958.

131. Allegre, O.J., Y. Jin, W. Perrie, J. Ouyang, E. Fearon, S.P. Edwardson, and G. Dearden, *Complete wavefront and polarization control for ultrashort-pulse laser microprocessing.* Optics Express, 2013. **21**(18): p. 21198-21207.

132. Jin, Y., O.J. Allegre, W. Perrie, K. Abrams, J. Ouyang, E. Fearon, S.P. Edwardson, and G. Dearden, *Dynamic modulation of spatially structured polarization fields for real-time control of ultrafast laser-material interactions.* Optics Express, 2013. **21**(21): p. 25333-25343.

133. Cai, M.Q., P.P. Li, D. Feng, Y. Pan, S.X. Qian, Y.N. Li, C.H. Tu, and H.T. Wang, *Microstructures fabricated by dynamically controlled femtosecond patterned vector optical fields.* Optics Letters, 2016. **41**(7): p. 1474-1477.

134. Hasegawa, S. and Y. Hayasaki, *Holographic Vector Wave Femtosecond Laser Processing.* International Journal of Optomechatronics, 2014. **8**(2): p. 73-88.

135. Hermens, U., M. Pothen, K. Winands, K. Arntz, and F. Klocke, *Automated polarization control for the precise alignment of laser-induced self-organized nanostructures.* Optics and Lasers in Engineering, 2018. **101**: p. 44-50.

136. Jia, T.Q., H.X. Chen, M. Huang, F.L. Zhao, J.R. Qiu, R.X. Li, Z.Z. Xu, X.K. He, J. Zhang, and H. Kuroda, *Formation of nanogratings on the surface of a ZnSe crystal irradiated by femtosecond laser pulses.* Physical Review B, 2005. **72**(12).

137. Cai, W.J., A.R. Libertun, and R. Piestun, *Polarization selective computer-generated holograms realized in glass by femtosecond laser induced nanogratings.* Optics Express, 2006. **14**(9): p. 3785-3791.

138. Beresna, M. and P.G. Kazansky, *Polarization Diffraction Grating Produced by Femtosecond Laser Nanostructuring in Glass.* 2010 Conference on Lasers and Electro-Optics (Cleo) and Quantum Electronics and Laser Science Conference (Qels), 2010.

139. Yao, J.W., C.Y. Zhang, H.Y. Liu, Q.F. Dai, L.J. Wu, S. Lan, A.V. Gopal, V.A. Trofimov, and T.M. Lysak, *Selective appearance of several laser-induced periodic surface structure patterns on a metal surface using structural colors produced by femtosecond laser pulses.* Applied Surface Science, 2012. **258**(19): p. 7625-7632.

140. Ji, X., L. Jiang, X.W. Li, W.N. Han, Y. Liu, A.D. Wang, and Y.F. Lu, *Femtosecond laser-induced cross-periodic structures on a crystalline silicon surface under low pulse number irradiation.* Applied Surface Science, 2015. **326**: p. 216-221.

141. Gregorcic, P., M. Sedlacek, B. Podgornik, and J. Reif, *Formation of laser-induced periodic surface structures (LIPSS) on tool steel by multiple picosecond laser pulses of different polarizations.* Applied Surface Science, 2016. **387**: p. 698-706.

142. Lam, B., J. Zhang, and C. Guo, *Generation of continuously rotating polarization by combining cross-polarizations and its application in surface structuring.* Optics Letters, 2017. **42**(15): p. 2870-2873.

143. Allegre, O.J., W. Perrie, K. Bauchert, D. Liu, S.P. Edwardson, G. Dearden, and K.G. Watkins, *Real-time control of polarisation in ultra-short-pulse laser micro-machining.* Applied Physics a-Materials Science & Processing, 2012. **107**(2): p. 445-454.

144. Graf', S. and F.A. Muller, *Polarisation-dependent generation of fs-laser induced periodic surface structures.* Applied Surface Science, 2015. **331**: p. 150-155.